Doctoral theses at NTNU, 2022:58

Bahareh Nikparvar

Modelling and analysis of the response of *Listeria monocytogenes* to high pressure processing

Doctoral thesis

NTNU
Norwegian University of Science and Technology
Thesis for the Degree of
Philosophiae Doctor
Faculty of Natural Sciences
Department of Chemical Engineering

NTNU
Norwegian University of
Science and Technology

Bahareh Nikparvar

Modelling and analysis of the response of *Listeria monocytogenes* to high pressure processing

Thesis for the Degree of Philosophiae Doctor

Trondheim, February 2022

Norwegian University of Science and Technology
Faculty of Natural Sciences
Department of Chemical Engineering

NTNU
Norwegian University of
Science and Technology

NTNU
Norwegian University of Science and Technology

Thesis for the Degree of Philosophiae Doctor

Faculty of Natural Sciences
Department of Chemical Engineering

ISBN 978-82-326-5717-9 (printed ver.)
ISBN 978-82-326-5411-6 (electronic ver.)
ISSN 1503-8181 (printed ver.)
ISSN 2703-8084 (online ver.)

Doctoral theses at NTNU, 2022:58

Printed by NTNU Grafisk senter

To my dear family.

This page intentionally left blank.

Abstract

The effects of environmental stresses on microorganisms have been well-studied, and cellular responses to stresses such as heat, cold, acids, and salts have been extensively discussed. Some previous works studied the membrane, protein system, and DNA as susceptible structures in bacteria to external stress. Although high pressure processing (HPP) is an emerging technology as a preservation method in the food industry, the dynamics of the response of bacteria and particularly *Listeria monocytogenes* as a foodborne pathogen to high pressure processing (HPP) has not been well-explored yet. *L. monocytogenes* is known to survive extreme conditions, including high pressure, and therefore gaining knowledge of its reaction to the stress produced by high pressure may help the food industry to increase the efficiency of HPP.

In this Ph.D. thesis, we employed synergy between various experimental techniques (such as flow cytometry, fluorescence microscopy, electron microscopy, and RNA sequencing) and modelling strategies to explore the cellular response of *L. monocytogenes* to HPP.

First, we found that high pressure stress could create membrane pores in *L. monocytogenes* after HPP at 400 MPa, 8 min. Using a common staining technique with propidium iodide (PI) combined with high-frequency fluorescence microscopy, we monitored the diffusion rate of PI molecules into hundreds of bacterial cells through these pores during four days after HPP. We found that the diffusion rate of PI into the cells decreased over the four consecutive days after exposure to HPP, indicating the existence of a repair mechanism for the pressure-created membrane pores. In addition, we developed a mathematical model based on mass transfer and passive diffusion laws, calibrated using our microscopy data, to evaluate the rate of repair of the membrane following HPP. The model predicted a temporal change in the size of pores until closure. To the best of our knowledge, this is the first time that pressure-created membrane pores have been quantitatively described and shown to diminish with time. In addition, we found that the membrane repair rate in response to HPP was linear (at pore sizes < 20 nm), and growth was temporarily arrested at the population level during the repair period.

Second, we used time-series RNA-seq transcriptome data of *L. monocytogenes* (strain ScottA) treated at 400 MPa for 8 min and combined it with current information in the literature to create a transcriptional regulation database, depicting the relationship between transcription factors (TFs) and their target genes (TGs) in *L. monocytogenes*. We then applied network component analysis (NCA), a matrix decomposition method, to reconstruct the activities of TFs over time. According

to our findings, *L. monocytogenes* responded to the stress applied during HPP by three significantly different gene regulation modes: a survival mode during the first 10 min post-treatment, a repair mode during one hour post-treatment, and a re-growth mode beyond six hours after HPP. We identified the TFs and their TGs that were responsible for each of the modes. We developed a plausible model that could explain the regulatory mechanism that *L. monocytogenes* activated through the well-studied CIRCE (controlling inverted repeat of chaperone expression) operon via the regulator HrcA during the survival mode.

Third, since the SOS response and the chaperonin systems were shown to be essential regulatory networks that counteract environmental stresses, we developed a mathematical model to get a deeper insight into the behavior and dynamics of these two networks as parts of an initial recovery process in response to HPP. The model was described by a system of ordinary differential equations (ODEs) and calibrated using a time-series RNA-seq data to estimate critical parameters. Our model outputs indicated the existence of a range of parameters that yielded damped oscillatory behavior in the time response of the SOS response-associated variables. This is in contrast to the chaperonin system-related variables that showed a single pulse response to HPP. We found that perturbing the parameters associated with HU, a histone-like protein involved in activation of RecA (a regulator of the SOS response), and consequently induction of the SOS response, had significant impacts on the characteristics of the response. Moreover, our results suggested a correlation between the frequency of oscillations of the SOS response and the resistibility of RO15 and ScottA (two strains of *L. monocytogenes*) to HPP. Additionally, our further analysis led us to formulate a hypothesis about the relationship between HPP parameters (pressure value and holding time) and the characteristics of oscillations in the SOS response. The results suggested that increasing pressure values and holding time affected the response by increasing the number of peaks (prolonging the damped oscillation) and the amplitude of the first peak, respectively. We believe that these results may guide the industry to adjust different parameters of HPP to achieve a more efficient preservation technology via pressurization.

This Ph.D. thesis presents a collection of journal and conference papers.

Acknowledgements

Firstly, I would like to express my sincere gratitude to my Supervisor, Prof. Nadav Bar, for the support of my Ph.D. study and related research. His comments and encouragements helped me in all the time of research and writing of this thesis. Besides my main supervisor, I would like to thank my co-supervisor, Prof. Sigurd Skogestad, for sharing his deep knowledge in process control and process systems engineering with me as one of his students.

Secondly, I would like to acknowledge my dear colleagues in the Process Systems Engineering group and particularly: Fabienne Rössler, Andrea Tuveri, Pedro Antonio Lira Parada, Haakon Holck, and Fernando Perez-Garcia, for the supports, inspiration, and great moments we had together.

Thirdly, I want to thank the people in SafeFood consortium, especially Alicia Subires, Margarita Andreevskaya, Marta Capellas, Petri Auvinen, and Christian Riedel, for productive collaborations we had together.

Finally, I must thank my real treasure in the world, my family, that finishing this journey without them was not possible for me: my dearest parents, my husband Majid, my brother Behnam, and my sister Behnoush for their supports and for being there every time I needed them, and the last but not the least my little angel Nahal Sophia for understanding that Mamma should work and cannot spend too much time for playing. I love you and I'm proud of you.

This page intentionally left blank.

Contents

Preface

This thesis is submitted in partial fulfillment of the requirements for the degree of Doctor of Philosophy (Ph.D.) at the Norwegian University of Science and Technology (NTNU). The work performed during this Ph.D. was carried out at the Department of Chemical Engineering from January 2017 to July 2021, under the supervision of Dr. Professor Nadav Bar and co-supervised by Dr. Professor Sigurd Skogestad. The original project was three years, but the project was extended due to teaching duties. The project was a part of the transnational SafeFood industrial biotechnology project united 8 groups from 6 countries across Europe, with the purpose to turn food safer, by inactivating *Listeria monocytogenes*, a foodborne pathogen. The consortium consisted of experts in different fields like bioinformatics, molecular biology, simulation and modelling, and food preservation industry.

During my Ph.D. studies I had the privilege to be trained and work at the high pressure pilot plant, flow cytometry, and fluorescence microscopy lab at the Autonomous University of Barcelona (UAB), for more than 1 month in 2019. The results of this collaboration led to two publications included in this thesis. Additionally I had the opportunity to visit the RNA-seq lab at the University of Helsinki in 2019 and collaborate with the bioinformaticians there to process and analyze the trancriptome data which resulted in two other publications as parts of this thesis. Besides that, I had the privilege to be trained at the Cellular and Molecular Imaging Core Facility (CMIC), Norwegian University of Science and Technology (NTNU) to work with an electron microscope.

This research work was supported within the ERA-IB2 consortium SafeFood (ID: ERA712IB-16- 247 014) by grants of the the Research Council of Norway, grant number 263499.

Declaration of Compliance

I hereby declare that the thesis is an independent work in agreement with the exam rules and regulations of the Norwegian University of Science and Technology (NTNU). This work is original and my own work, and the sources I used were properly cited and acknowledged.

Oslo, February 9, 2022
Bahareh Nikparvar

Chapter 1

Introduction

Bacteria in nature can grow in various habitats such as soil, water, animals' intestines, radioactive waste, and even arctic ice and glaciers. In this wide range of environments, bacteria may be exposed to different types of stresses such as high or low temperatures, radiation, osmotic pressure, and antimicrobial compounds. Bacteria possess a well-developed adaptability system to overcome such adversities, that allows them to modify themselves to fluctuating environmental conditions [33]. This modification is mainly facilitated through changes in the pattern of gene expression, which leads to the production of required proteins to combat stresses [22, 33].

High pressure processing (HPP) is becoming more popular as a preservation technique in the food industry to inactivate pathogenic bacteria such as *Listeria monocytogenes*, *Salmonella*, and *Escherichia coli* as an alternative for more traditional treatments like heating, adding salt, and changing pH [50]. However, although the bacterial response to stresses such as heat/cold shock, oxidative stress, nutrient depletion, acid, and antibiotics have been studied extensively [11, 18, 28, 57], the mechanisms that are activated in response to high pressure are still largely unknown despite the proven effectiveness of HPP in the food preservation industry and its increasing use (Figure 1.1) [15, 34, 47].

1.1 High pressure processing (HPP)

HPP, which is considered as an alternative to thermal treatments to prolong shelf life and preserve the quality of the food, is becoming more popular in the food industry (Figure 1.1). This method can be used alone or in combination with other techniques to produce high quality and minimally processed safe foods [37].

In this pasteurization technique, food is exposed to a high level of hydrostatic pressure (300-800MPa) lasting for a time range of a few min to an hour [48]. The processing cycle consists of filling the process vessel with the product, pumping water as the pressure transmission fluid into the vessel, pressurizing the product for a specific pressure value and holding time and in a desired temperature, and finally taking out the product from the vessel after decompression (Figure 1.2).

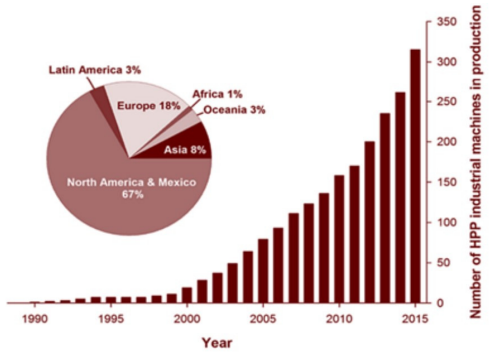

Figure 1.1: World growth of the food industry use of HPP technology [4].

The product is then kept in a low temperature to eliminate bacterial growth during storage.

Since hydrostatic pressure acts instantaneously and uniformly throughout the sample, it provides a gentle food treatment with minimum side effects on the flavor and texture of foods [50, 65]. As HPP is normally performed during final packaging, the risk of re-contamination from any step of the production chain becomes minimum [50]. The ability of sub-lethally injured cells to recover after treatment is a major concern in the food preservation industry which demands more efficient and promising approaches to eliminate pathogenic bacteria in food [13, 36, 38].

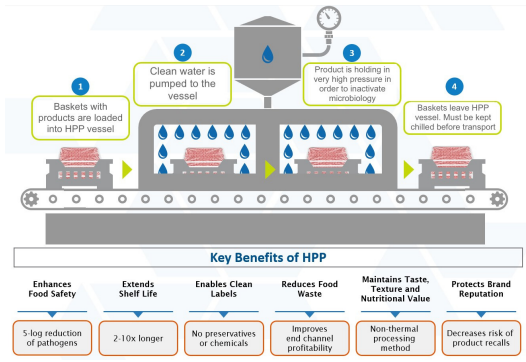

Figure 1.2: HPP cycle in the food industry [3].

1.2 *L. monocytogenes*

L. monocytogenes is a Gram-positive, non-spore-forming, rod-shaped, pathogenic bacterium that causes the infection listeriosis, a disease with increased health and economic issues in Europe. The U.S. Food and Drug Administration (FDA) claims that although listeriosis is rare, it has a high mortality rate of 20-30% and hos-

pitalization rate of 90%. Elderly, newborns, and pregnant women are at a higher risk due to their weaker immune systems. According to the latest annual epidemiological report published by European Centre for Disease Prevention and Control (ECDC) in 2020 [2], more than 2500 confirmed cases of Listeria and 220 deaths were reported in Europe in 2017. The report stated that the number of cases shows a statistically significant increasing trend from 2013 to 2017. Listeria is commonly found in soil, water, and particularly decaying plant material, but it can also contaminate food products such as raw vegetables and meat. *L. monocytogenes* is known to have tolerance for different extreme environmental conditions such as refrigeration temperatures [5].

1.3 Bacterial response to stress

Bacteria, like other living organisms, have the capability of sensing and responding to conditions that stress their homeostatic mechanisms. These mechanisms help bacteria to prevent death and survive different inhospitable environments. One of the main bacterial strategies to respond to stress is to re-model their protein complexes and produce required proteins critical for withstanding the stress [22, 33]. It was shown that modulating the pattern of gene expression through, for instance, two-component signal transduction systems (TCS) or by activating sigma factors [43] is an important way to express and maintain these essential proteins. In this work, and especially for the modelling procedure, we focused on these two elements, described in more detail below.

1.3.1 Two-component signal transduction system (TCS)

A TCS system consists of a histidine kinase which is typically a membrane-associated protein and a response regulator, which conveys a change in cell physiology by regulation of gene expression. The histidine kinase monitors the environmental conditions and when it receives an external input, autophosphorylates a histidine residue. The phosphoryl group is then transferred to an aspartic residue of the response regulator which is alternatively called transcription factor and is capable of binding to DNA and regulates gene expression [35, 64, 72]. AgrAC, VirRS, ResDE, LisRK, and CesRK are some examples of reported TCSs in *L. monocytogenes* [24]. In addition to regulators, sigma factors (explained below) also contribute to the regulation of gene expression by determining which sets of genes should be transcribed.

1.3.2 Sigma factors

Transcription of DNA is carried out by the enzyme RNA polymerase, which catalyzes the synthesis of RNA using DNA as a template. Bacterial cells have a single kind of RNA polymerase that synthesizes all three major classes of RNA; mRNA, tRNA, and rRNA. The enzymes from different bacteria are quite similar, and the RNA polymerase from *E. coli* has been especially well characterized. It is a large protein consisting of two α subunits, two β subunits that differ enough to be identified as β and β', and a dissociable subunit called the sigma (σ) factor. Although

the core enzyme lacking the sigma subunit is competent to carry out RNA synthesis, the holoenzyme (complete enzyme containing all of its subunits) is required to ensure initiation at the proper sites within a DNA molecule. The sigma subunit plays a critical role in this process by promoting the binding of RNA polymerase to specific DNA sequences, called promoter, found at the beginning of genes. Bacteria contain a variety of different sigma factors that selectively initiate the transcription of specific categories of genes [33].

1.4 Bacterial structures susceptible to pressure-induced damages

Although bacteria have the capability of activating a highly advanced defense mechanism in response to inhospitable conditions, they cannot withstand all kinds of stresses. Treatments with pressures higher than 400 MPa may lead to a reversible or irreversible cleavage of intermolecular and intramolecular bonds and therefore result in lethal damages such as structural changes in the membrane or inactivation of vital enzymes [34, 39].

An intact bacterial membrane is a robust permeability barrier that prevents both the leakage of essential intracellular molecules outside the cell and the uptake of many particles from outside the cell. However, exposure to undesired conditions may cause the membrane to become permeable to molecules such as fluorescent ones (which are widely used for staining techniques) that otherwise could not pass through the intact membrane. Heat treatment, adding agents, and pulsed electric field are among membrane-acting stressors that may cause loss of membrane integrity. In [40, 63] the authors observed damage to the cytoplasmic membrane in bacteria after heating. Cortezzo et al. [17] showed that treatment with oxidizing agents can damage the inner membrane of spores of *Bacillus subtilis*. Some authors reported damage to the cell membrane as one of the critical events leading to cell inactivation by pulsed electric field [8, 27].

By considering this unique feature of the bacterial membrane and using different tools such as fluorescence microscopy techniques, several authors investigated the impact of the HPP on the cell envelope and particularly the membrane as one of the most susceptible structures in bacteria to stress [26, 42, 61]. For example, in [61] the authors demonstrated increased uptake of exogenous fluorescent molecules propidium iodide (PI) in *Lactobacillus plantarum* exposed to high pressure, indicating a damaged membrane. In [26] changes in the kinetics of outer and cytoplasmic membrane permeability in *E. coli* after exposure to high pressure (300, 500, 600 MPa) was shown by staining of treated cells with PI and 1-N-phenylnaphthylamine. Furthermore, a few studies have detected cellular proteins or adenosine triphosphate (ATP) molecules outside the cell after pressurization [42, 61]. One such example is a study that reported the detection of intracellular proteins outside pressure-treated *E. coli* cells (200 MPa, 8 min), indicating a membrane leakage [42].

Proteins are macromolecules that play major roles in the metabolic activity of all living cells. The protein structure is normally described in terms of four different aspects of covalent bonds and folding patterns known as primary, secondary, tertiary, and quaternary structures. The primary structure, which is the simplest

level of protein structure, is the sequence of amino acids in a polypeptide chain. The next level, the protein secondary structure, is the three-dimensional form of local segments of proteins. The overall three-dimensional structure of a polypeptide is called its tertiary structure. The tertiary structure is primarily due to interactions between the R groups of the amino acids that make up the protein. The last level, i.e., the quaternary structure of a protein is the association of several subunits into a packed arrangement where each of the subunits has its own primary, secondary, and tertiary structure [51]. In order to be biologically functional, a protein chain is translated to a native three-dimensional structure through a physical process, typically a "folded" conformation. Protein folding and particularly the tertiary and quaternary structure of proteins are extremely susceptible to different types of stress [34]. Protein denaturation and enzyme inactivation make structural and functional proteins a prime target for heat treatment [58]. Oxidative stress can damage the protein structure as well by inducing covalent modifications that destabilize and therefore inactivate proteins [21]. High pressure may change protein folding as well although HPP-induced protein denaturation can be reversible depending on treatment conditions such as temperature, time, and pressure [16]. Chaperones and heat-shock proteins are specific macromolecules that protect the cell against stress-inducible denaturation by correcting the folding of proteins [33]. The induction of heat-shock and chaperone proteins after pressure treatment has been reported by several authors [6, 20, 69], suggesting a role for these groups of the proteins in the protection of the protein system against pressure-induced damages. For example it has been shown that the genes *dnaK* and *clpP* (from chaperonin group) differentially expressed in *E. coli* after exposure to sublethal pressures 75 and 150 MPa for 15 min [6]. An up-regulation of chaperone and peptidases genes such as *clpE*, *clpP*, *groEL*, *groES*, *hrcA*, *dnaK*, and *dnaJ* in *L. monocytogenes* at early time points after HPP at 400 MPa, 8 min was observed as well [20].

Undesired stressful conditions can lead to DNA damage as well. This damage mostly appears as double-strand breaks in DNA and the formation of ssDNA (single-stranded DNA). For example, UV radiation may induce DNA damages that if are not repaired, cause death [10]. Exposure to oxidative stress and antibiotics are other types of stress that can lead to lethal or sublethal damage in bacteria [10]. The authors of [6] could detect DNA damages in *E. coli* after pressure treatment (up to 300 MPa) using a differential fluorescence induction screening. Perturbed cell division and nucleoid structure were reported after high pressure exposure as well [1, 69], which again suggests the presence of DNA damage due to treatment.

1.5 Pressure-mediated damage in bacteria can be repairable

Several previous works investigated the existence of a repair process in bacteria after pressure treatment by growth evaluation and observed that some treated bacteria could start to proliferate again, potentially after an accomplished repair process during storage [13, 36, 38]. For instance, although no colony formation in different bacteria (including *L. monocytogenes*) was detected in selective or non-selective agar immediately after HPP at 550 MPa, growth evaluation after six days

storage at 4 °C and one day storage at 22 and 30 °C indicated some growing bacteria in both selective and non-selective agar [13]. This observation suggested a transient inactivation phase in bacteria right after treatment, followed by an effort to recover damages and maintain the homeostasis phase. According to another work [36], even a pressure treatment of 900 MPa could not stop growth in some *L. monocytogenes* cells during storage at 30 °C. Another examination [38] indicated that the leaky membrane of a pressure-resistant strain of *E. coli* was able to reseal after getting damaged under high pressure (up to 700 MPa) as PI uptake occurred only during treatment but not after pressure release.

As mentioned earlier, heat-shock proteins and chaperone systems assist for correct protein folding. The up-regulation of genes encoding for chaperones after pressure treatment (in comparison with untreated cells) was observed by several groups [6, 20, 69], suggesting the activation of a protein repair process after pressure exposure. Two operons (dnaKJ and groESL) encoding for molecular chaperones were identified in the previous decades as the CIRCE (controlling inverted repeat of chaperone expression) operon [14, 59]. *hrcA* (heat-shock regulation at CIRCE) is the gene encoding for the repressor protein binding to the CIRCE element. The GroE chaperonin system is responsible for creating an equilibrium between active and inactive forms of the repressor HrcA, where the inactive form is unable to bind to its operator [59]. The activity of the repressor HrcA is modulated after stress by the GroE chaperonin system. In the absence of stress, HrcA is maintained in an active conformation able to bind to CIRCE through the GroE system. Under stress, since unfolded proteins titrate the GroE chaperonin system, it is no longer available to activate HrcA, leading to an increase in the amount of inactive repressor HrcA and transcription of the groE and dnaK operons [55, 59].

SOS response is a broad regulatory network in bacteria that can be induced in response to external stimuli to manage DNA damage and survive. The activation of the SOS response leads to the expression of genes with different functions, including excision repair, homologous recombination, translesion DNA replication, and cell division arrest. Therefore the induction of the SOS response can be interpreted as an effort to accomplish DNA repair before restarting the growth [7, 44]. The regulation of the SOS response in bacteria is mainly achieved by interactions between two regulators (TFs), LexA and RecA [44, 52]. LexA protein is a repressor and normally regulates transcription of SOS response-associated genes (among them its own gene, *lexA*, and *recA*) negatively by binding to the promoter and thereby blocking RNA polymerase. However, if DNA is damaged and ssDNA is accumulated under stress conditions (such as high pressure or UV irradiation), the positive regulator RecA is activated and makes a filament with ssDNA. The interaction between LexA and RecA/ssDNA leads to autocleavage of LexA, thereby facilitating the transcription of the SOS response operon [7, 60, 67]. Figure 1.3 shows the principle of the SOS response induction schematically.

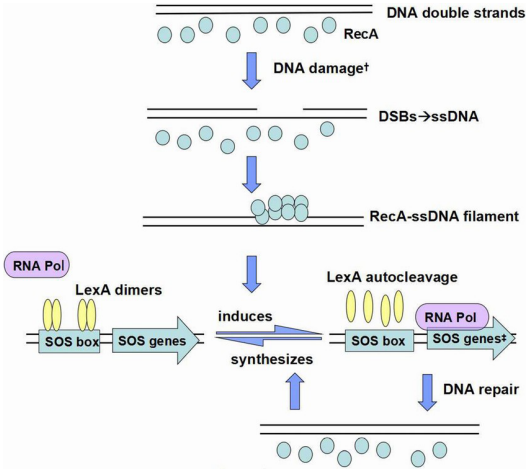

Figure 1.3: The induction of the SOS response is regulated by two regulators, LexA as a repressor and RecA as an activator. Under normal conditions, LexA inhibits the transcription of the SOS operon by binding to the promoter and blocking RNA polymerase. The accumulation of ssDNA originated from DNA damage under stressful conditions results in the activation of RecA, which then makes a filament with ssDNA. The interaction between this filament and LexA leads to autocleavage of LexA and facilitates the transcription of the SOS response operon. †: UV irradiation, chemicals or oxidative compounds, acids, organic mutagens, some antibiotics, high pressure, etc.; ‡: the transcription of SOS genes is hindered by blocking RNA-polymerase activity. Figure from [53].

1.6 Use of ordinary differential equations (ODEs) to model time-dependent processes

ODEs are a very useful tool to express mathematically the dynamical consequences of a molecular interaction network [62]. To get from a wiring diagram to a set of ODEs, it is possible to think about a network as a dynamical system whose state is changing from one moment of time to the next. A single state variable $X(t) =$ the concentration of species X, is then assigned to each species in the diagram. The collection of values of all these variables $\{X_1(t), X_2(t), X_3(t), ...\}$ at any point in time constitutes the state of the system. Then, for each molecular species, a differential equation is written which describes how its concentration changes over time due to its interactions with the other species in the network. In this paradigm, the dynamical consequences of a reaction network are determined by a system of nonlinear ODEs,

$$\dot{X}_i = F_i\{X_1, X_2, ..., X_n, p_1, p_2, ...p_m\},\ i = 1, 2, ..., n \tag{1.1}$$

where $\{p_1, p_2, ...p_m\}$ is the set of all rate constants needed to describe the reactions in a molecular interaction network, or simply parameters. It is possible to estimate

parameters by fitting the simulated data (solution of ODEs) to the experimental points. A major challenge with such models is that they often possess a large number of parameters (usually more than measured experimental points) whose values can significantly affect model behavior. In fact, there is a trade-off between the level of detail included in the model and the amount of data available for parameter estimation. This issue is usually addressed by performing sensitivity analysis to determine the most critical parameters of the model.

1.7 Research questions, and the outline of the thesis

In this Ph.D. work, we combined the knowledge of modelling with data analysis and experimental methods to answer three research questions. The thesis chapters were organized according to these three questions and the answers we suggested to address these questions. The outline of the thesis is summarized in Figure 1.4:

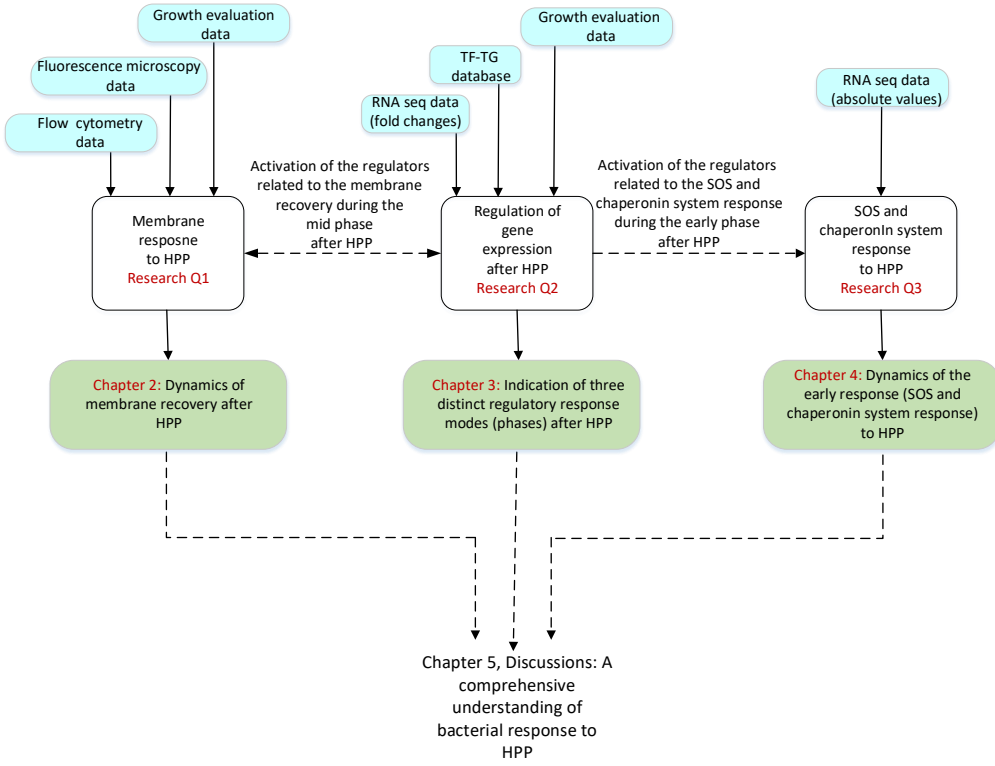

Figure 1.4: Outline of the thesis. The thesis was organized into six chapters, chapter 1: introduction, chapters 2-4: answering three research questions, chapter 5: Discussion, and chapter 6: Conclusion and future work. A summary of the research questions and the chapters that address them is shown in the figure.

1.7.1 Research question 1

The previous knowledge presented in sections 1.5 and 1.4 indicating that high pressure can affect the structure of the membrane has led us to the following research question:
Research question 1: *What is the impact of HPP on the bacterial membrane and how does the bacterium respond to any potential pressure-induced damage?*

Chapter 2. To answer this question, we employed three independent techniques to: 1) observe and gather information about the cellular structure and particularly the permeability of the membrane in pressure-treated bacteria, 2) to quantify the scale of potential damages, and 3) to model the strategy of bacteria to withstand this stress (by activating a repair process). These three techniques that form the topic of this chapter are summarized here:

1. **Electron microscopy (transmission electron microscopy: TEM and scanning electron microscopy: SEM):** As the first step to answer this research question, we looked at the morphology of the pressure-treated *L. monocytogenes* (400 MPa, 15 min) and compared it with untreated cells using electron microscopy, TEM and SEM (Figure 1.5). The HPP treatment was done at the Norwegian Institute of Food, Fisheries and Aquaculture Research (also known as NOFIMA), in Stavanger, Norway in attendance of the Ph.D. candidate. The candidate was trained at Cellular and Molecular Imaging Core Facility (CMIC), Norwegian University of Science and Technology (NTNU) to collect images with an electron microscope. After comparing the morphology of treated with untreated bacteria, we could detect some sites of leakage on the membrane of some pressurized cells (Figure 1.5 as representatives). While this observation provided us a qualitative overview of pressure-induced damages in the membrane, the next two analyses gave us a detailed and quantitative measure of the response of the membrane to HPP.

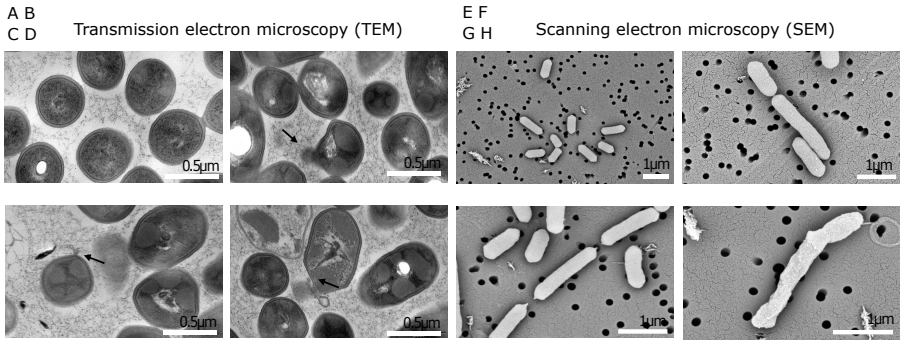

Figure 1.5: ABCD. TEM images of A. untreated (control) and B, C, D. pressure-treated (HPP: 400 MPa, 15 min) *L. monocytogenes* cells. The black arrows show the sites of damages on the membrane. EFGH. SEM images of E. untreated (control) and F, G, H. pressure-treated (HPP: 400 MPa, 15 min) *L. monocytogenes* cells.

2. **Flow cytometry:** We used the high throughput data obtained from this laser-based technology to analyze the characteristics of the bacterial membrane. The principle of this method is briefly explained in Figure 1.6. Sample preparation, pressure treatments (at 400 MPa, 8 and 20 min, 8 °C), and flow cytometry experiments were performed at the Autonomous University of Barcelona (UAB), Spain, as one of the project collaborators, in the presence and with the assistance of the Ph.D. candidate. We developed a model calibrated by data collected from a flow cytometer to quantify membrane damages and estimate the pathogen's recovery time following HPP.
3. **Fluorescence microscopy:** As a further analysis to achieve a more accurate estimation of pressure-created damages, we increased the level of monitoring to each individual pressure-treated cell by using a high frequency fluorescence microscopy technique. HPP was performed in a discontinuous isostatic press (Alstom ACB, Nantes, France) at the Autonomous University of Barcelona (UAB) at 400 MPa, 8 min, 8 °C. Pressurized samples were kept in ice before being further processed for fluorescence microscopy analysis. We used a common staining technique involving propidium iodide (PI) combined with high-frequency fluorescence microscopy and monitored the diffusion rate of PI molecules into hundreds of bacterial cells through permeable membrane of pressurized cells. PI molecules that can only penetrate cells with a damaged membrane, bind to DNA and emit fluorescence intensity, making damaged cells detectable within a population. The experimental setup is shown in Figure 1.7A schematically. To add PI molecules to the sample during a live microscopy process, a delivery system consisted of a syringe coupled to a plastic tube (shown in Figure 1.7B) was used that was in turn attached to a holed plate lid on top of the plate containing the sample. The rate of PI diffusion into a cell depends on the scale of membrane damage that we considered as a pore area. Therefore, it is possible to estimate the pore size by measuring the difference in fluorescence intensity resulting from the increased number of PI molecules bound to DNA. The microscopy experiments were performed over four days after treatment (days 0, 1, 2, 3, and 4) to measure the PI diffusion rate through the pores and thereby to investigate the existence of a recovery process in the membrane (i.e., resealing pores). The principle of the work is shown in Figure 1.8. The microscopy experiments were performed at the Autonomous University of Barcelona (UAB) by the Ph.D. candidate. All obtained images are available on Dryad Digital repository A.1. We developed a dynamic model capable of quantifying membrane damages (specifically membrane pores) created by high pressure. The combination of our diffusion model and microscopy experiments revealed that some pressure-treated *L. monocytogenes* cells repaired their damaged membrane approximately linearly on a time scale of days.

1.7.2 Research question 2

Once we established the existence of damage on the cellular membrane, and the existence of recovery mechanisms of the membrane, the question that naturally arises is how the regulatory network enables this recovery. More specifically:

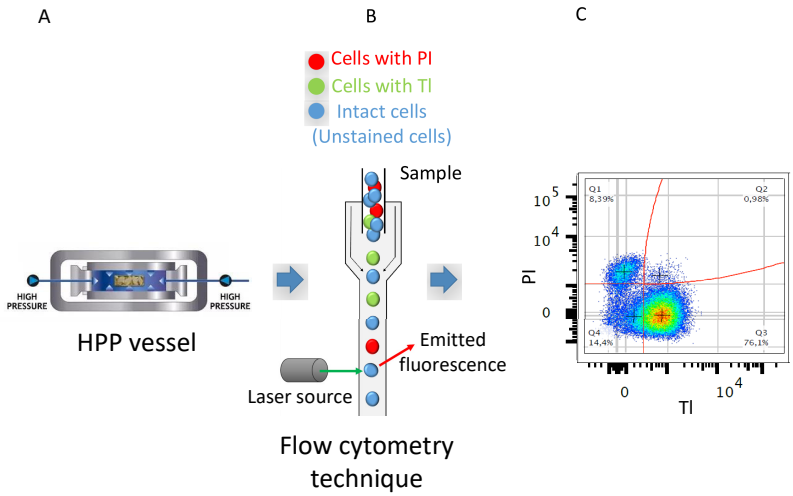

Figure 1.6: Flow cytometry is a technology that is used to analyze the physical and chemical characteristics of particles in a fluid as it passes through at least one laser. Cell components are fluorescently labelled and then excited by the laser to emit light at varying wavelengths. Up to thousands of particles per second can be analyzed as they pass through the liquid stream. After HPP treatment (part A), pressurized bacteria were processed for further analysis in a flow cytometer (part B). The flow cytometry device we used could measure the fluorescent intensity for each cell at a high frequency (over 40000 cells in approximately 20 seconds). Two different fluorescent molecules, propidium iodide (PI) and FluxOR II-thallium (FluxOR II-Tl) that have different molecular sizes, were used to estimate the size of the membrane pores in damaged cells (PI radius: 0.6 nm and Tl radius: 0.2 nm [12]). Both molecules can only penetrate the cells with damaged membranes. Molecules of PI emit red (630 nm) fluorescence, and molecules of FluxOR II-Tl emit green (525 nm) fluorescence after binding to DNA. C. The expected fluorescence pattern as the output of the flow cytometer. The x and y axes represent the intensity of green and red fluorescence (emitted from FluxOR II-Tl and PI, respectively), respectively. Depending on the emitted intensity from each individual cell in a population, cells are categorized into four groups: Q1, Q2, Q3, and Q4. Q1, Q3, and Q4 correspond to highly damaged, less damaged, and intact cells (Q2 was less important in our work). The percentage of total cells detected in each population is shown in the plot as well.

Research question 2: *What is the impact of HPP on gene regulatory network and regulators' activities in L. monocytogenes?*

Chapter 3. As mentioned earlier in section 1.3, modulation of gene expression pattern is one of the main bacterial approaches to withstand stress condi-

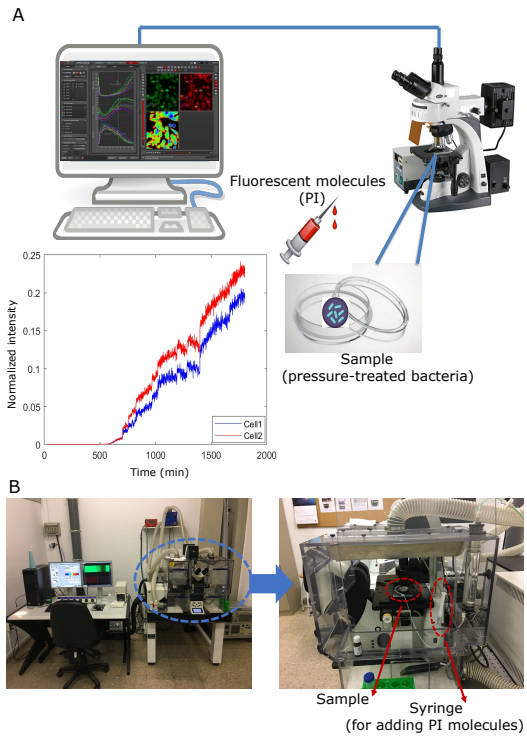

Figure 1.7: A. The experimental setup included a fluorescence microscope connected to a computer for time-lapse image acquisition of diffusion of fluorescent molecules PI into damaged bacteria. The average intensity for each cell in every single frame of the image stacks was then calculated (shown as blue and red curves for two representative cells) after image processing. B. The delivery system for PI molecules consisted of a syringe coupled to a plastic tube that was in turn attached to a holed plate lid on top of the sample.

tions. The gene expression pattern can be studied by several advanced methods such as RNA-seq, microarray, and quantitative polymerase chain reaction (qPCR). RNA-seq is a technique that can examine the quantity and sequences of RNA in a sample by analyzing the transcriptome of gene expression patterns encoded within RNA. For the first time, a time-series RNA-seq of *L. monocytogenes*, strains ScottA and RO15 (untreated and pressure-treated) was performed at the University of Helsinki, Finland as a collaborator of the project. The mRNA counts for 2953 genes of the ScottA strain and 3021 genes of the RO15 strain were obtained from the RNA-seq data (at least three replicates for each untreated/treated sample). The data is available in the European Nucleotide Archive (ENA) under accession code PRJEB34771 (A.3). Pairwise differential expression analysis between the treated samples and corresponding controls at all time points was conducted to determine significantly differentially expressed genes ($pvalue \leq 0.05$, $|\log_2 \text{fold change}| > 0.6$,

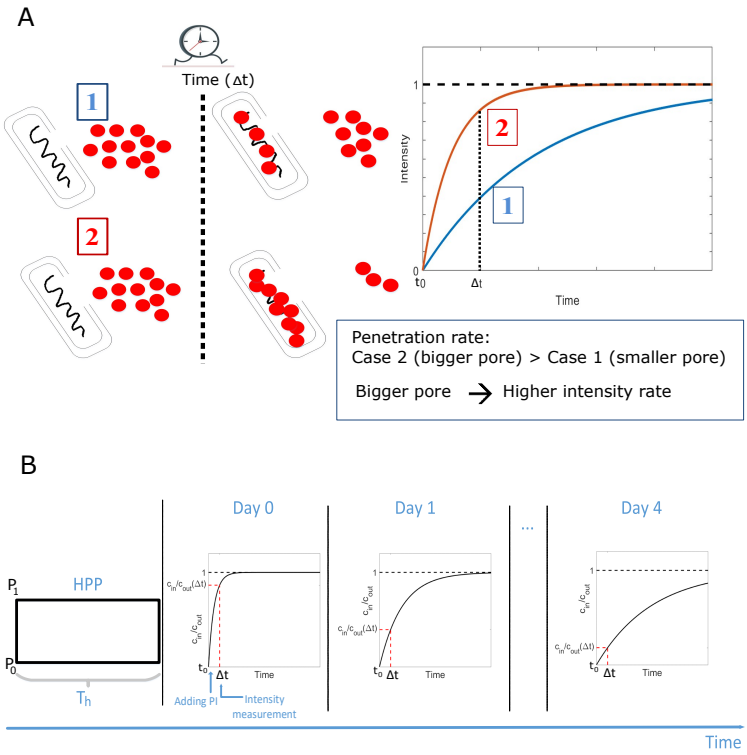

Figure 1.8: A. Fluorescent molecules (PI), shown as red circles, can only penetrate the cells with damaged membrane, bind to DNA, and emit red fluorescence intensity. We assumed that the penetration rate for a cell with a bigger pore (case 2) is higher than for a cell with a smaller pore (case 1). Therefore, by passing a specific time Δt after adding PI molecules to a sample of pressure-treated bacteria, a cell with a bigger pore emits a higher fluorescence intensity than a cell with a smaller pore. The plot shows that intensity increases until it reaches saturation which happens when the concentration of PI molecules inside and outside the cell (C_{in} and C_{out}, respectively) becomes equal. B. We repeated fluorescence microscopy experiments at days 0, 1, 2, 3, and 4 following HPP with a specific pressure value $P_1 = 400$ MPa and for a holding time of $T_h = 8$ min. We interpreted the observed reduction in the PI penetration rate over the four consecutive days as a recovery process in the membrane after HPP.

where fold change $= \log_2(counts_{tr}/counts_{utr})$, tr: treated, utr: untreated) after HPP. A detailed explanation about the RNA-seq data analysis is provided by [20]. As explained earlier in section 1.3, TFs/response regulators are one of the main building blocks of the gene regulatory network in bacteria reacting to stress. Therefore, studying the behavior of TFs is a prerequisite for the achievement of a deep understanding of bacterial response to stress. We employed Network Component Analysis (NCA) [25, 41, 66] to predict the activities of TFs/response regulators in

L. monocytogenes following HPP. Traditional statistical methods such as principal component analysis (PCA) and independent component analysis (ICA) ignore the underlying network structures and provide decompositions based purely on a priori statistical constraints on the computed component signals. The resulting decomposition thus provides a phenomenological model for the observed data and does not necessarily contain physically or biologically meaningful signals. However, in NCA a topology matrix **A** is used as an input to the algorithm which represents and matches the real biological system [41].

We used RNA-seq transcriptome data of *L. monocytogenes* (ScottA) treated at 400 MPa, 8 min, 8°C (performed at the University of Galati, Romania, as one of the project partners) together with a transcriptional regulation database as inputs of the NCA to obtain reconstructed activity of TFs as an output. The transcriptional regulation database that we built depicts the relationship between TFs and their TGs in *L. monocytogenes* (A.2). Our results indicated that the regulatory network in *L. monocytogenes* strain ScottA responded to high pressure stress in three distinct phases:

- Survival phase lasting 0-10 min after HPP, and based on our database, regulating genes responsible for immediate survival and structural integrity (mostly the SOS response-associated and chaperones-regulation genes).
- Repair phase, in which gene expressing enzymes and proteins related to the membrane repair were regulated during 30-60 min after HPP.
- Pre-growth phase, in which genes that are responsible for energy metabolism and re-growth were regulated during 6-48 h after HPP.

1.7.3 Research question 3

Once we mapped and understood the gene regulatory network, and found the three distinctive phases, we focused on constructing a model including main genes, proteins, and interactions among them that enable rescuing the cell from the high pressure stress at the early-phase.

Research question 3: *How can we employ a system modelling approach to develop a comprehensive multi-scale model that describes the initial response of L. monocytogenes to HPP?*

Chapter 4. As mentioned in section 1.5, a few authors discussed about a potential repair process in bacteria in response to HPP. However, explanatory and predictive models that can provide a comprehensive overview of the response of bacteria to pressure treatment are still missing. As explained in chapter 3, the results of gene regulation analysis indicated a timely-structured response in *L. monocytogenes* to high pressure stress via a highly-ordered activation of TFs. We realized that the TFs involved in the regulation of the SOS response and chaperonin system were among the ones which regulated the early response of *L. monocytogenes* to HPP. Moreover, we showed that the expression of both SOS response- and chaperonin system- associated genes were enriched during the early phase using gene set enrichment analysis (GSEA). We developed a multi-scale model to describe the dynamics of the SOS response and chaperonin system regulation in *L. mnocyto-*

gens exposed to HPP at 200 and 400 MPa, 8 min, 8°C and at nine time points post-treatment (0, 5, 10, 30, 45, 60 min, and 6, 24, and 48 h). The model was calibrated using RNA-seq data (absolute mRNA counts) through a parameter estimation task. According to the model's outputs, we found an oscillatory behavior for the expression of the genes that encode for the main SOS response regulators, i.e., LexA and RecA. Moreover, our results suggested that the characteristics of oscillations are affected by HPP parameters (pressure value and holding time) as well as types of strain (ScottA or RO15). Additionally, our simulation results indicated a single-pulse response for the model variables related to the chaperonin system (mRNA counts for *hrcA* and *groEL* genes) following the experimental points. We used a set ODEs to describe the model:

$$\begin{aligned} \dot{\boldsymbol{x}}(t) &= f(\boldsymbol{u}(t), \boldsymbol{x}(t), \boldsymbol{P}) \\ \boldsymbol{y}(t) &= g(\boldsymbol{x}(t), \boldsymbol{m}) + \boldsymbol{\epsilon}(t) \end{aligned} \tag{1.2}$$

with model states $\boldsymbol{x}(t)$, model input $\boldsymbol{u}(t)$, parameter set $\boldsymbol{P}$, a function g as a mapping of the states to the observable variables $\boldsymbol{y}(t)$ involving parameters $\boldsymbol{m}$, and the measurement noise $\boldsymbol{\epsilon}(t)$. The function f defines the relationship between the model input $\boldsymbol{u}(t)$ and parameters ($\boldsymbol{P} = p_1, p_2, ..p_q$) with the model output.

In general the ODE that formulates gene expression as output Z of a genetic module under control of signal (regulator) S (Figure 1.9) is given by [62]:

$$\begin{aligned} \dot{M} &= a \pm \frac{k_{tr} \cdot S^n}{K^n + S^n} \cdot M^{\mu} - d_M \cdot M \\ \dot{Z} &= k_{tl} \cdot M - d_Z \cdot Z \end{aligned} \tag{1.3}$$

where M is the mRNA concentration, a is the rate constant associated with signal-independent (basal) gene transcription, and k_{tr} is the rate constant associated with transcription. The '+' and '−' operators are used to distinguish between the case of activation or repression by signal S, respectively. To avoid obtaining negative values for M in case of repression by S, we defined the constant μ which is equal to 1 for repression and equal to zero for activation by S. The constants K and n are the Hill constant and Hill coefficient, respectively. The Hill constant gives the value of the input signal that yields 50% response, and the Hill coefficient gives the slope of the signal-response curve at this input signal. Z represents the concentration of protein, k_{tl} is the rate constant associated with translation and d_M and d_Z are the mRNA and protein decay constants, respectively. As the protein Z may have two active and inactive modes, we considered this as a linear enzymatic reaction in Figure 1.9 as well.

RNA-seq analysis provides the mRNA counts and not concentration, therefore we reformulated Eq. 1.4 to obtain mRNA counts instead of mRNA concentration by introducing a dimensionless concentration $m = M/X$ and $z = Z/X$ (similar to [62]), where m represents the mRNA counts, z is a dimensionless concentration of protein, and X is the maximum value of each variable in our work.

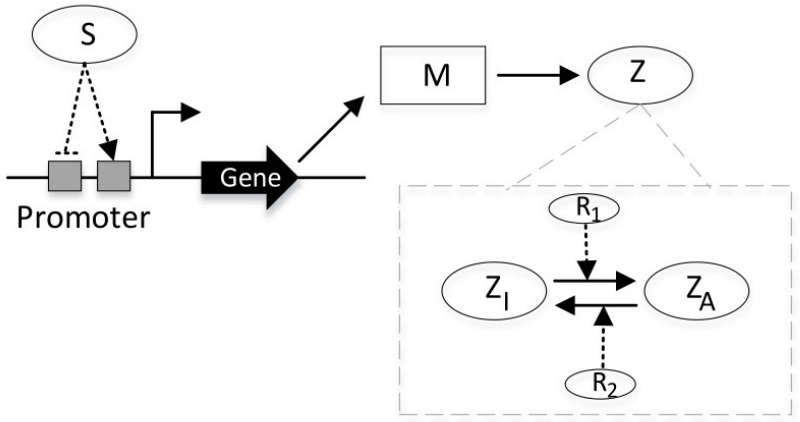

Figure 1.9: The architecture of a gene expression regulatory module. M, Z, and S are the mRNA, protein, and the regulator concentration, respectively. The regulator S can act as an activator or a repressor that binds to the operator site in the prompter region of the gene and facilitate or inhibit the transcription. The protein Z may have two active and inactive conformations (Z_A and A_I, respectively) that can be converted to each other through a reversible reaction. R_1 and R_2 are two regulators (e.g. enzyme proteins) that facilitate these reversible conversions.

$$\begin{aligned} \dot{m} &= a' \pm \frac{k'_{tr} \cdot s^n}{K'^n + s^n} \cdot m^\mu - d'_M \cdot m \\ \dot{z} &= k'_{tl} \cdot m - d'_Z \cdot z \end{aligned} \tag{1.4}$$

with $a' = a/X$, $k'_{tr} = k_{tr}/X^{1-\mu}$, $s = S/X$, $K' = K/X$, $d'_M = d_M$, $K'_{tl} = K_{tl}$, and $d'_Z = d_Z$.

The obtained results, which provide a fundamental understanding of the bacterial response to high pressure, may guide the industry to increase the efficiency of HPP by targeting the critical players belonging to the bacterial protection system against high pressure.

Chapters 5 and **6** present the Discussion and Conclusion, respectively, where we discuss the outcomes of the three previous chapters, summarize the main findings, and provide some suggestions for future works.

1.8 Thesis contributions

In general, the results of the work give a detailed, novel understanding of the dynamics of the bacterial response to HPP. The findings of this work, which have

been obtained from a synergy between modelling and pre-designed experiments, not only revealed the main sites of pressure-induced damages in bacteria but also could explore a well-structured repair mechanism activated as the bacterial effort to survive stress. In specific, the contributions of this work are the following:

- We compared the morphology of pressure-treated and untreated *L. monocytogenes* cells by using TEM and SEM techniques to detect any potential pressure-induced membrane damages (Figure 1.5).
- We quantified the scale of membrane damages in pressure-treated bacteria by developing a model based on a systems biology approach which was calibrated using experimental data obtained from the flow cytometry technique.
- We could detect pressure-induced membrane pores and monitor the dynamics of pore-closing as part of a recovery process in pressure-treated bacteria by designing a set of high-frequency fluorescence microscopy experiments.
- We developed a diffusion model to quantify membrane damage and membrane repair process in *L. monocytogenes* exposed to high pressure based on fluorescence microscopy data.
- We built a database that can explain the regulatory network between TFs and TGs in *L. monocytogenes*. This database is available in A.2.
- We conducted an analysis to explore the temporal gene regulation of pressurized *L. monocytogenes* based on time-series transcriptome data which revealed distinct regulatory response modes in bacteria after exposure to HPP.
- We proposed an integrative model to explain the early response of *L. monocytogenes* to HPP, including the regulation of the SOS response and chaperonin system as bacterial reactions to pressure-induced DNA damages and protein denaturation.

1.9 List of publications

The work on this Ph.D. project and thesis has resulted in the main authorship by the Ph.D. candidate (the author of the thesis) of three journal papers, one conference paper, and the co-authorship of three other journal papers. The list of papers together with (co)authors' contributions are given in the following:

1. An original research paper published in Frontiers in Microbiology Journal. The paper has been a collaboration among the Norwegian University of Science and Technology, The Autonomous University of Barcelona, and Ulm University:

   Bahareh Nikparvar, Alicia Subires, Marta Capellas, Manuela Hernandez-Herrero, Peter Crauwels, Christian U. Riedel, and Nadav Bar. A diffusion model to quantify membrane repair process in *Listeria monocytogenes* exposed to high pressure processing based on fluorescence microscopy data. *Frontiers in Microbiology*, 12(598739), 2021,

https://doi.org/10.3389/fmicb.2021.598739 (Chapter 2).

Bahareh Nikparvar conceptualized the study, designed the methodology, analyzed data, visualized the results, and wrote the manuscript.
Alicia Subires designed the methodology, analyzed data, and wrote the manuscript.
Marta Capellas supervised, provided the resources, reviewed and edited the manuscript.
Manuela Hernandez-Herrero supervised and provided the resources.
Peter Crauwels Visualized the results, reviewed and edited the manuscript.
Christian U. Riedel supervised, reviewed and edited the manuscript.
Nadav Bar supervised, conceptualized the study, analyzed data, provided resources, reviewed and edited the manuscript.

2. A published paper in a conference proceeding (12th IFAC Symposium on Dynamics and Control of Process Systems, including Biosystems). The paper has been a collaboration between the Norwegian University of Science and Technology and The Autonomous University of Barcelona:

   Bahareh Nikparvar, Alicia Subires, Marta Capellas, Manuela Hernandez-Herrero, and Nadav Bar. A dynamic model of membrane recovery mechanisms in bacteria following high pressure processing. *IFAC-PapersOnLine*, 52(1):243–350, 2019,
   https://doi.org/10.1016/j.ifacol.2019.06.069 (Chapter 2).

   Bahareh Nikparvar conceptualized the study, designed the methodology, analyzed data, visualized the results, and wrote the manuscript.
   Alicia Subires designed the methodology, analyzed data, and wrote the manuscript.
   Marta Capellas supervised, provided the resources, reviewed and edited the manuscript.
   Manuela Hernandez-Herrero supervised and provided the resources.
   Nadav Bar supervised, conceptualized the study, designed the methodology, analyzed data, provided resources, reviewed and edited the manuscript.

3. A research article published in BMC Genomics Journal. The paper has been a collaboration among the Norwegian University of Science and Technology, University of Helsinki, University of Galati, and Ulm University:

   Bahareh Nikparvar, Margarita Andreevskaya, Ilhan C. Duru, Florentina I. Bucur, Leontina Grigore-Gurgu, Daniela Borda, Anca I. Nicolau, Christian U. Riedel, Petri Auvinen, and Nadav Bar. Analysis of temporal gene regulation of *Listeria monocytogenes* revealed distinct regulatory response modes after exposure to high pressure processing. *BMC Genomics*, 22(1), 2021,

https://doi.org/10.1186/s12864-021-07461-0 (Chapter 3).

Bahareh Nikparvar conceptualized the study, built the TF-TG dataset, performed the NCA and statistical analysis, made the Cytoscape visualization, wrote the manuscript.
Margarita Andreevskaya built the TF-TG dataset, wrote the manuscript.
Ilhan C. Duru made the Cytoscape visualization, wrote the manuscript.
Florentina I. Bucur collected the experimental samples, performed the pressure treatments, and wrote the manuscript.
Leontina Grigore-Gurgu collected the experimental samples, performed the pressure treatments, read and commented the manuscript.
Daniela Borda collected the experimental samples, performed the pressure treatments, read and commented the manuscript.
Anca I. Nicolau collected the experimental samples, performed the pressure treatments, read and commented the manuscript.
Christian U. Riedel built the TF-TG dataset, read and commented the manuscript.
Petri Auvinen read and commented the manuscript.
Nadav Bar supervised, conceptualized the study, performed the NCA and statistical analysis, and wrote the manuscript.

4. A research paper ready to be submitted in a journal. This paper has been a collaboration among the Norwegian University of Science and Technology, University of Helsinki, and Ulm University:

   Bahareh Nikparvar, Ilhan C. Duru, Petri Auvinen, Christian U. Riedel, and Nadav Bar. Modelling of the SOS response and chaperonin system regulation in *Listeria monocytogenes* after exposure to high pressure processing *to be submitted in a journal* (Chapter 4).

   Bahareh Nikparvar conceptualized the study, developed the model, analyzed data, visualized the results, wrote the manuscript.
   Ilhan C. Duru visualized the results and edited the manuscript.
   Petri Auvinen edited the manuscript.
   Christian U. Riedel edited the manuscript.
   Nadav Bar supervised, conceptualized the study, and edited the manuscript.

The Ph.D. candidate contributed in three journal papers as a co-author (two accepted and one submitted), but they are not part of this Ph.D. thesis:

1. A research article published in BMC Genomics Journal. The paper has been a collaboration among the University of Helsinki, University of Galati, Norwegian University of Science and Technology, Nofima: Norwegian Institute of Food, Fisheries and Aquaculture Research, and Ulm University:

Ilhan Cem Duru, Florentina Ionela Bucur, Margarita Andreevskaya, **Bahareh Nikparvar**, Anne Ylinen, Leontina Grigore-Gurgu, Tone Mari Rode, Peter Crauwels, Pia Laine, Lars Paulin, Trond Løvdal, Christian U. Riedel, Nadav Bar, Daniela Borda, Anca Ioana Nicolau, and Petri Auvinen. High-pressure processing-induced transcriptome response during recovery of *Listeria monocytogenes*. *BMC Genomics*, 22(1), 2021, https://doi.org/10.1186/s12864-021-07407-6.

Bahareh Nikparvar collected the samples and performed the pressure treatments and viable cell count, and read and edited the manuscript.

2. A research note published in BMC Genomics Journal. The paper has been a collaboration among the University of Helsinki, University of Galati, Ulm University, Norwegian University of Science and Technology, and Nofima: Norwegian Institute of Food, Fisheries and Aquaculture Research.

   Ilhan Cem Duru, Florentina Ionela Bucur, Margarita Andreevskaya, Anne Ylinen, Peter Crauwels, Leontina Grigore-Gurgu, **Bahareh Nikparvar**, Tone Mari Rode, , Pia Laine, Lars Paulin, Trond Løvdal, Christian U. Riedel, Nadav Bar, Daniela Borda, Anca Ioana Nicolau, and Petri Auvinen. The complete genome sequence of *Listeria monocytogenes* strain S2542 and expression of selected genes under high-pressure processing. *BMC Genomics*, 14(1), 2021, https://doi.org/10.1186/s13104-021-05555-2.

   Bahareh Nikparvar collected the samples and performed the pressure treatments and viable cell count, and read and edited the manuscript.

3. An original research paper submitted to an international journal.

   Nadav Bar, **Bahareh Nikparvar**, Naresh Doni Jayavelu, and Fabienne Krystin Roessler. Constrained Fourier estimation of time-series gene expression data reduces noise and improves post-processing predictions. Submitted.

   Bahareh Nikparvar implemented the algorithm to RNA-seq data and analyzed the results, wrote, and edited the manuscript.

Chapter 2

Modelling the response of bacterial membrane to high pressure processing

Available online at www.sciencedirect.com

ScienceDirect

IFAC PapersOnLine 52-1 (2019) 243–250

IFAC Papers Online CONFERENCE PAPER ARCHIVE

A Dynamic Model of Membrane Recovery Mechanisms in Bacteria following High Pressure Processing

B. Nikparvar * **A. Subires** ** **M. Capellas** ** **M. Hernandez** ** **N. Bar** *

* *Department of Chemical Engineering, NTNU, Trondheim, Norway (e-mail: bahareh.nikparvar@ntnu.no, nadi.bar@ntnu.no).*
** *Department of Animal and Food Science, UAB, Barcelona, Spain (e-mail: alicia.subires@uab.cat, marta.capellas@uab.cat, manuela.hernandez@uab.cat).*

Abstract: High pressure processing (HPP) in the food industry is considered as an alternative to conventional thermal treatments for inactivation of pathogenic bacteria. However, a major concern in this field is the ability of some pathogens such as *Listeria monocytogenes* to recover pressure-induced damages after HPP even during cold temperature storage. Based on our observation using electron microscopy and flow cytometry techniques, membrane of *Listeria monocytogenes* is one of the main structures in this microorganism which is damaged by pressurization. We quantify this damage by estimating the radius of holes created on the membrane after pressure exposure of 400 [MPa] lasting for 8 and 20 [min]. The flow cytometry result with two fluorescent molecules at different time points after pressurization supports the existence of a recovery process. We propose a novel model consisting of six ordinary differential equations, wired by a feedback regulatory network to investigate the dynamics of hole recovery after HPP. The model is developed based on a hypothesized repair mechanism, similar to the well-established pathways that bacteria activate in response to general types of stress. Simulation results show a nonlinear behaviour of the hole recovery and fitted to the experimental points very well. The maximum estimated hole radius is approximately 0.9 [nm] and 0.7 [nm] for 400 [MPa], 8 [min] and 400 [MPa], 20 [min], respectively. The model provides a valuable tool to estimate the membrane damage and recovery in live bacteria following HPP.

Keywords: High pressure processing, Dynamic model, Feedback, Pathogenic bacteria, Membrane recovery

1. INTRODUCTION

High Pressure Processing (HPP) as a food preservation method is becoming more popular. It not only prolongs the shelf-life of food, but also causes minimum sensory and nutritional side-effects compared to conventional food preservation methods like heating (Farkas and Hoover (2000), Torres and Velazquez (2005), Oey et al. (2008)). To guarantee the elimination of pathogens in ready-to-eat food, the food processing industry exposes the food to pressure values over 600 [MPa]. Applying this amount of pressure is not always profitable due to the operation costs and is only suitable for limited food types. HPP affects different structures in bacteria, such as the cell wall, membrane, intra-cellular protein synthesis and DNA copy and repair pathways. However, the exact mechanisms which affect these structures are not well understood. We are missing quantitative descriptions of the underlying mechanisms triggered by HPP, including repair of structural deformations, models that can help to reduce the effective pressure levels, and inactivate bacteria at pressures as low as 300 [MPa].

Several studies reported that membrane, the barrier which protects the bacteria from outer environment, is affected when exposed to high pressure or high temperature (Pagan and Mackey (2000), Winter and Jeworrek (2009), Kurata et al. (2001)). This stress potentially damages the membrane by creating surface holes. HPP study of Smelt et al. (2006) enforced this hypothesis when the authors observed increased uptake of exogenous fluorescent dyes by a fraction of pressure-treated bacterial cells while untreated cells remained unstained. Tholozan et al. (2000) and Manas and Mackey (2004) observed leakage of ATP and small proteins from cells into extra-cellular medium when the cells were subjected to pressure, which is an indication of membrane damage as well.

Although food-borne bacteria cannot avoid injury during high values of pressure, some authors like Ritz et al. (2001) and Bozoglu et al. (2004) showed evidence that some pathogens such as *Listeria monocytogenes* can repair their damaged membrane after HPP and restart the growth, although the manner these pathogens repair was not explained.

10.1016/j.ifacol.2019.06.069

In general, when bacteria sense adverse conditions, they activate mechanisms to adapt to the changes in the environment. Through the adaptation, the bacteria employ complex feedback regulation systems to alter their gene expression pattern and to encode genes involved in defense mechanism (Wright and Lewis (2007)). Since the cells' ability to increase their resistance against stress is limited, it takes time for the cells to activate the protective system and synthesize elements that can repair damages (Corradini and Pelegt (2009)).

The present knowledge on membrane repair following high pressure stress is scarce and purely qualitative. We wish to quantify the response of bacteria to pressure damage in order to obtain a better understanding of the microbial stress recovery systems, their timely response to high pressure, and the genes that are involved in the recovery mechanisms. However, considering all the mechanisms involved in stress response in one single model is challenging due to the system's complexity and lack of experimental data.

We therefore developed a dynamic model which describes the response of *Listeria monocytogenes* to the membrane damage induced by HPP. To the best of our knowledge, this is the first computational model describing the effect of high pressure stress on the bacterial membrane. We employed flow cytometry techniques to measure the scale of damage and then used this data to estimate several parameters of the model by nonlinear optimization. The remaining parameters were set based on our knowledge. We demonstrated quantitatively the manner the membrane was repaired and estimated the pathogen's recovery time following HPP. This knowledge has practical relevance in the development of antimicrobial treatments in the food preservation industry.

2. MODEL DEVELOPMENT

2.1 Main assumptions

According to our observation using transmission electron microscopy (TEM), we assumed that high pressure creates membrane holes, which cause a defect in membrane integrity by destruction of main membrane components, phospholipids and transmembrane proteins. Figure 1, shows cells in control and pressure-treated samples, observed under TEM.

Being both environmental stresses affecting the cellular membrane, we considered the response of bacteria to high pressure similar to their response to high temperature (Kurata et al. (2001), El-Samad et al. (2003)).

The state space model we present here consists of six states wired by a feedback regulatory network that responds to reseal pressure-induced holes on the membrane of *Listeria monocytogenes*. Our model framework includes a set of nonlinear equations in the following form:

$$\dot{x} = f(x, u, t) \tag{1}$$

where $x \in \mathbb{R}^n$ and $n = 6$. The model we developed relies on protein concentrations and mass balance equations, but since the signaling and enzymatic pathways that activate the repair process are complex and still largely

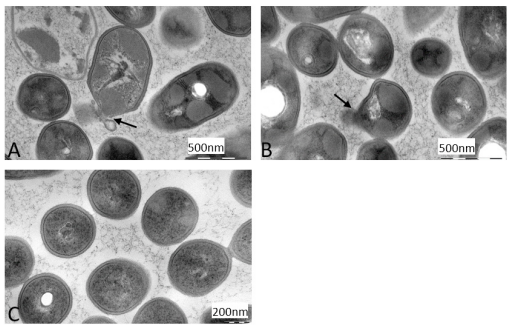

Fig. 1. Transmission electron microscopy (TEM). A, B) Pressure-treated sample, 400 [MPa], 15 [min]. C) Control sample. The arrow shows the location of the hole on the membrane.

unknown, we simplified these mechanisms and assumed a representative for each group of proteins and regulators.

We defined an index between zero and one as membrane integrity state for intact and damaged membrane, shown in Figure 2 by $Memb_d$ and $Memb_{in}$, respectively, such that:

- $Memb_d + Memb_{in} = 1$.
- For a membrane with full integrity: $Memb_{in} = 1$, $Memb_d = 0$.
- For a membrane that has lost its integrity completely: $Memb_{in} = 0$, $Memb_d = 1$.
- For a damaged membrane (intermediate damage): $0 < Memb_{in} < 1$, $0 < Memb_d < 1$.

Based on the proposed mechanisms in literature for response of bacteria to different types of stress and particularly to high temperature (Kurata et al. (2001), El-Samad et al. (2003), Schaik and Abee (2005)), we hypothesized that by sensing high pressure via a signal transduction system, bacteria activate a feedback response to increase the activity of required regulators, change the gene expression pattern, and finally produce proteins which are needed for the repair. A proposed block diagram for this regulatory system is shown in Figure 3.

We considered a feedback loop through two main pathways (Figure 2):

(1) By sensing the stress (the membrane damage induced by HPP), the status of one or a group of proteins changes from an inactive form ($RsbV_i$) to an active form ($RsbV_a$). Although Several proteins may be activated in response to the membrane damage, we chose $RsbV$ as a representative of this group. Sigma factor (Sig_B) which is a regulator molecule, under non-stress condition is bound (and thus inactive) to an anti-sigma factor. When $RsbV$ is activated due to the stress, it can bind to the anti-sigma factor. This leads to the release of Sig_B from its complex with the anti-sigma factor. The freed Sig_B then binds to the promoter region on DNA and initiates encoding of a group of proteins called chaperones, which are involved in the repair process by refolding denatured proteins (Wright and Lewis (2007), Impens et al. (2017)). The refolded proteins play different roles inside the cell and among them

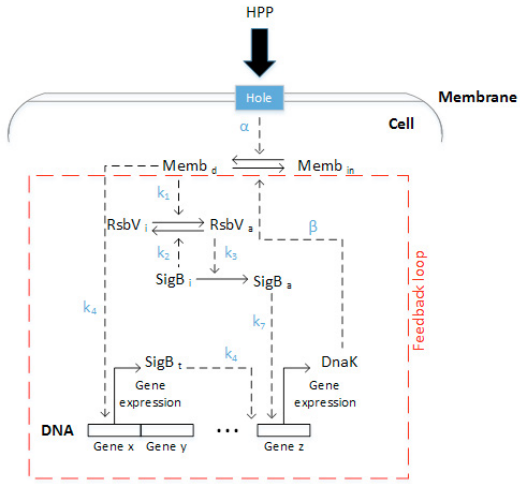

Fig. 2. A schematic of our proposed regulatory pathway for the response of *Listeria monocytogenes* to the membrane damage caused by HPP.

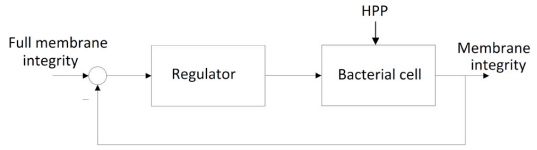

Fig. 3. The proposed Block diagram for the internal regulatory system embedded in bacterial cell to respond to HPP.

is synthesis of membrane components like phospholipids and transmembrane proteins. We considered $DnaK$ as the representative for the chaperones group.

(2) By sensing the membrane damage, a signal is sent to the promoter region on DNA to increase the expression of the gene which produces the regulator molecule ($SigB_t$).

2.2 Model equations

Our model consists of six differential equations describing the response of the bacterial membrane to damage following HPP. We assumed that an intact membrane loses its integrity under HPP and is changed to a damaged membrane (the intact membrane index, $Memb_{in}$, decreases and the damaged membrane index, $Memb_d$, increases). When the pressure is released and returned to its atmospheric value, the damaged membrane is gradually repaired until it regains its full integrity ($Memb_{in}$ increases and $Memb_d$ decreases), therefore:

$$\frac{d[Memb_d]}{dt} = \gamma_1(P)\cdot Memb_{in} - \gamma_2(P,T_h)\cdot Memb_d\cdot[DnaK] \quad (2)$$

, where we assumed that the degree of damage, $\gamma_1(P)$, is a linear function of the pressure strength P, such that $\gamma_1(P) = \alpha \cdot P$. The second parameter, $\gamma_2(P,T_h)$, defines the effect of pressure strength and holding time (T_h, which is the period for pressure exposure) on the membrane recovery rate and was formulated as $\gamma_2(P,T_h) = \frac{\beta}{T_h \cdot P}$. We assumed that the recovery process is inversely proportional to P and T_h. The concentration of chaperons ($[DnaK]$) works as a positive signal for the recovery mechanism.

We modeled the gene expression and the activation-inactivation of the proteins by the Hill and Michaelis-Menten kinetics, respectively (Szallasi et al. (2010)).

It was assumed that by sensing the pressure-induced damage on the membrane, the status of $RsbV$ protein changes from inactive to active form, formulated as the Michaelis-Menten kinetics:

$$\frac{d[RsbV_a]}{dt} = \frac{k_1 \cdot Memb_d \cdot [RsbV_i]}{K_{m1} + [RsbV_i]} - \frac{k_2 \cdot [RsbV_a] \cdot [SigB_i]}{K_{m2} + [RsbV_a]} \quad (3)$$

where $[RsbV_a]$ and $[RsbV_i]$ are the concentration in active and inactive forms, respectively. $k1$ and $k2$ are activation and inactivation rates. The damaged membrane ($Memb_d$) signals the activation of RsbV. K_{m1} and K_{m2} are the Michaelis-Menten constants.

The activated $RsbV$ molecules then alter the status of the regulator (sigma factor) from inactive ($SigB_i$) to active ($SigB_a$) manner by binding to the anti-sigma factor (as explained in 2.1). $RsbV_{occ}$ and $RsbV_f$ represent the active $RsbV$ molecules which have already been occupied with the anti-sigma factor molecules, and the free active $RsbV$ molecules, respectively:

$$\frac{d[RsbV_{occ}]}{dt} = k_3 \cdot [SigB_i] \cdot [RsbV_f] \quad (4)$$

We assumed that $SigB$ is produced with a constant rate k_5 and degraded with a constant rate k_6, proportional to $[SigB_t]$. Here $[SigB_t]$ represents the total concentration of regulator, which is the sum of active regulator concentration and inactive regulator concentration. k_4 is the rate of increase in $SigB$ production resulted from the change in the gene expression pattern under HPP. Signal from the damaged membrane ($Memb_d$) plays the role of an activator for this reaction, which is formulated as the Hill function:

$$\frac{d[SigB_t]}{dt} = \frac{k_4 \cdot (\frac{Memb_d}{K_{m4}})^m}{1 + (\frac{Memb_d}{K_{m4}})^m} + k_5 - k_6 \cdot [SigB_t] \quad (5)$$

where K_{m4} is the Hill parameter, representing the strength of the signal $Memb_d$ when $[SigB_t]$ is at its half maximum. m is the Hill coefficient, affecting the shape of the Hill curve for production of $SigB_t$.

According to (4), the inactive regulator molecules become active by binding to the free $RsbV$ molecules:

$$\frac{d[SigB_i]}{dt} = -k_3.[SigB_i] \cdot [RsbV_f] + k_5 - k_6 \cdot [SigB_i] \quad (6)$$

We formulated $DnaK$ dynamics similar to $SigB_t$. We assumed that $DnaK$ is produced with a constant rate k_8 and degraded with a constant rate k_9, proportional to $[DnaK]$. k_7 is the rate of increase in $DnaK$ production resulted from the change in the gene expression pattern under HPP. The active regulator molecules ($SigB_a$) work as activator signals for this reaction, which is modeled as the Hill function:

$$\frac{d[DnaK]}{dt} = \frac{k_7 \cdot (\frac{[SigB_a]}{K_{m7}})^m}{1 + (\frac{[SigB_a]}{K_{m7}})^m} + k_8 - k_9 \cdot [DnaK] \quad (7)$$

where K_{m7} is the Hill parameter and m is the Hill coefficient.

Mass-balance equations are listed in (8) to (10) and relate the total quantity of a species in the system to its active, inactive, free, and occupied concentration.

$$[RsbV_a] + [RsbV_i] = 1 \quad (8)$$
$$[RsbV_{occ}] + [RsbV_f] = [RsbV_a] \quad (9)$$
$$[SigB_a] + [SigB_i] = [SigB_t] \quad (10)$$

The variables and the parameters of the model and their descriptions are listed in Tables 1 and 2, respectively.

We hypothesized that there is a linear correlation between the rate of hole recovery (i.e. the change in the hole radius R) and the membrane integrity index, such that when the membrane is fully intact ($Memb_{in} = 1$ and $Memb_d = 0$), the hole radius is zero; when the membrane loses its integrity completely ($Memb_{in} = 0$ and $Memb_d = 1$), the hole radius is maximum, therefore:

$$R = \kappa \cdot Memb_d \quad (11)$$

The slope (κ) was calculated by considering two points of the line: ($Memb_d = 0, R = 0$) and ($Memb_d = 1, R = max$).

Table 1. Variables and their descriptions.

Variable	Description
$Memb_d$	Damaged membrane (index between zero and one)
$Memb_{in}$	Intact membrane (index between zero and one)
$[RsbV_a]$	Concentration of active $RsbV$ molecules
$[RsbV_i]$	Concentration of inactive $RsbV$ molecules
$[RsbV_{occ}]$	Concentration of occupied $RsbV$ molecules
$[RsbV_f]$	Concentration of free $RsbV$ molecules
$[SigB_t]$	Total concentration of regulator
$[SigB_a]$	Concentration of regulator in active form
$[SigB_i]$	Concentration of regulator in inactive form
R	Hole radius
P	Pressure value
T_h	Holding time

3. ANALYSIS

3.1 Hole size estimation

The purpose of this section is to explain briefly the method we used to provide experimental data to calibrate the model. The experimental procedure is explained in the Appendix with more details.

The developed model consists of 16 parameters (except for κ) that need to be evaluated. We used nonlinear least square algorithm (Matlab) to estimate four parameters α, β, k_7, and k_9, that we chose based on sensitivity analysis (explained in 3.2). The parameter estimation task was done by fitting the simulation results to the experimental data. To provide the experimental data, we pressurized *Listeria monocytogenes*, strain ScottA (CIP103575) in a high hydrostatic pressure machine (ACB) at 400 [MPa] for 8 or 20 [min] ($T_h = 8$ or 20 [min]) at 8°C. In order to quantify the scale of the membrane damage we employed flow cytometry technique in which the exclusion of fluorescent molecules by cells with intact membrane is employed as a reliable test for membrane integrity (Bowman et al. (2010), Subires et al. (2014)). We hypothesized that the pressure-induced damage appeared as holes with circular areas on the membrane. Using flow cytometry technique, we categorized the cells in a sample into three different populations based on the degree of damage. This led us to a distinctive hole size range (R_1, R_2, R_3) for the cells in each population (more information is provided in the Appendix). Figure 4A shows the percentage of total cells detected in each population immediately (0), 1, 2, 3, 4, and 48 [h] after HPP at 400 [MPa], 8 [min]. Figure 4B provides the percentage of total cells observed in each population immediately, 1, 2, and 24 [h] after pressure treatment at 400 [MPa], 20 [min].

Table 3 summarizes the range of the expected hole size for the cells detected in each population.

As it is shown in Figure 4A, the number of cells in the population 2 (hole size=R_2) decreased gradually during the first four hours after HPP. This could be interpreted as progressing recovery of less damaged cells. However, since the percentage of cells in the population 1 remained approximately constant during the first four hours, we concluded that larger holes needed more time to reseal. Through 24-48 hours recovery, the number of cells in this population decreased drastically. Accordingly, we believe that during 24-48 hours, cells with large holes (the population 1) had enough time to recover the membrane holes relatively, such that the cells in this population transferred to the population 2 (less damaged cells). The increase in the number of cells in the population 2 after 24-48 hours enforced this hypothesis.

Table 2. Parameters, constants, and their descriptions.

Parameter	Description
α	Rate that HPP induced damage on the membrane
β	Rate of memb. recovery
k_1	Rate of $RsbV$ activation
K_{m1}	Michaelis-Menten constant
k_2	Rate of $RsbV$ inactivation
K_{m2}	Michaelis-Menten constant
k_3	Rate of activation for $SigB$ molecules
k_4	Rate of gene exp. for $SigB_t$
K_{m4}	Hill parameter
K_5	Constant production of $SigB_t$
K_6	Rate of constant degradation of $SigB_t$
k_7	Rate of gene exp. for $DnaK$
K_{m7}	Hill parameter
k_8	Constant production of $DnaK$
k_9	Rate of constant degradation of $DnaK$
m	Hill coefficient
κ	Correlation factor between integrity index and R

Table 3. The range of the hole size (R) for each of the three populations.

Population	Hole size range
1	$0.6\ nm \leq R_1 < 1.2\ nm$
2	$0.2\ nm \leq R_2 < 0.6\ nm$
3	$0\ nm \leq R_3 < 0.2\ nm$

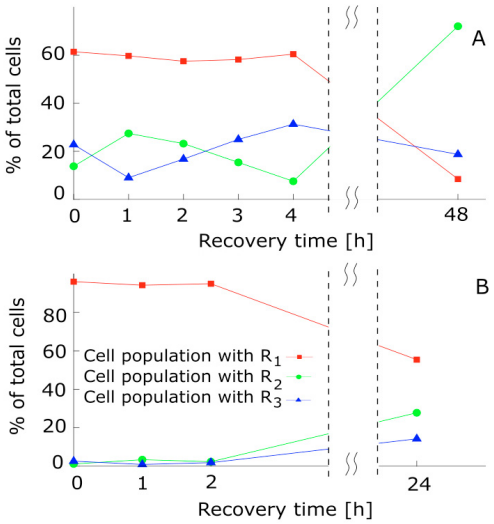

Fig. 4. By investigating the flow cytometry results, we could classify the cells in a sample into three populations based on the hole size range. The figures show the percentage of the total cells detected in each population: A) After HPP at $P = 400$ [MPa], $T_h = 8$ [min], different recovery times. B) After HPP at $P = 400$ [MPa], $T_h = 20$ [min], different recovery times.

Using the information in Table 3, we estimated the average hole size in a pressurized sample at a specific recovery time (Table 4). The estimation method is described in the Appendix (A.2) in details.

Table 4. The estimated radius for the pressure-induced membrane holes at different recovery times.

Recovery time	Estimated radius (400 [MPa], 8 [min])	Estimated radius (400 [MPa], 20 [min])
1 [h]	0.69 [nm]	0.88 [nm]
2 [h]	0.65 [nm]	0.87 [nm]
3 [h]	0.62 [nm]	-
4 [h]	0.61 [nm]	-
24 [h]	-	0.65 [nm]
48 [h]	0.39 [nm]	-

3.2 Parameter estimation

We calculated the membrane integrity index ($Memb_d$) by substituting the resulted value for the hole size in (11) as the experimental data. As stated earlier, we used nonlinear least square algorithm in Matlab to estimate four parameters α, β, k_7, and k_9, chosen by sensitivity analysis explaiend in the following.

Equation (12) was used to determine the sensitivity of the model variable x to perturbations in each parameter (p_i):

$$|S_i| = |\frac{g_{(p_i)} - g_{(p_i + p_i \cdot \Delta p_i)}}{p_i \cdot \Delta p_i}| \qquad (12)$$
$$g = \|x_{sim} - x_{exp}\|$$

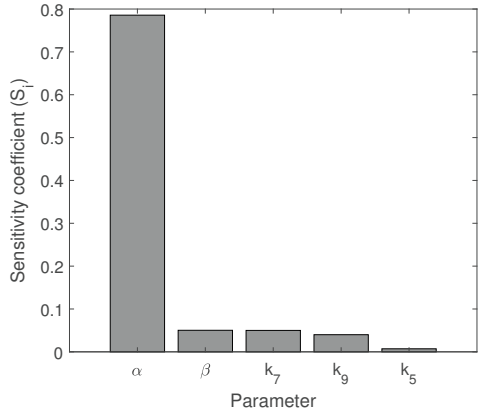

Fig. 5. The integrity index for damaged membrane ($Memb_d$) was highly sensitive to parameter α, the rate of the membrane damage creation resulted from pressure exposure. In the Figure we present the four other parameters that Mem_b was the most sensitive to. Sensitivity to the other parameters was negligible ($|S_i| < 0.005$).

where $|S_i|$ is the sensitivity coefficient, $x_{sim} - x_{exp}$ is the deviation between simulated (x_{sim}) and experimental (x_{exp}) values for the variable, and $\|.\|$ is the Euclidean norm. Figure 5 shows the sensitivity of $x = Memb_d$ (the membrane integrity index) to one percent perturbation ($\Delta p_i = 0.01$) in each parameter. As the sensitivity of this variable to α, β, k_7, and k_9 was higher than its sensitivity to the rest of the parameters, these four parameters were selected to be estimated using nonlinear algorithm in Matlab.

We estimated the remaining parameters based on Monte Carlo simulations, and chose the set which yielded minimum deviation between simulations and experimental results. Despite the scarce experimental data, the estimated parameter values were comparable with values reported for other types of foodborne pathogens. For example, we estimated the degradation rates $k_6 = 0.01$ $[min^{-1}]$ and $k_9 = 0.2$ $[min^{-1}]$, which are in the ranges that Kurata et al. (2001) and El-Samad et al. (2003) reported as degradation rates for proteins in bacteria *E. coli* exposed to heat. The parameter values are listed in Table 5.

3.3 Simulation results

The solid line in Figure 6A and 6B shows the simulated result for the membrane integrity index ($Memb_d$) at $P = 400$ [MPa], $T_h = 8$ [min] and $P = 400$ [MPa], $T_h = 20$ [min], respectively. The experimental points are marked for different recovery times (immediately, 1, 2, 3, 4, 24, and 48 hours after HPP) by circles.

According to the figure, the dynamics during recovery time was non-linear. Despite of non-linearity, the model could reproduce the experimental data quite well.

Figure 7 presents the simulated dynamics for some other variables of the model.

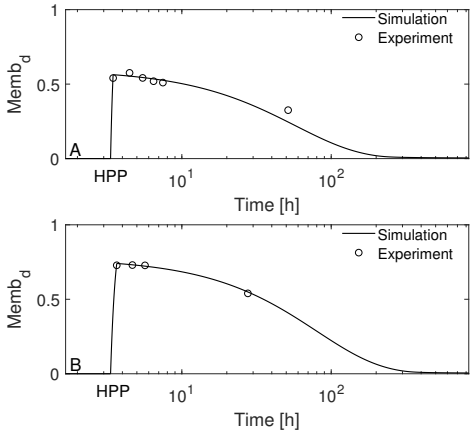

Fig. 6. The simulated dynamics (solid line) for $Memb_d$ at A) $P = 400$ [MPa], $T_h = 8$ [min] and B) $P = 400$ [MPa], $T_h = 20$ [min]. Experimental data is marked with ('o'). The time axis is shown in the logarithmic scale.

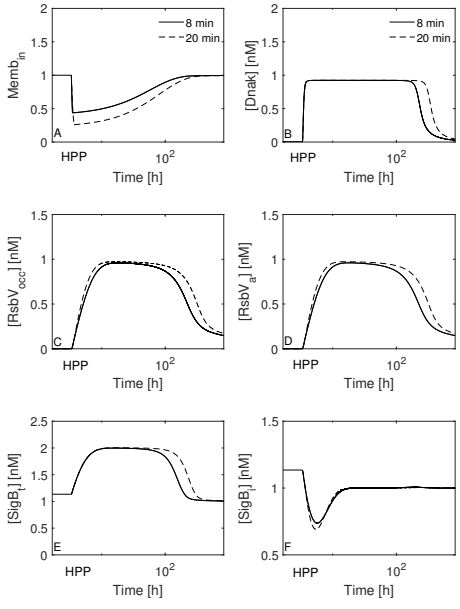

Fig. 7. The simulated dynamics for A) $Memb_{in}$, B) $[DnaK]$, C) $[RsbV_{occ}]$, D) $[RsbV_a]$, E) $[SigB_t]$, and F) $[SigB_i]$ at $P = 400$ [MPa], $T_h = 8$ [min] (solid line) and $P = 400$ [MPa], $T_h = 20$ [min] (dashed line). The time axis is shown in the logarithmic scale.

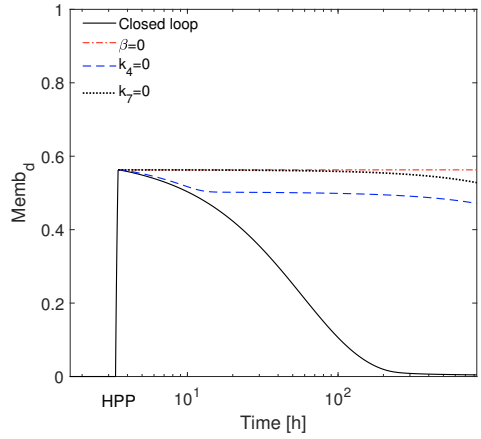

Fig. 8. The dynamics of $Memb_d$ when the feedback loop became open by inserting $\beta = 0$ or $k_4 = 0$ or $k_7 = 0$. The time axis is shown in the logarithmic scale.

In order to analyze the role of the feedback loop parameters in the recovery response, we cut the loop by inserting one single parameter (β or k_4 or k_7) equal to zero each time, while the others were kept at their estimated values (Figure 8). In the case of $\beta = 0$, the membrane remained at its damaged status and the recovery process was not started at all. when $k_4 = 0$, since there was no signal from the membrane to the promoter to increase the production of the regulator molecule $SigB_t$, the recovery was not fulfilled completely, although it was started through the path with k_1-k_3-k_7-β (Figure 2). Inserting $k_7 = 0$, inhibited the recovery procedure to be started after HPP as well. The critical role of the parameter β and k_7 in compare to k_4 is also obvious from Figure 2: By inserting either $\beta = 0$ or $k_7 = 0$, the main feedback loop was open while in the case of $k_4 = 0$, although the path including k_4 was open, the main feedback loop still remained closed through the other path including k_1 and k_3.

Table 5. Parameters and constants values.

Parameter/Constant	Value
α	$(2.58^*, 1.69^{**})10^{-4}$ $[min^{-1} \cdot MPa^{-1}]$
β	1^*, 1.8^{**} $[MPa \cdot nM^{-1}]$
k_1	0.07 $[nM \cdot min^{-1}]$
K_{m1}	5 $[nM]$
k_2	0.001 $[min^{-1}]$
K_{m2}	3 $[nM]$
k_3	2 $[nM^{-1} \cdot min^{-1}]$
k_4	0.01 $[nM \cdot min^{-1}]$
K_{m4}	0.05
K_5	0.01 $[nM \cdot min^{-1}]$
K_6	0.01 $[min^{-1}]$
k_7	0.18 $[nM \cdot min^{-1}]$
K_{m7}	0.05 $[nM]$
k_8	0.001 $[nM \cdot min^{-1}]$
k_9	0.2 $[min^{-1}]$
m	2
κ	1.2 $[nm]$

* 400 [MPa], 8 [min]
** 400 [MPa], 20 [min]

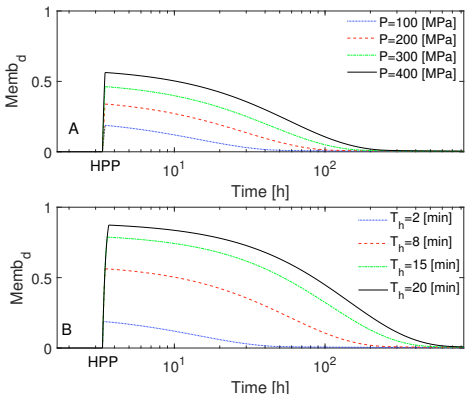

Fig. 9. The simulated result for $Memb_d$ dynamics in A) different P values, $T_h = 8$ [min] and B) different T_h values, $P = 400$ [MPa]. The time axis is shown in the logarithmic scale.

To investigate the effect of the pressure and holding time values on the maximum damage and rate of membrane recovery, we simulated incremental changes of these two factors (Figure 9). The results suggested that both pressure and time values had impact on the maximum value of $Memb_d$, and consequently on the maximum estimated hole radius. The rate of recovery was slower for longer holding times as seen in Figure 9B.

4. DISCUSSION

The main objective of this study was to develop a quantitative model for the response of foodborne pathogens to the membrane damage induced by HPP. Unlike other types of stressful conditions (e.g. high temperature), we still lack knowledge about the response of bacteria to high pressure, its impact on the cellular membrane, and the mechanisms that regulate the repair process.

The model consisted of a set of ODEs with six states and 17 parameters which determined the dynamics of the hole recovery after HPP. We estimated several critical parameters of the model by fitting the simulated data to the result from experiments we designed. Due to the limited measurement data and nonlinear dynamics, the parameter estimation task was challenging. At this moment we had a few experimental points only for one of our model variables ($Memb_d$). Therefore, we chose to estimate with optimal least square method only the most important parameters (α, β, k_7, and k_9, described in Figure 2 and Table 2) based on sensitivity analysis. The remaining parameters were fixed by values based on literature and our knowledge.

As it is stated in the literature, in the case of HPP, the degree of bacterial inactivation depends on the pressure level (P) and holding time (T_h). We considered both factors as variables in our model. We estimated the parameters of the model for two pressure treatments both taken at $P = 400$ [MPa] but for different holding times $T_h = 8$ min and $T_h = 20$ min. Except for the two parameters α (The rate that HPP induced damage on the membrane) and β (rate of membrane recovery), the obtained values for the remaining parameters were independent of the holding time T_h. The dependency of α and β to T_h led us to conclude that the impact of holding time, which has usually been underestimated by the industry in compare to the effect of the pressure strength (P), is determining in efficiency of high pressure treatment. Our simple model requires an extension with the two functions γ_1 and γ_2 in (2) to include the effect of T_h in greater details.

Regarding our results, the average hole size was approximately 0.7 [nm] and 0.9 [nm] immediately after HPP at $P = 400$ [MPa], $T_h = 8$ [min] and $P = 400$ [MPa], $T_h = 20$ [min], respectively. The hole radius decreased with a characteristic half-life of 37 hours and 52 hours after HPP at $P = 400$ [MPa], $T_h = 8$ [min] and $P = 400$ [MPa], $T_h = 20$ [min], respectively. Importantly, the calculated recovery time was comparable with the period Bozoglu et al. (2004) mentioned as the time that bacteria needed to restart growth after pressurization, indicating that the model had a good prediction ability despite the low number of measurements.

Simulation results showed a non-linear behaviour for the hole recovery dynamics and was fitted to the experimental points well (Figure 6). The proposed simplified model for the membrane repair showed that the regulation response is achieved by a network of interactions among diverse types of molecules such as proteins, regulators, and DNA through a feedback loop. In our model, the feedback closed loop response resulted in a full recovery process. In order to compare the significance of the parameters in the feedback loop for the membrane recovery, we analyzed the model under zero kinetics (loop rate constants were set to zero). The simulated results (Figure 8) suggested that the parameters β and k_7 play key roles in the feedback loop. This information may guide the industry to find target components inside the cell to be attacked by using additives in conjunction with HPP to increase the efficiency of the pressure treatment.

ACKNOWLEDGEMENTS

The SAFEFOOD project is supported by the Norwegian Research Council grant number 263499, under the European ERA Industrial Biotechnology (IB2) Program. We would like to thank N.E. Skogaker for technical assistance in transmission electron microscopy that performed at the Cellular and Molecular Imaging Core Facility (CMIC), Norwegian University of Science and Technology (NTNU).

REFERENCES

Bowman, A., Nesin, O., Pakhomova, O., and Pakhomov, A. (2010). Analysis of plasma membrane integrity by fluorescent detection of $thallium^+$ uptake. *J. Membrane Biol.*, 236, 15–26.

Bozoglu, F., Alpas, H., and Kaletunc, G. (2004). Injury recovery of food-borne pathogens in high hydrostatic pressure treated milk during storage. *FEMS Immunol. and Med. Microb.*, 40, 243–247.

Corradini, M. and Pelegt, M. (2009). Dynamic model of heat inactivation kinetics for bacterial adaptation. *Appl. and Environ. Microb.*, 75, 2590–2597.

El-Samad, H., Khammash, M., and Doyle, J. (2003). Feedback regulation of the heat shock response in *E. coli*. *Multidisciplinary Research in Control*, 289, 115–128.

Farkas, D. and Hoover, D. (2000). High pressure processing. *J. of Food Sci.*, 65, 47–64.

Impens, F., Rolhion, N., Redoshevich, L., Becavin, C., Duval, M., Mellin, J., Portillo, F., Pucciarelli, M., Williams, A.H., and Cossart, P. (2017). N-terminomics identifies prli42 as a membrane miniprotein conserved in firmicutes and critical for stressosome activation in *Listeria monocytogenes*. *Nat. Microbiol.*, 2:17005.

Kurata, H., El-Samad, H., Yi, T., Khammash, M., and Doyle, J. (2001). Feedback regulation of the heat shock response in *E. coli*. *Proceedings of the 40th IEEE, conference on Decision and Control*, Orlando, Florida, USA, 837–842.

Manas, P. and Mackey, B. (2004). Morphological and physiological changes induced by high hydrostatic pressure in exponential- and stationary-phase cells of *Escherichia coli*: Relationship with cell death. *Appl. and Environ. Microb.*, 70, 1545–1554.

Oey, I., Plancken, I., Loey, A., and Hendrickx, M. (2008). Does high pressure processing influence nutritional aspects of plant based food systems? *Trends in Food Sci. and Tech.*, 19, 300–308.

Pagan, R. and Mackey, B. (2000). Relationship between membrane damage and cell death in pressure-treated *Escherichia coli* cells: Differences between exponential- and stationary-phase cells and variation among strains. *Appl. and Environ. Microb.*, 66, 2829–2834.

Ritz, M., Tholozan, J., Federighi, M., and Pilet, M. (2001). Morphological and physiological characterization of *Listeria monocytogenes* subjected to high hydrostatic pressure. *Appl. and Environ. Microb.*, 67, 2240–2247.

Schaik, W. and Abee, T. (2005). The role of σ^B in the stress response of gram-positive bacteria – targets for food preservation and safety. *Current Opinion in Biotechnology*, 16, 218–224.

Smelt, J., Rijke, A., and Hayhurst, A. (2006). Possible mechanism of high pressure inactivation of microorganisms. *J. of High Pressure Research*, 12, 199–203.

Subires, A., Yuste, J., and Capellas, M. (2014). Flow cytometry immunodetection and membrane integrity assessment of *Escherichia coli* o157:h7 in ready-to-eat pasta salad during refrigerated storage. *International J. of Food Mic.*, 168, 37–56.

Szallasi, Z., Stelling, J., and Periwal, V. (eds.) (2010). *System Modelling in Cellular Biology*. The MIT Press (February 26, 2010).

Tholozan, J., Ritz, M., Jugiau, F., Federighi, M., and Tissier, J. (2000). Physiological effects of high hydrostatic pressure treatments on *Listeria monocytogenes* and *Salmonella typhimurium*. *J. of Appl. Microb.*, 88, 202–212.

Torres, J. and Velazquez, G. (2005). Commercial opportunities and research challenges in the high pressure processing of foods. *J. of Food Eng.*, 67, 95–112.

Winter, R. and Jeworrek, C. (2009). Effect of pressure on membrane. *The Royal Soc. of Chem.*, 5, 3157–3173.

Wright, J. and Lewis, R. (2007). Stress responses of bacteria. *Current Opinion in structural Biology*, 17, 755–760.

Appendix A. APPENDIX

A.1 Details of Experimental Method

Flow cytometry technique: We measured the intensity of fluorescent dye cell by cell in a sample and used the intensity value to determine the scale of the membrane defect. The flow cytometry device we used could measure the fluorescent intensity for each cell at a high frequency (over 40000 cells in approximately 20 seconds). Two different fluorescent molecules, propidium iodide (PI) and FluxOR II-thallium (FluxOR II-Tl) that have different molecular sizes, were used to estimate the size of the holes in damaged cells (PI radius $\approx$ 0.6 nm and Tl radius $\approx$ 0.2 nm, Bowman et al. (2010)). Both molecules can only penetrate the cells with damaged membrane. The dye molecules of PI emit red (630 nm) fluorescence and the molecules of FluxOR II-Tl emit green (525 nm) fluorescence. Based on the detected color for each cell, we could categorize the cells in a sample into highly damaged (red), less damaged (green), and intact cells (unstained). The fraction of cells belonged to each population calculated as a percentage value and shown in Figure 4.

We hypothesized that the largest hole size in a sample was twice the size of the PI molecule (1.2 [nm]). Accordingly, cells emitting red fluorescence (Population 1) might have hole sizes in the range $R_{PI} \leq R < 2R_{PI}$ (R_{PI}: radius of PI). Table A.1 summarizes the range of the expected hole size for the cells detected in each population.

Table A.1. Population information

Population	fluorescence color	Hole size
1	Red cells	$R_{PI} \leq R < 2R_{PI}$
2	Green cells	$R_{Tl} \leq R < R_{PI}$
3	Unstained cells	$0 \leq R < R_{Tl}$

A.2 Hole size estimation

To estimate the average hole size at each recovery time, we assigned a random number with a normal distribution as the hole radius R to each cell. This random number for the cells in each population followed the range mentioned in the third column of Table A.1. Normal distribution was chosen since the histogram of intensity for both red and green fluorescence in each quadrant showed approximately a normal distribution (data not shown). By calculating the mean value of assigned numbers for all cells in a sample (three populations), we got a number which was interpreted as the average value for R at a specific recovery time (Table 4).

frontiers in Microbiology

ORIGINAL RESEARCH
published: 13 May 2021
doi: 10.3389/fmicb.2021.598739

A Diffusion Model to Quantify Membrane Repair Process in *Listeria monocytogenes* Exposed to High Pressure Processing Based on Fluorescence Microscopy Data

*Bahareh Nikparvar[1], Alicia Subires[2], Marta Capellas[2], Manuela Hernandez-Herrero[2], Peter Crauwels[3], Christian U. Riedel[3] and Nadav Bar[1]**

[1] Department of Chemical Engineering, Norwegian University of Science and Technology, Trondheim, Norway, [2] Department of Animal and Food Science, Autonomous University of Barcelona, Barcelona, Spain, [3] Department of Biology, Institute of Microbiology and Biotechnology, Ulm University, Ulm, Germany

OPEN ACCESS

Edited by:
Teresa Zotta,
University of Basilicata, Italy

Reviewed by:
Hui Li,
Chinese Academy of Agricultural Sciences, China
Jose A. Egea,
Spanish National Research Council, Spain
Didier Cabanes,
University of Porto, Portugal

***Correspondence:**
Nadav Bar
nadi.bar@ntnu.no

Specialty section:
This article was submitted to Food Microbiology, a section of the journal Frontiers in Microbiology

Received: 25 August 2021
Accepted: 12 April 2021
Published: 13 May 2021

Citation:
Nikparvar B, Subires A, Capellas M, Hernandez-Herrero M, Crauwels P, Riedel CU and Bar N (2021) A Diffusion Model to Quantify Membrane Repair Process in Listeria monocytogenes Exposed to High Pressure Processing Based on Fluorescence Microscopy Data. Front. Microbiol. 12:598739. doi: 10.3389/fmicb.2021.598739

The effects of environmental stresses on microorganisms have been well-studied, and cellular responses to stresses such as heat, cold, acids, and salts have been extensively discussed. Although high pressure processing (HPP) is becoming more popular as a preservation method in the food industry, the characteristics of the cellular damage caused by high pressure are unclear, and the microbial response to this stress has not yet been well-explored. We exposed the pathogen *Listeria monocytogenes* to HPP (400 MPa, 8 min, 8°C) and found that the high pressure created plasma membrane pores. Using a common staining technique involving propidium iodide (PI) combined with high-frequency fluorescence microscopy, we monitored the rate of diffusion of PI molecules into hundreds of bacterial cells through these pores on days 0, 1, 2, 3, and 4 after pressurization. We also developed a mathematical dynamic model based on mass transfer and passive diffusion laws, calibrated using our microscopy experiments, to evaluate the response of bacteria to HPP. We found that the rate of diffusion of PI into the cells decreased over the 4 consecutive days after exposure to HPP, indicating repair of the pressure-created membrane pores. The model suggested a temporal change in the size of pores until closure. To the best of our knowledge, this is the first time that pressure-created membrane pores have been quantitatively described and shown to diminish with time. In addition, we found that the membrane repair rate in response to HPP was linear, and growth was temporarily arrested at the population level during the repair period. These results support the existence of a progressive repair process in some of the cells that take up PI, which can therefore be considered as being sub-lethally injured rather than dead. Hence, we showed that a subgroup of bacteria survived HPP and actively repaired their membrane pores.

Keywords: high pressure processing, *Listeria monocytogenes*, mathematical modeling, membrane damage, repair process, fluorescence microscopy

1. INTRODUCTION

Bacteria in nature are exposed to various environmental stresses, including changes in temperature or pH, radiation, antimicrobial compounds, and osmotic pressure. Pressurization of bacteria that normally grow in atmospheric conditions may trigger response mechanisms that enable them to adapt to the new pressure condition and survive. Although the cell envelope and particularly the membrane structure have been reported to be susceptible to high pressure processing (HPP) (Pagán and Mackey, 2000; Winter and Jeworrek, 2009; Gänzle and Liu, 2015), the mechanisms that bacteria activate as a response to this stress are still largely unknown. Moreover, the potential existence of a membrane repair machinery in bacteria that responds to pressure-induced damage has not been well-investigated. This phenomenon is of particular importance in the food industry, where exposure to HPP is used as a preservation method to inactivate foodborne bacteria.

Release of low-molecular-weight metabolites, including nucleotides, amino acids, and inorganic ions, from bacterial cells exposed to different types of stress such as antibiotics or bacteriocins has been proposed as an indicator of membrane damage (Lambert and Hammond, 1973; Gilbert et al., 1977; Broxton et al., 1983; Zhen et al., 2013; Singh et al., 2016). Two decades ago, high pressure stress had already been shown to cause deformation of the cell membrane and create surface pores (Ritz et al., 2001). Several authors demonstrated increased uptake of exogenous fluorescent molecules by pressurized cells. For example, membrane damage in *Lactobacillus plantarum* exposed to high pressure was shown by staining cells with the fluorescent dye propidium iodide (PI) (Smelt et al., 1994). In the same work, leakage of ATP from these cells was observed, indicating a leaky membrane (Smelt et al., 1994). Gänzle and Vogel (2001) showed changes in the kinetics of outer and cytoplasmic membrane permeability in *Escherichia (E.) coli* after exposure to high pressure (300, 500, 600 MPa) by staining of treated cells with PI and 1-N-phenylnaphthylamine. Furthermore, a few studies have detected cellular proteins outside the cell after exposure to high pressure (Smelt et al., 1994; Gänzle and Vogel, 2001; Mañas and Mackey, 2004). One such example is the study of Mañas and Mackey (2004), which detected intracellular proteins outside pressure-treated *E. coli* cells (200 MPa, 8 min), indicating membrane leakage.

Several previous experiments showed that pressure-mediated damage in bacteria could be repairable such that the cells could potentially grow after repair of the site of injury during storage (Bozoglu et al., 2004; Jofré et al., 2010; Klotz et al., 2010). Bozoglu et al. (2004) observed no colony formation in selective or non-selective agar immediately after pressure treatment at 550 MPa, suggesting that all cells were inactivated. However, they detected growth in both selective and non-selective agar after 6 days at 4°C, and after 1 day at 22 and 30°C, probably due to a recovery process. Jofré et al. (2010) reported that even after a high pressure treatment of 900 MPa, some *Listeria (L.) monocytogenes* cells remained viable and were able to recover at 14°C. Klotz et al. (2010) examined the susceptibility of cell membranes in *E. coli* to pressure-induced damage (500, 600, and 700 MPa) and found that in a pressure-resistant strain, uptake of PI occurred only during exposure but not after pressure release, indicating that the cells were able to reseal their leaky membranes. This again supports the hypothesis of the presence of a recovery process in sub-lethally injured cells, and adds to the evidence in the literature that, in contrast to what has been traditionally assumed, cells that take up PI are not always dead (Shi et al., 2007; Davey and Hexley, 2011; Subires et al., 2013; Yang et al., 2015).

Several authors have proposed simple models to describe inactivation of pressure-treated bacteria and their growth behaviors (Koseki et al., 2007; Bover-Cid et al., 2010; Hereu et al., 2014; Valdramidis et al., 2015; Rubio et al., 2018). However, although a few of these studies reported the existence of a repair process, they did not identify the underlying mechanisms that allow bacteria to recover.

Here, we focused on foodborne pathogenic bacteria *L. monocytogenes* and the effects of HPP (400 MPa, 8 min, 8°C) on its membrane. We developed a dynamic model that could estimate pressure-induced membrane damage over time.

Our predictions and findings suggest that sub-lethally injured pressurized cells were able to repair their membranes by resealing the surface pores after decompression. To the best of our knowledge, this is the first time that the repair of membrane pores following HPP has been shown in bacteria.The estimated time required for resealing the pore area could be useful for the food industry to adjust the high pressure strategy applied (particularly by adjusting the pressure strength and holding time) to design a more effective food preservation process.

2. MATERIALS AND METHODS

2.1. Experiments

2.1.1. Bacterial Strain and Culture Conditions

The *L. monocytogenes* Scott A strain used in this study was provided by the Collection of Institut Pasteur (CIP 103575; Paris, France) and selected based on its increased high pressure resistance and widespread use as a reference strain in food preservation technology testing (Alpas et al., 1999; Briers et al., 2011; Duru et al., 2020). Stock cultures grown in tryptone soya broth supplemented with 0.6% w/v yeast extract (TSBYE; Oxoid/ThermoFisher Scientific, Hampshire, UK) were stored at −80°C in glycerol (33% v/v). A loopful of the glycerol stock was inoculated into 20 mL TSBYE and incubated at 37°C overnight in a shaking (80 rpm) water bath. To prepare working cultures in the early stationary phase, the overnight culture was diluted to 1:100 in 20 mL of fresh TSBYE and incubated under the same conditions for 18 h. The time to reach this growth phase was established by monitoring the optical density at 600 nm (Bioscreen C; Oy Growth Curves AB, Helsinki, Finland) in a separate experiment.

Abbreviations: *E. coli*, *Escherichia coli*; FI, Fluorescence intensity; HPP, High pressure processing; *L. monocytogenes*, *Listeria monocytogenes*; LOD, Limit of detection; LOQ, Limit of quantification; PI, Propidium iodide.

2.1.2. High Pressure Processing (HPP)

Early stationary phase cultures were transferred to 30-mL HDPE bottles with screw caps (BNH0030PN, SciLabware Limited, Stoke-on-Trent, UK), avoiding the presence of air bubbles. Bottles had previously been sterilized with a 70% v/v ethanol solution overnight, rinsed three times with sterile distilled water, and dried at 60°C in an incubator. The possible presence of ethanol residues after this procedure was ruled out, as growth of untreated samples was not reduced (data not shown). To prevent hazardous culture spills, caps were sealed with laboratory film, and bottles were vacuum packed in sterile plastic bags. Samples were then cooled to 8°C in ice before HPP (approximately 30 min).

HPP was performed in a discontinuous isostatic press (Alstom ACB, Nantes, France) fitted with a 2-L pressure chamber containing water. The temperature of the pressure chamber and transmission fluid was adjusted to the treatment temperature (8°C) using an external continuous cooling system. The samples were then placed inside the chamber, allowed to re-equilibrate to 8°C for 5 min, and pressurized at 400 MPa for 8 min. The temperature was selected according to the common HPP conducted in the industry (Muntean et al., 2016). The come-up time and the decompression time were both 2 min. Pressurized samples were kept in ice before being further processed for fluorescence microscopy analysis, and then stored at 8°C for the subsequent days of analysis. The storage temperature was selected to simulate the temperature deviations that occur in the cold chain/storage of refrigerated food products, i.e., abuse temperature (Alvarez-Ordóñez et al., 2015).

2.1.3. Cell Preparation and Fluorescence Microscopy Analysis

Pressure-treated cells were pelleted (13,000 g, 1 min) and resuspended in Dulbecco's phosphate-buffered saline (DPBS, pH 7.4) immediately before microscopy analysis at 1 h (day 0), and on days 1, 2, 3, and 4 post-treatment. Sixty microliters of this cell suspension was pipetted into the center of a glass-bottomed microwell plate (35 mm petri dish, 14 mm microwell, coverglass No. 1.5; MatTek Corporation, Ashland, USA). To immobilize cells and provide a stationary frame for real-time imaging, 200 μL of a 2% w/v low-gelling-temperature agarose (Sigma-Aldrich, Saint Louis, USA) solution was carefully dispensed over the cell suspension drop, first surrounding and then covering it. Approximately 2 mL of a staining solution containing 1.25 μM PI (final concentration; 20 mM stock solution in DMSO, Life Technologies/ThermoFisher Scientific, Darmstadt, Germany) in DPBS was carefully dispensed over the cell suspension and agarose mixture during real-time imaging. The delivery system consisted of a syringe coupled to a plastic tube that was in turn attached to a holed plate lid. Untreated and heat-treated (80°C for 40 min) cell suspensions were prepared as described above and used as a negative and a positive control for PI staining, respectively.

Time-lapse image acquisition was performed with a Leica TCS SP5 (Leica Microsystems, Wetzlar, Germany) confocal microscope using a 63x oil objective (NA 1.4), filters for PI detection (excitation at 575–625 nm; emission at 660–710 nm), and a hybrid detector. For each sample and field, images were captured for 30 min at 1 frame per second (fps). The maximum achievable fluorescence intensity (FI) was obtained from the heat-treated sample, which was used every day as the reference to set the microscope gain parameter.

2.1.4. Culture-Based Cell Counting

The number of viable *L. monocytogenes* cells was determined by the spread plate count method before exposure to HPP (untreated) and on days 0, 1, 2, 3, and 7 after the treatment (400 MPa, 8 min, 8 °C). Samples were serially diluted at the designated time points in peptone saline solution (1 g/L neutralized bacteriological peptone [Oxoid/ThermoFisher Scientific] and 8.5 g/L NaCl in water). Appropriate dilutions were spiral-plated (Eddy Jet; IUL, Barcelona, Spain) on the non-selective medium tryptone soya agar supplemented with 0.6% (w/v) yeast extract (Oxoid/ThermoFisher Scientific). Plates were then incubated at 37°C for 48 h before colony counting. The limit of detection (LOD) and the limit of quantification (LOQ) (i.e., the lower limit of acceptably accurate cell counts) of this method were 1.00 and 2.40 log CFU/mL, respectively.

2.2. Post-processing of Microscopy Data

We used Fiji software, RRID:_SCR_002285 (an image-processing package based on ImageJ), RRID:_SCR_003070, and MATLAB, RRID:_SCR_001622 to derive the mean red FI value for each cell in every single frame of the image stacks (images were captured for 30 min at 1 fps as described above). On each consecutive day, we monitored several fields of view (FOV) such that the total numbers of PI-positive cells (n) studied on days 0–4 were 118, 49, 21, 44, and 27, respectively. We analyzed a total of 318 bacteria in 30 FOV during the 4 days. The lowest and the average number of bacteria analyzed per day were 20 and 45 cells, respectively. We monitored on average 3 FOV per day and 10 bacteria per FOV.

One reason that the cell number was different on different days was that cells at the edges or those with improper orientation for image processing were ignored. Another reason could have been a reduction in the number of red cells (cells with PI molecules inside) over the 4 days.

The FI curves for each day were grouped into separate clusters based on the rate of PI diffusion into the cell, as the treated sample was not homogeneous in terms of pressure-induced damage. This was because cells might react differently to high pressure; therefore, differences in the degree of damage and ability to repair would lead to differences in the rate of change of FI and in the rate of PI diffusion through pores. We used the k-means algorithm to cluster the FI curves, where the optimal number of clusters (k) was determined using the elbow method (Kassambara, 2017). The procedure was as the following: First, we considered the last point of each intensity curve (i.e., FI value at $t = 30$ min) to create a database for each day. Then we used MATLAB, RRID:_SCR_001622 to run the k-means algorithm for different numbers of clusters of the database for each day: $k = 1, , 2, ..., 10$. For each k, we calculated the sum of the squared distance (SSE) between the centroid of a cluster and each member of that cluster. We looked at the SSE as a function of the number of clusters and chose a number of clusters so that adding another cluster did not

improve much better the SSE. The mean and standard deviation of the FI for each cluster of cells were calculated separately for each time point.

To normalize the FI values and therefore make them comparable over the 4 days, on each consecutive day we divided the values obtained from the pressure-treated sample by the maximum intensity value achieved from the positive control sample on that day. This normalized FI value was then used to estimate the pore size.

2.3. Statistical Analysis

We used MATLAB, RRID:_SCR_001622 to run analysis of variance (one-way ANOVA) and multi-comparison tests to investigate whether the estimated radius for the pore size on each day significantly differed from the values estimated for the other days. In the multi-comparison analysis, two clusters with specific mean values were considered to be significantly different if their intervals were disjoint, and not significantly different if their intervals overlapped. We used the Bonferroni method to calculate the intervals.

Additionally, We ran the Bartlett test of the null hypothesis that the estimated radius over the 4 days comes from normal distributions with the same variance.

We fitted a weighted least square model (regression model) to the estimated pore values on each day where weights were determined according to the number of cells monitored each day. We used MATLAB, RRID:_SCR_001622 command "fitnlm" to fit our linear regression model ($y = ax + b$, where a and b are the fitting parameters) to the estimated values.

2.4. A Computational Model to Describe Membrane Recovery

We developed a modified version of the model that Zarnitsyn et al. (2008) proposed for the transmembrane diffusion of small molecules through membrane wounds in human cells after sonication. Our proposed model was constructed based on several assumptions.

First, as stated in the literature (Pagán and Mackey, 2000; Winter and Jeworrek, 2009; Gänzle and Liu, 2015) and evidenced by our previous work using flow cytometry (Nikparvar et al., 2019), the bacterial membrane is one of the main structures in the cell that is damaged by HPP. We investigated the morphology of the bacterial membrane after exposure to high pressure using transmission electron microscopy (TEM) and found that the membrane was damaged and became perforated under pressure (**Figures 1A–D**). We assumed that the main damage occurred in a single pore area. This assumption is valid for our model, because the estimated pore area in our work could be interpreted as an effective area (or total area) regardless of the number of pores. It is mathematically possible to estimate the number of large pores by dividing the effective pore area by the size of the reference molecule (PI), which led us again to one large pore area (for all 4 consecutive days). A schematic geometry for the described membrane pore is shown in **Figure 1E**.

Second, the membrane, which is otherwise impermeable to fluorescent molecules such as PI, allows the diffusion of these molecules within the pressure-induced membrane pore,

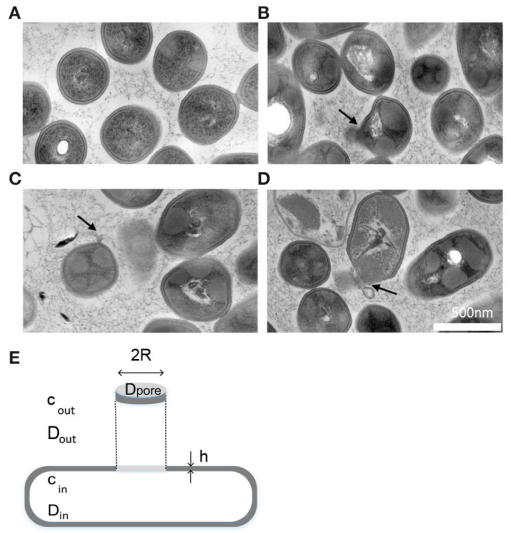

FIGURE 1 | Morphology of pressure-treated cells. **(A–D)** TEM images showed that HPP could create membrane pores (Nikparvar et al., 2019). **(A)** Untreated sample, **(B–D)** Pressure-treated sample, 400 MPa, 15 min. The black arrows show the location of the pore area on the membrane. **(E)** A schematic model showing the morphology of a created membrane pore area under high pressure. The geometry of the bacterium and its plasma membrane with thickness h is simplified as a rod shape. c_{in} and c_{out} are the concentration of fluorescent molecules inside and outside the cell, respectively, and D_{in}, D_{out}, and D_{pore} are the diffusion coefficient of the fluorescent molecules inside, outside, and within the pore area, respectively. Symbols are defined in **Table 1**.

provided the size of the pore area is greater than the size of the molecules. We assumed that the mechanism responsible for the movement of PI molecules was diffusion caused by random molecular motion. The rate of PI diffusion into the cell depends on the size of the pore area; therefore, it is possible to estimate the pore size by measuring the difference in FI resulting from the increased number of PI molecules bound to DNA. Based on the mass balance of PI molecules, we can write:

$$V_{cell}\frac{dc_{in}}{dt} = A_{pore}k(c_{out}(t) - c_{in}(t)), \quad (1)$$

where V_{cell} is the cell volume (m^3); c_{in} and c_{out} are the intracellular and extracellular concentration of PI molecules (mol/m^3), respectively; t is time (s); A_{pore} is the pore area (m^2); and k is the mass transfer coefficient (1/s), which is independent of the pore area and the cell volume but varies with the diffusion coefficient, D (m^2/s), of PI molecules. The expressions on the left and right sides of the equation above (with the unit mol/s) represent the accumulation of PI molecules inside the cell and the rate of the transport into the cell through the pore, J (mol/s), respectively. If we assume that PI molecules were added to the

sample at $t = 0$, $c_{in}(t = 0) = 0$, and $c_{out}(t = 0)$ changes from 0 to $c_{out_{ss}}$, solving Equation (1) gives:

$$c_{in}(t) = c_{out_{ss}}(1 - exp(-Kt)), \tag{2}$$

where $K = \frac{Ak}{V_{cell}}$. Here, we assume that A_{pore}, k, and V_{cell} are constant during the integrating time, i.e., the period between adding PI molecules to the sample and the time when the FI is saturated (saturation occurred when the intracellular concentration of PI molecules reached the concentration level outside, i.e., $c_{in} = c_{out_{ss}}$).

According to Equation (2) and by measuring c_{in} experimentally at time t, the quantity K can be calculated:

$$K = \frac{1}{t} \ln\left(\frac{1}{1 - \frac{I(t)}{I_{max}}}\right), \tag{3}$$

where assuming that the relationship between the concentration of fluorescent molecules and the FI is linear (Kim et al., 2020), we have $\frac{c_{in}(t)}{c_{out_{ss}}} = \frac{I(t)}{I_{max}}$ ($I(t)$ and I_{max} are the intensity at time t and maximum intensity, respectively).

Third, as discussed previously by Zarnitsyn et al. (2008), we considered a three-part process for the diffusion of PI molecules into a cell: diffusion from the extracellular point to the pore; diffusion across the cell membrane within the pore; and diffusion away from the pore in the cytosol. The flow J (mol/s) is given by:

$$J = \frac{c_{out} - c_{in}}{\frac{h}{D_{pore}A_{pore}} + \frac{1}{4D_{out}R} + \frac{1}{4D_{in}R}}, \tag{4}$$

where h is the membrane thickness; R represents the pore radius; and D_{pore}, D_{out}, and D_{in} are the diffusion coefficients of PI molecules inside the pore, outside the cell, and inside the cell, respectively. Symbols are defined in **Table 1**.

By substituting $A_{pore} = \pi R^2$ (where R is the pore radius), K can be expressed as a function of D and R:

$$K = \frac{1}{V_{cell}\left(\frac{h}{D_{pore}\pi R^2} + \frac{1}{4D_{out}R} + \frac{1}{4D_{in}R}\right)}. \tag{5}$$

As mentioned earlier, we immobilized the cells in agarose gel; therefore, the extracellular diffusion coefficient (D_{out}) was the rate of the diffusion for PI molecules in agarose gel (D_g) and equal to σD_w, where D_w is the diffusion coefficient in aqueous solution (**Table 2**). σ was taken from the literature (Pluen et al., 1999):

$$\sigma = 1 - 2.1444(R_a/R_g) + 2.08877(R_a/R_g)^3 - 0.94813(R_a/R_g)^5 - 1.372(R_a/R_g)^6 + 3.87(R_a/R_g)^8 - 4.19(R_a/R_g)^9, \tag{6}$$

where R_a and R_g are the radii of the PI molecule and gel pore respectively, with the values given in **Table 2**.

TABLE 1 | Definition of symbols.

Symbol	Definition
V_{cell} (m^3)	Cell volume
D_{out} (m^2/s)	Extracellular diff. coeff. of PI
D_{in} (m^2/s)	Intracellular diff. coeff. of PI
D_{pore} (m^2/s)	Diff. coeff. of PI inside the pore
A_{pore} (m^2)	Pore area
D_g (m^2/s)	Diff. coeff. of PI in agarose gel
D_w (m^2/s)	Diff. coeff. of PI in aqueous solution
c_{out} (mol/m^3)	Extracellular concentration of PI
c_{in} (mol/m^3)	Intracellular concentration of PI
h (m)	Membrane thickness
R (m)	Pore radius
R_a (m)	Radius of PI molecule
R_g (m)	Radius of gel pores
k_B (J/K)	Boltzmann constant
T (K)	Temperature
η ($N.s/m^2$)	Viscosity of plasma membrane

TABLE 2 | Constant values.

Constant	Value	Reference
V_{cell}	$0.7 * 10^{-18}$ (m^3)	For *E. coli* (Yu et al., 2014)
D_w	$4 * 10^{-10}$ (m^2/s)	Stokes-Einstein relation[a]
h	$4 * 10^{-9}$ (m)	For *E. coli* (Briegel et al., 2009)
R_a	$6 * 10^{-10}$ (m)	(Bowman et al., 2010)
R_g	$8 * 10^{-7}$ (m)	(Pluen et al., 1999)
k_B	$1.38 * 10^{-23}$ (J/K)	-
T	296 (K)	-
η	$5 * 10^{-9}$ ($N.s/m^2$)	(Daniels and Turner, 2007)

[a] $D_w = k_B T/(6\pi\eta_w R_a)$, where η_w is the viscosity of water.

We used the expression that Verkman (2002) introduced to estimate the diffusion coefficient of small molecules (with size and mass approximately equal to those of the PI molecule) in cytoplasm: $D_{in} \approx 0.25 D_w$. This approximation agrees with the intracellular diffusion coefficient that Zarnitsyn et al. (2008) used to estimate the wound radius in human cell membranes after sonication.

As shown in **Figure 1E**, the diffusion of fluorescent molecules within the pore can be modeled as diffusion of molecules in a tube of length h and radius R. We used the expression that Daniels and Turner (2007) proposed for calculating the diffusion coefficient of proteins along long thin membrane tube to express D_{pore}:

$$D_{pore} = \frac{k_B T}{4\pi\eta}\left[ln\left(\frac{R}{R_a}\right) + O(1) + O\left(\frac{R_a}{R}\right) + ...\right], \tag{7}$$

where k_B is the Boltzmann constant, T is the temperature in Kelvin, η is the viscosity of the membrane, and R_a is the particle (PI) radius (all values in **Table 2**). O(.) elements are neglected terms from the Taylor series representation. We obtained the measured value for K by inserting $I(t)$ and I_{max} (Equation 3) and

tried to fit our simulated value for K (Equation 5) to the measured value for K (Equation 3). By doing so, and by substituting other parameters from the literature and physics of the cells (**Table 2**), we estimated the parameter R in Equation (5) which gave us the pore radius R. The time dependent value K made the link between our model and experimental data and since we calculated it from the measured data, it specifically affected the final estimation of the pore size, thereby calibrating the model for a specific experimental condition.

Fourth, as we followed an identical protocol for microscopy, it was assumed that the impact of photobleaching (if it occurred) did not interfere with the results.

3. RESULTS

3.1. Monitoring the Diffusion of PI Molecules Into Damaged Bacterial Cells Through Membrane Pores

To measure the diffusion rate of PI molecules through a damaged membrane, we measured red FI for each bacterial cell (*L. monocytogenes*) after adding PI molecules for 30 min at a rate of 1 fps (**Figure 2**). All obtained images and videos can be found in the Dryad Digital Repository (Nikparvar et al., 2020). Owing to variability in cell resistance, cells showed different degrees of pressure-induced damage. We used the k-means algorithm to cluster the intensity curves using a certain number of clusters (determined by the elbow method) for days 0, 1, 2, 3, and 4 after pressure exposure based on the rate of PI diffusion through membrane pores (see section 2.2). The mean intensity curve for each cluster on each evaluation day is shown in **Figures 3A–E**. In the negative control sample (untreated cells), the cells remained uncolored during the observation period, indicating that PI molecules did not diffuse into the cells (**Figure 3F**). By contrast, in the positive control sample (heat-treated cells), the intensity reached its maximum value after 30 min, indicating substantial membrane damage. The numbers of untreated, heat-treated, and pressure-treated cells in each cluster for days 0–4 are reported in **Table 3**.

First, we found that for all evaluation days, the FI started to increase after a delay of about 8 min, probably owing to the time taken for the PI molecules to diffuse from the extracellular medium to the cells through the agarose gel.

Second, Equation (2) implies that the higher the slope of the intensity curve, the faster PI molecules diffuse inside the cell. According to Equations (2) and (5), the diffusion rate of PI molecules (slope of the curves in **Figure 3**) was positively correlated with the membrane pore size. This suggests that the curves belonging to the cluster with the lowest slope of the intensity curve correspond to the cells with the smallest pore sizes. The intensity curve for the group with the lowest slope displayed an upward trend toward saturation as the time approached 30 min (**Figure 3**). Conversely, the clusters with the highest slope of the intensity curve correspond to the cells with the largest pore sizes.

Most importantly, we detected a general decrease in the rate of PI diffusion into the cells on consecutive days. This was consistent for the cluster of cells with the lowest rate of diffusion, in which the final FI value (shown with a dashed line in **Figure 3**) changed from 0.14 on day 0 to a final value of 0.02 on day 4, i.e., a seven-fold decrease. This is a strong indication that the pore size decreased over the 4 days after the pressure treatment.

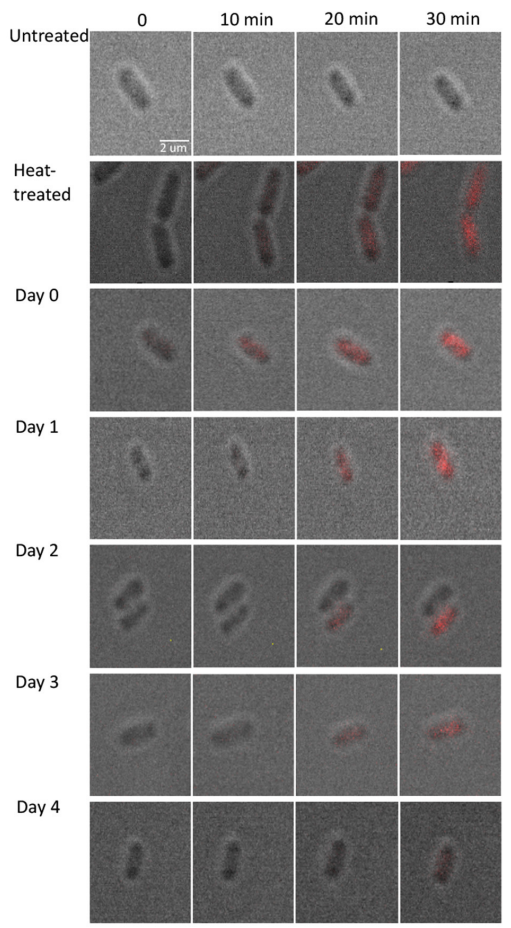

FIGURE 2 | Fluorescence microscopy images for pressure-treated (400 MPa, 8 min, 8°C) and control samples. To measure the diffusion rate of PI molecules through a damaged membrane, we measured red FI for each bacterial cell (*L. monocytogenes*) after adding PI molecules for 30 min at a rate of 1 fps. All images and videos are available from the Dryad Digital Repository (Nikparvar et al., 2020).

3.2. Estimation of the Pore Area

As discussed earlier, we assumed that the cluster corresponding to the curves with the lowest slope of the intensity curve was associated with the least-damaged bacteria. As we could detect a decay in the rate of PI uptake for this group of cells from day 0

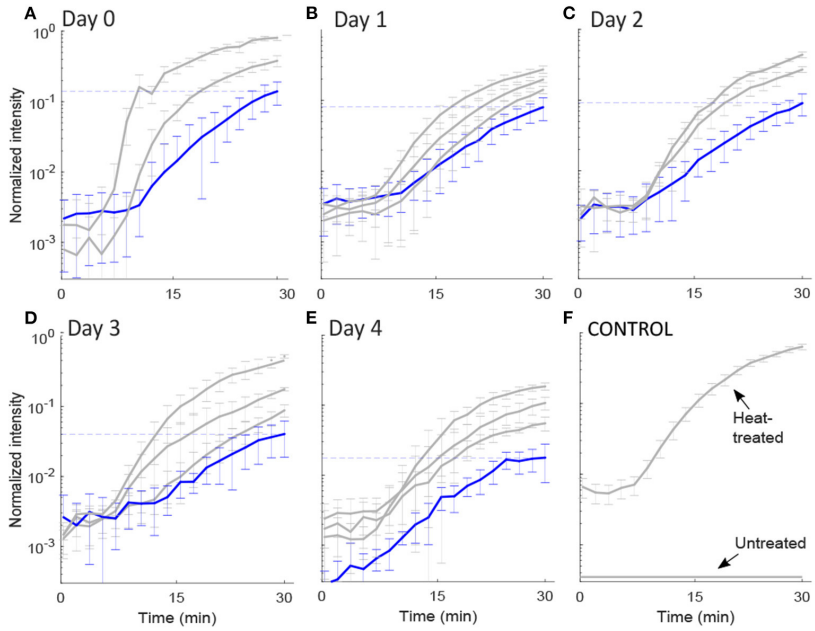

FIGURE 3 | Intensity plots. The normalized mean and standard deviation of the red fluorescence intensity, FI, emitted from: **(A–E)** each pressure-treated cell on days 0–4 following HPP, and **(F)** two control samples. The FI values were extracted from images captured by the fluorescence microscopy technique for 30 min after PI addition. We used the k-means algorithm to cluster the intensity curves through a certain number of clusters (determined by the elbow method) for days 0, 1, 2, 3, and 4 after pressure exposure based on the rate of PI diffusion through membrane pores (see 2.2). The y-axis is in log scale. The intensity value after 30 min for the group of cells with the lowest slope (shown in blue) decreased with the days from 0.14 to 0.02, represented by the dashed lines. Intensity values for each cell (raw data) are available in **Supplementary File 1**.

TABLE 3 | Number of studied untreated (Untr), heat-treated (H-T), and pressure-treated (PI-positive) cells in each cluster on days 0–4 (D0-D4).

Cluster	D0	D1	D2	D3	D4	Untr	H-T
Lowest slope	98	12	11	10	7	–	
Mild slope[a]	5	28	3	30	12	–	
Highest slope	15	9	7	4	8	–	
Total	118	49	21	44	27	20	39

[a] *The number of cells in the mild-slope cluster equals to the number of cells belonging to the clusters other than the lowest- and the highest-slope clusters.*

to day 4, we used this group to calibrate the model that estimates the pore size.

By substituting the FI value corresponding to this cluster for each evaluation day into Equations (3–7), the mean value for pore size was estimated. First, the results of the model calibration showed that the mean radius of the pore decreased from 1.3 to 0.8 nm over the 4 days (**Figure 4A**).

Second, we ran one-way ANOVA and multi-comparison tests using the Bonferroni method (see section 2.3) and found that the mean value of the estimated pore radius on day 0 (mean = 1.338, SD = 0.0014) was significantly ($p < 10^{-6}$) higher than on the other days (**Figure 4A**). The mean values of the pore radius for day 1 (mean = 1.191, SD = 0.0039) and day 2 (mean = 1.221, SD = 0.0041) were significantly different ($p < 10^{-6}$) from those on days 3 (mean = 0.964, SD = 0.0043) and 4 (mean = 0.809, SD = 0.0051). Although we observed a general reduction in the PI uptake during the 4 days (**Figure 4B**), we did not observe a reduction from day 1 to day 2 probably owing to high variability in the results or due to other reasons such as a lag time before starting the recovery process. Furthermore, because of the small sample size on day 4 (due to a low number of PI-positive cells detected on day 4 which most likely resulted from the partial recovery of the membrane), we could not show a significant reduction from day 3 to day 4. Estimated pore size values for the cluster with the lowest slope are presented in **Table 4**. The decay in the pore size suggests the presence of an embedded membrane repair mechanism in bacteria, which was activated in response to HPP (see section 4). The Bartlett test reported insufficient evidence to say the variances are different with a *P*-value higher than 0.05.

Once the model was calibrated, we fitted a weighted least squares model to the estimated pore size values on each day for the cluster with the lowest slope (**Figure 5A**). Based on the

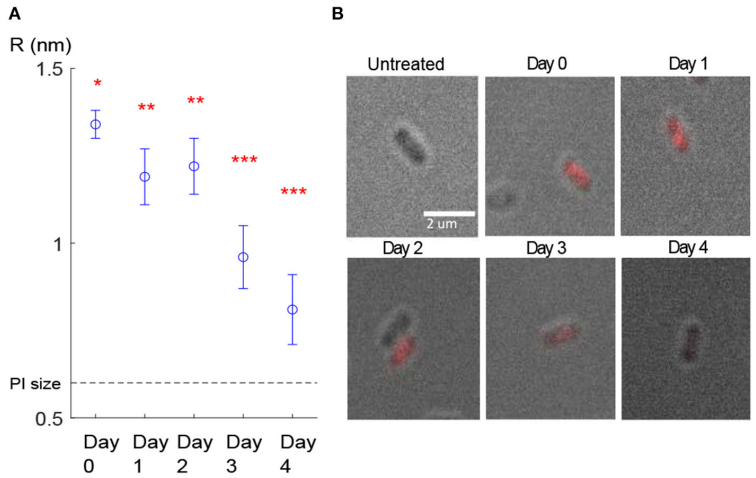

FIGURE 4 | Pore size estimation. **(A)** Estimated pore radius of the cells belonging to the cluster with the lowest slope. The mean value of pore radius for day 0 was significantly ($p < 10^{-6}$) different than the rest of the days. The mean value of the pore radius for days 1–2 was significantly different than days 3–4 (stars represent statistically different groups). Error bars show the confidence intervals, calculated using the Bonferroni method for multi-comparison (see 2.3). **(B)** The last frame (t = 30 min monitoring) of the fluorescence microscopy image stacks obtained in each evaluation day. Here only one cell as a representative for each day is shown.

TABLE 4 | Estimated pore radius for the cluster with the lowest slope (**Figure 4**).

Day post-pressure	*R* (nm)	Confidence interval[a] (nm)
D0	1.338	(1.296–1.380)
D1	1.191	(1.113–1.269)
D2	1.221	(1.139–1.303)
D3	0.964	(0.878–1.051)
D4	0.809	(0.702–0.915)

[a] *The Bonferroni method.*

assumption that cells with different pore sizes in the range <5 nm are repaired at the same rate (Zarnitsyn et al., 2008), we used the same weighted least squares model to fit the remaining cell groups (**Figure 5B**). Given an initial FI value on day 0, this model could predict the pore radius as a function of time. It was then possible to estimate the time that the bacterial cell needed to regain its membrane integrity. In our case, this occurred when the pore radius became smaller than the radius of the PI molecule (dashed horizontal line, **Figure 5B**). Although extrapolation outside the region of experimental measurements may risk entering different dynamics/regions, where the assumptions do not apply anymore, we believe that such error will not matter in our work because this is when the pores are too small to have consequences on the cell (death).

This information could be useful for food industry to design more efficient pressure treatments by adjusting HPP strategy (the pressure strength and holding time).

Figure 6 gives a better understanding of pore size in terms of allowing for the leakage of solutes with different molecule sizes through the pore. A literature search revealed that small solutes, such as ions, amino acids, ATP, etc. (size <700 Da) could pass through 1-nm pores. Larger molecules such as ribosomes and DNA were found to pass through pores larger than 2 nm (**Figure 6**). Although estimation of cell life expectancy requires extensive statistical experiments, it can be safely assumed that large pore sizes can cause leakage of larger essential compounds, e.g., DNA, from the cell through pores (**Figure 6**). In other words, the cell is more likely to die when the pore sizes are large.

To investigate how sensitive the model prediction R was to different parameters (e.g., V_{cell}, σ, η, h, and D_{in}), we perturbed each parameter by $\Delta p = \pm 10\%$, while the input c_{in} was 50% of its maximum value, 1 (local sensitivity analysis). We found that the model was sensitive to V_{cell}, η, and h. The relative sensitivity coefficient ($S = |\frac{R_{(p)} - R_{(p+\Delta p)}}{\Delta p} \cdot \frac{p}{R}|$) is listed in **Table 5**, where p is the parameter and Δp is its perturbation.

To evaluate how sensitive our linear regression model was to variations in the cell volume (i.e., the most sensitive parameter in our model; **Table 5**), we perturbed the parameter V_{cell} ($\Delta p = \pm 10\%$ and $\pm 50\%$) and checked the deviation in the predicted value R each day. Importantly, for both $\Delta p = \pm 10\%$ and $\Delta p = \pm 50\%$, the local sensitivity of the regression model to the perturbation decreased over time (**Figure 7**), such that the estimated time for regaining the membrane integrity did not alter significantly. We also examined the other two sensitive parameters, i.e., membrane thickness h and viscosity of the plasma membrane η, and found similar results. These results together with the fact that the size of *L. monocytogenes* is in the range defined by 10 and 50% perturbation from the size of *E. coli* (Jamshidi and Zeinali, 2019) indicate that the model predictions of temporal recovery were robust to the uncertainty

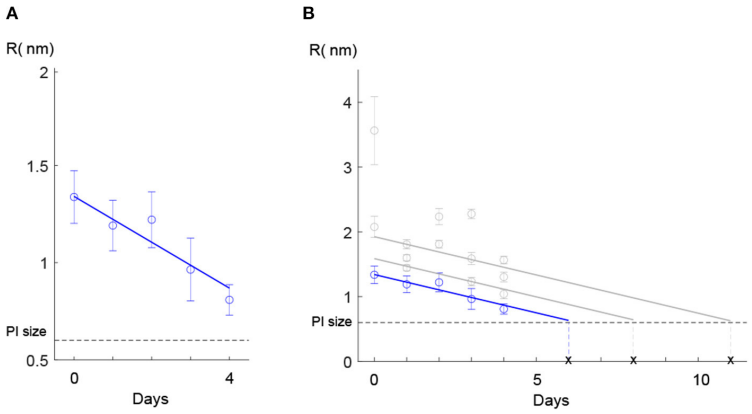

FIGURE 5 | Regression model for the pore size. **(A)** A weighted regression model showed that the estimated values of the pore size for the cluster with the lowest slope in the intensity curve decayed linearly over the four days. **(B)** The linear model was fitted to the data of the remaining clusters. Error bars in both **(A,B)** show the standard deviation for the estimated pore radius. The solid blue line shows the fitted linear model to the data for the least damaged cells (the cluster with the lowest slope in the intensity curve) and the solid gray lines show the predicted linear approach for resealing pores over evaluation days for the rest of the clusters. With this linear model, we could predict the time interval needed for each group to recover the membrane.

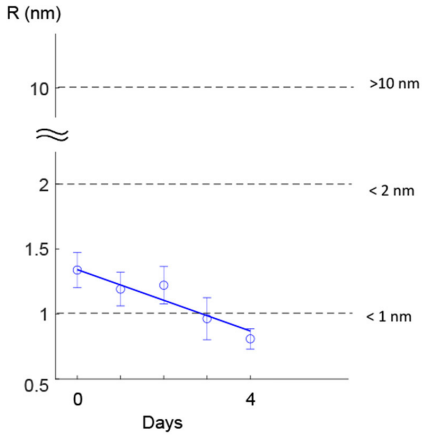

Solute	Size	Mass
Ribosome 70S	10 nm	2.5 MDa
DNA chain	1 nm	660 Da (1 base pair)
Glucose	1 nm	180 Da
ATP	0.7 nm	500 Da
Water	0.3 nm	18 Da
Cl^-	0.18 nm	35 Da
K^+	0.13 nm	35 Da
Na^+	0.09 nm	23 Da
Mg^{2+}	0.07 nm	24 Da

FIGURE 6 | Leak of solutes through small pores. Literature research in filter membranes shows that solutes such as glucose, some ions, and ATP are small enough to pass through pores up to 1 nm size. Bigger pores may allow pass of bigger molecules such as DNA and dextrans[1].

of parameters such as V_{cell} (which was substituted from values specified for *E. coli*, **Table 2**).

3.3. Population Growth Behavior of Pressure-Treated *L. monocytogenes*

Absence of growth at the population level during the recovery period was confirmed by measurement of viable plate counts. Exposure of *L. monocytogenes* to 400 MPa, 8 min, 8°C led to a 7.79 ± 0.82 *log* CFU/mL decrease in viable cell counts, corresponding to a cell concentration below the LOQ of the method (**Figure 8**). Viable cell counts in the pressure-treated sample remained constant and below the LOQ during the subsequent 4 days, whereas the growth of the total population was only observed 7 days after HPP. This trend is compatible with the existence of a lag phase of at least 4 days, followed by the onset of the exponential growth phase.

[1]London Health Science Centre (2020). https://www.lhsc.on.ca/critical-care-trauma-centre/principles-of-crrt/ (accessed July 24, 2020).

4. DISCUSSION

We exposed *L. monocytogenes* cells to HPP of 400 MPa, 8 min, 8°C. Our results showed that some of the cells in the sample that were exposed to HPP became permeable to PI molecules, which otherwise could not pass through the intact membrane, suggesting the formation of pores in the cellular envelope under high pressure. Although the exact mechanism of pressure-induced membrane permeabilization is not known, it has been linked to the denaturation of membrane proteins, as well as to the phase transition of membrane phospholipids from the physiological liquid-crystalline phase to the gel phase, which results from lateral compression and increased packing of the acyl chains (Pagán and Mackey, 2000; Casadei et al., 2002; Winter and Jeworrek, 2009; Patterson, 2014). To evaluate the degree of membrane damage, we measured the rate of FI change inside each cell after adding PI molecules to the extracellular medium. First, we detected large variations in the degree of membrane damage among single cells, which were clustered into groups (**Figure 3**) using the k-means algorithm (see section 2.2). This was consistent with a study by Ritz et al. (2001), in which HPP followed by PI staining and flow cytometry analysis of *L. monocytogenes* revealed a broad distribution of red FIs for cells taking up PI, probably arising from different structural strengths of the cellular envelope. Entry of a bacterial population into the stationary phase, as analyzed in this study, is related to an increased resilient cell envelope and the synthesis of stress response proteins (Casadei et al., 2002; Huang et al., 2014). However, this phenotype is subject to various possible drivers of intrapopulation heterogeneity, including stochasticity in gene expression, the effects of which

TABLE 5 | Relative sensitivity coefficient for 10% perturbation in each parameter.

Parameter	Relative sensitivity $\|S\|$
V_{cell}	0.3799
η	0.3798
h	0.3798
σ	$9.758 * 10^{-6}$
D_{in}	$3.188 * 10^{-5}$

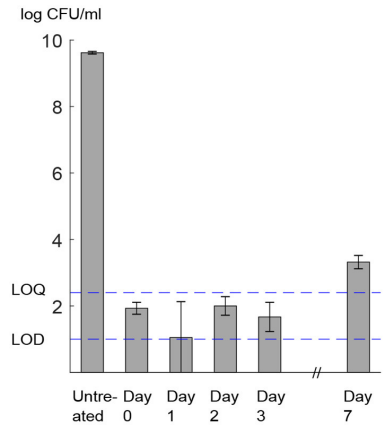

FIGURE 8 | *L. monocytogenes* viable cell counts (log *CFU*/*mL*). Assessment was done by plating on non-selective medium before (untreated) and after HPP (day 0) and during storage at 8°C (day 1–7). LOD, limit of detection; LOQ, limit of quantification. Error bars show standard deviation of three biologically independent replicates. Raw data is available in **Supplementary File 2**.

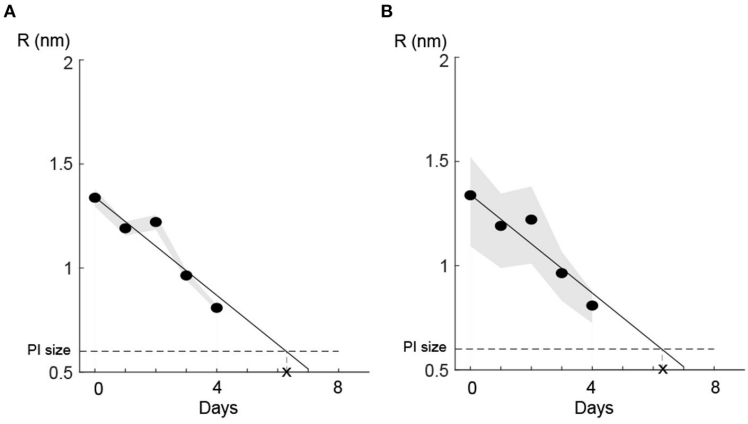

FIGURE 7 | Parametric uncertainty of the linear prediction for the cell volume (**Table 5**) diminished with pore size. **(A)** 10% perturbation and **(B)** 50% perturbation in $p = V_{cell} = 0.7 * 10^{-18}$ (m^3). Shaded bounds show the deviation of the predicted R values from its nominal values (black solid line) due to parameter (V_{cell}) uncertainty. For both perturbations of 10 and 50% of the nominal parameter value, the uncertainty region diminished as pores were resealed.

are amplified for low-abundance molecules such as mRNAs and regulatory proteins; cell cycle and aging stage; and epigenetic regulation (Avery, 2006; Veening et al., 2008). Moreover, phenotypic heterogeneity is an inherent feature of bacterial populations and, most importantly, is considered to be a component of their adaptation and survival strategy (Booth, 2002).

Second, the synergy of our mass transfer mechanistic model (Equations 1–7) with specially tailored experiments to test the membrane recovery hypothesis allowed us to estimate the total size of the pressure-created pores at any time point after treatment at 400 MPa, 8 min, 8°C. Our observations indicated that the rate of diffusion of PI, particularly in the cluster with the lowest slope (corresponding to the least-damaged cells), was reduced during the 4 days after exposure (**Figure 4**). The existence of a recovery process in the bacterial membrane investigated in this work is consistent with the results of our previous works (Duru et al., 2021; Nikparvar et al., 2021), where by using a time-series RNA sequencing data and conducting a network component analysis we proved the presence of a repair process in the membrane after HPP.

Most importantly, we found that the estimated pore size decayed (most likely) linearly as a function of time (**Figure 5**). If the trend is not linear, then the rate of repair (decay of size) must be increased (e.g., log decay) or decreased (e.g., exponential decay). We see no reason for an accelerated repair because cells will likely mobilize most of their resources to repair damage when it is at its maximum level. There is no reason to assume that the cells will increase their repair resources (and thus the rate) as the pore size decreases. An exponential decay (decelerating rate of repair) is otherwise more likely, but as pores are becoming smaller, the repair process will likely proceed faster. However, at that stage the cells likely divert resources to other essential damaged sites than the membrane, and therefore the rate remains nearly linear. The linear repair rate is consistent with a previous study of membrane recovery in human cells (Zarnitsyn et al., 2008), in which the authors measured membrane wound closure using several fluorescent molecules. They found an exponential decay for wound sizes on the scale of hundreds of nanometers over time, followed by an approximately linear decay for wound sizes less than 20 nm.

The model suggested in this work for quantifying the membrane damage is based on several assumptions (see 2.4). The assumption that the main pressure-induced membrane damage occurred in a single effective pore area (total area of membrane pores) may affect the prediction of the size of individual pores. To date, pores smaller than fluorescent molecules (such as PI) are difficult to measure by direct methods. Thus, the model predictions may appear biased when the number of small pores (smaller than PI size) is large. Importantly, the total diffusion of molecules through the cell membrane is only dependent on the total surface of the pores (Zarnitsyn et al., 2008), so cell fate, which is strongly affected by the total diffusion via the loss of cytosol material, will not be affected by the wrong estimation of the number of pores. Additionally, there is no evidence supporting that high pressure causes multiple small pores: once high pressure damages the membrane structure in a certain area, additional pressure buildup will most likely concentrate around the same area which is structurally weaker than the remaining parts of the membrane. Finally, finer resolution of pore sizes can be estimated by using several fluorescent molecules as in a previous work (Zarnitsyn et al., 2008) the authors compensated for this assumption (single pore area) by using a series of fluorescent molecules with different sizes. The linear relationship between the concentration of PI molecules and the FI is another fundamental assumption in our model development. This assumption may limit the accuracy of the result if saturation occurs i.e., when the increase in the PI concentration does not affect the intensity anymore. However, because we used heat-treated bacteria as positive control cells (see 2.1.3), in which the membrane damaged was highest, we guaranteed that for each day the intensity in pressure-treated bacteria was not saturated.

The intensity curves for the cluster with the lowest slope (**Figure 3**) displayed an increasing trend until reaching a near-saturation level. However, as the intensity approaches saturation, the sensitivity of the signal decreases. An inaccurate saturation value may cause to underestimate the pore size through Equation (5), particularly for days 0–2. For days 3 and 4, the intensity curve for the lowest-slope cluster stayed at a steady state after 30 min and therefore the estimation of the pore size for these 2 days is more accurate. However, the underestimation of the pore size on days 0–2 does not affect our conclusion of the existence of a recovery process, because even if the actual pore sizes for days 0–2 were larger than the estimated values, the damage was still recovered over days 3 and 4.

Leakage of intracellular components due to membrane damage following various treatments with antibiotics, bacteriocins, or high pressure was demonstrated for both Gram-positive and Gram-negative bacteria. In an early study, leakage of low-molecular-weight solutes upon treatment of *E. coli* with different concentrations of 2-phenoxyethanol was proposed as an indicator of the disorganization of the cytoplasmic membrane (Gilbert et al., 1977). In line with this, membrane damage induced by poly-hexamethylene biguanides resulted in leakage of potassium ions and inorganic phosphates in *E. coli* (Broxton et al., 1983). Lambert and Hammond (1973) showed leakage of potassium to be a primary indicator of membrane damage. Depending on the extent of membrane damage, larger solutes such as ATP or DNA (500–700 Da) are also released from the cell (Zhen et al., 2013; Singh et al., 2016). Although bacteria possess membrane repair mechanisms, the duration and the extent of membrane damage (i.e., pore size) may lead to bacterial cell death (Wortman and Bissonnette, 1988; Vigouroux et al., 2020). As the model developed in this work predicts the timely repair of pores, it could be integrated with future work to estimate the cumulative probability of survival and life expectancy.

We did not observe a marked increase in the number of cells able to form colonies in the culture medium during the 4 days of the experiments, i.e., cell counts remained stable and below the LOQ. However, as we could observe a decay in the membrane pore radius by time, we inferred that the growth process (mass accumulation and division) of these individual cells was arrested,

yet they were not dead. Although a population growth curve does not provide information about the physiological state of cells giving rise to the exponential growth phase, single-cell studies have revealed that the presence of a non-growing fraction of cells is the main cause of the extended apparent population lag when stress conditions at the growth limit are applied (Koutsoumanis, 2008; Aguirre and Koutsoumanis, 2016), as in the present study. Moreover, several studies have shown an increased length of the lag phase, both at the population and single-cell levels, after exposure of *L. monocytogenes* to stress conditions, including high pressure (Robinson et al., 1998; Francois et al., 2006; Muñoz-Cuevas et al., 2013). The increased time required to start division can be attributed to the metabolic processes needed for repair of damaged cell components and is therefore indicative of the presence of sub-lethally injured cells (Guillier et al., 2005; Métris et al., 2008). In our experiments, cell counts exceeded the LOQ only after 7 days. Thus, it is likely that the cells that resealed their membrane pores started to proliferate and, along with a small fraction of non-injured cells (Aguirre and Koutsoumanis, 2016), contributed to the observed growth at the population level. Our observation of growth arrest at the first days after pressure treatment led us to hypothesize that for each day the cells in the group with the lowest slope came either from the cells belonging to the lowest-slope group in previous days or injured cells from other groups such as mild-slope group that transferred to the lowest-slope group as they managed to recover partially. Therefore, we knew that the less number of PI-positive cells obtained over the 4 days could not be due to proliferation of new cells but likely due to an increasing number of recovered cells.

We note that it is impossible to infer the rate of membrane damage repair from the microscopy observations alone, because of the large biological variations and the number of cell clusters (**Figure 3**). It was the synergy of our dynamic model, trained by our experimental data and tested on a subset of experiments, that enabled us to calculate the repair rate of any pore size on this scale (<20 nm) until the cellular envelope was repaired. This could help to predict the duration time of growth arrest after exposure to HPP until the cells restart the growth process. It should be noted that the results obtained in this work were specifically related to the pressure treatment of *L. monocytogenes* in 400 MPa, 8 min, 8°C, thereby generalizing the result to other HPP conditions and other microorganisms may not be valid. However, what we presented in this study may pave the road for future works such that the method suggested here can be applied for other HPP conditions or other microorganisms and fluorescent molecules. Repeating similar experiments with different pressure values and holding times can increase the fidelity of the model.

5. CONCLUSION

The recovery process in bacteria after exposure to high pressure has not been investigated well. Here, we focused on foodborne pathogenic bacteria *L. monocytogenes* and the effects of high pressure (400 MPa, 8 min, 8°C) on its membrane. We added PI molecules to the pressure-treated bacteria at time point 0 (immediately after treatment) and on days 1, 2, 3, and 4 after HPP, and measured the FI emitted by DNA-bound PI molecules using a fluorescence microscopy technique. We developed a dynamic model to quantify the degree of damage in pressure-treated bacteria. The synergy between our diffusion model and microscopy experiments revealed that some *L. monocytogenes* cells exposed to HPP repaired their damaged membrane approximately linearly on a time scale of days. This is the first time that membrane pores created by HPP have been quantitatively described and shown to diminish.

DATA AVAILABILITY STATEMENT

The original contributions presented in the study are publicly available. This data can be found here: https://datadryad.org/stash/share/bP2iD9QM03-5tCl8njy_0BNrcQAHgX5dZvCwznZwmvw.

AUTHOR CONTRIBUTIONS

BN: conceptualization, methodology, software, formal analysis, investigation, and writing—original draft, visualization. AS: methodology, investigation, and writing—original draft. MC: resources, writing—review and editing, and supervision. MH-H: resources and supervision. PC: visualization and writing—review and editing. CR: writing—review and editing and supervision. NB: conceptualization, validation, formal analysis, investigation, resources, writing—review and editing, supervision, and project administration. All authors contributed to the article and approved the submitted version.

FUNDING

This study was supported within the ERA-IB2 consortium SafeFood (ID: ERA712IB-16- 247 014) by grants of the the Research Council of Norway (to NB, grant number 263499), the Spanish Government (to MC, grant number PCIN-2016-072), and the German Ministry for Education and Research (to CR, grant number 031B0268). The funders had no role in the design of the study and collection, analysis, and interpretation of data and in writing the manuscript.

ACKNOWLEDGMENTS

The authors thank Judit Pampalona Sala for technical assistance with fluorescence microscopy experiments performed at Servei de Microscopia at Autonomous University of Barcelona and Pedro A. Lira-Parada and Dr. Gerd M. Seibold for discussions.

SUPPLEMENTARY MATERIAL

The Supplementary Material for this article can be found online at: https://www.frontiersin.org/articles/10.3389/fmicb.2021.598739/full#supplementary-material

REFERENCES

Aguirre, J., and Koutsoumanis, K. (2016). Towards lag phase of microbial populations at growth-limiting conditions: the role of the variability in the growth limits of individual cells. *Int. J. Food Microbiol.* 224, 1–6. doi: 10.1016/j.ijfoodmicro.2016.01.021

Alpas, H., Kalchayanand, N., Bozoglu, F., Sikes, A., Dunne, C., and Ray, B. (1999). Variation in resistance to hydrostatic pressure among strains of food-borne pathogens. *Appl. Environ. Microbiol.* 9, 4248–4251. doi: 10.1128/AEM.65.9.4248-4251.1999

Alvarez-Ordóñez, A., Broussolle, V., Colin, P., Nguyen-The, C., and Prieto, M. (2015). The adaptive response of bacterial food-borne pathogens in the environment, host and food: implications for food safety. *Int. J. Food Microbiol.* 213, 99–109. doi: 10.1016/j.ijfoodmicro.2015.06.004

Avery, S. (2006). Microbial cell individuality and the underlying sources of heterogeneity. *Nat. Rev. Microbiol.* 4, 577–587. doi: 10.1038/nrmicro1460

Booth, I. (2002). Stress and the single cell: intrapopulation diversity is a mechanism to ensure survival upon exposure to stress. *Int. J. Food Microbiol.* 78, 19–30. doi: 10.1016/S0168-1605(02)00239-8

Bover-Cid, S., Belletti, N., Garriga, M., and Aymerich, T. (2010). Model for *Listeria monocytogenes* inactivation on dry-cured ham by high hydrostatic pressure processing. *Food Microbiol.* 28, 804–809. doi: 10.1016/j.fm.2010.05.005

Bowman, A., Nesin, O., Pakhomova, O., and Pakhomov, A. (2010). Analysis of plasma membrane integrity by fluorescent detection of Tl+ uptake. *Membr. Biol.* 236, 15–26. doi: 10.1007/s00232-010-9269-y

Bozoglu, F., Alpas, H., and Kaletunç, G. (2004). Injury recovery of foodborne pathogens in high hydrostatic pressure treated milk during storage. *FEMS Immunol. Med. Microbiol.* 40, 243–247. doi: 10.1016/S0928-8244(04)00002-1

Briegel, A., Ortega, D., Tocheva, E., Wuichet, K., Li, Z., Chen, S., et al. (2009). Universal architecture of bacterial chemoreceptor arrays. *Proc. Natl. Acad. Sci. U.S.A.* 106, 17181–17186. doi: 10.1073/pnas.0905181106

Briers, Y., Klumpp, J., Schuppler, M., and Loessner, M. (2011). Genome sequence of *Listeria monocytogenes* Scott A, a clinical isolate from a food-borne listeriosis outbreak. *J. Bacteriol.* 193, 4284–4285. doi: 10.1128/JB.05328-11

Broxton, P., Woodcock, P. M., and Gilbert, P. (1983). A study of the antibacterial activity of some polyhexamethylene biguanides towards *Escherichia coli* ATCC 8739. *J. Appl. Bacteriol.* 54, 345–353. doi: 10.1111/j.1365-2672.1983.tb02627.x

Casadei, M., Mañas, P., Niven, G., Needs, E., and Mackey, B. (2002). Role of membrane fluidity in pressure resistance of *Escherichia coli* nctc 8164. *Appl. Environ. Microbiol.* 68, 5965–5972. doi: 10.1128/AEM.68.12.5965-5972.2002

Daniels, D., and Turner, M. (2007). Diffusion on membrane tubes: a highly discriminatory test of the saffman-delbruck theory. *Langmuir* 23, 6667–6670. doi: 10.1021/la0635000

Davey, H., and Hexley, P. (2011). Red but not dead? Membranes of stressed *Saccharomyces cerevisiae* are permeable to propidium iodide. *Environ. Microbiol.* 13, 163–171. doi: 10.1111/j.1462-2920.2010.02317.x

Duru, I. C., Andreevskaya, M., Laine, P., Rode, T. M., Ylinen, A., Løvdal, T., et al. (2020). Genomic characterization of the most barotolerant *Listeria monocytogenes* RO15 strain compared to reference strains used to evaluate food high pressure processing. *BMC Genomics* 21:455. doi: 10.1186/s12864-020-06819-0

Duru, I. C., Bucur, F. I., Andreevskaya, M., Nikparvar, B., Ylinen, A., Grigore-Gurgu, L., et al. (2021). High-pressure processing-induced transcriptome response during recovery of *Listeria monocytogenes*. *BMC Genomics* 22:117. doi: 10.1186/s12864-021-07407-6

Francois, K., Devlieghere, F., Standaert, A., Geeraerd, A., Impe, J. V., and Debevere, J. (2006). Effect of environmental parameters (temperature, ph and aw) on the individual cell lag phase and generation time of *Listeria monocytogenes*. *Int. J. Food Microbiol.* 108, 326–335. doi: 10.1016/j.ijfoodmicro.2005.11.017

Gänzle, M., and Liu, Y. (2015). Mechanisms of pressure-mediated cell death and injury in *Escherichia coli*: from fundamentals to food applications. *Front. Microbiol.* 6:599. doi: 10.3389/fmicb.2015.00599

Gänzle, M., and Vogel, R. (2001). On-line fluorescence determination of pressure mediated outer membrane damage in *Escherichia coli*. *Syst. Appl. Microbiol.* 24, 477–485. doi: 10.1078/0723-2020-00069

Gilbert, P., Beveridge, E. G., and Crone, P. B. (1977). The lethal action of 2-phenoxyethanol and its analogues upon *Escherichia coli* NCTC 5933. *Microbios* 19, 125–141.

Guillier, L., Pardon, P., and Augustin, J. (2005). Influence of stress on individual lag time distributions of *Listeria monocytogenes*. *Appl. Environ. Microbiol.* 71, 2940–2948. doi: 10.1128/AEM.71.6.2940-2948.2005

Hereu, A., Dalgaard, P., Garriga, M., Aymericha, T., and Bover-Cida, S. (2014). Analysing and modelling the growth behaviour of *Listeria monocytogeneson* RTE cooked meat products after a high pressure treatment at 400 MPa. *Int. J. Food Microbiol.* 186, 84–94. doi: 10.1016/j.ijfoodmicro.2014.06.020

Huang, H.-W., Lung, H.-M., Yang, B. B., and Wang, C.-Y. (2014). Responses of microorganisms to high hydrostatic pressure processing. *Food Control* 40, 250–259. doi: 10.1016/j.foodcont.2013.12.007

Jamshidi, A., and Zeinali, T. (2019). Significance and characteristics of *Listeria monocytogenes* in poultry products. *Int. J. Food Sci.* 2019, 1–7. doi: 10.1155/2019/7835253

Jofré, A., Aymerich, T., Bover-Cid, S., and Garriga, M. (2010). Inactivation and recovery of *Listeria monocytogenes*, *Salmonella enterica* and *Staphylococcus aureus* after high hydrostatic pressure treatments up to 900 MPa. *Int. Microbiol.* 13, 105–112. doi: 10.2436/20.1501.01.115

Kassambara, A. (2017). *Practical Guide to Cluster Analysis in R, 1 Edn*. CreateSpace Independent Publishing Platform, Scotts Valley, California.

Kim, Y., Shin, E., Jung, W., Kim, M. K., and Chong, Y. (2020). A near-infrared turn-on fluorescent sensor for sensitive and specific detection of albumin from urine samples. *Sensors* 20:1232. doi: 10.3390/s20041232

Klotz, B., Mañas, P., and Mackey, B. (2010). The relationship between membrane damage, release of protein and loss of viability in *Escherichia coli* exposed to high hydrostatic pressure. *Int. J. Food Microbiol.* 137, 214–220. doi: 10.1016/j.ijfoodmicro.2009.11.020

Koseki, S., Mizuno, Y., and Yamamoto, K. (2007). Predictive modelling of the recovery of *Listeria monocytogenes* on sliced cooked ham after high pressure processing. *Int. J. Food Microbiol.* 119, 300–307. doi: 10.1016/j.ijfoodmicro.2007.08.025

Koutsoumanis, K. (2008). A study on the variability in the growth limits of individual cells and its effect on the behavior of microbial populations. *Int. J. Food Microbiol.* 128, 116–121. doi: 10.1016/j.ijfoodmicro.2008.07.013

Lambert, P. A., and Hammond, S. M. (1973). Potassium fluxes, first indications of membrane damage in micro-organisms. *Biochem. Biophys. Res. Commun.* 54, 796–799.

Mañas, P., and Mackey, B. (2004). Morphological and physiological changes induced by high hydrostatic pressure in exponential- and stationary-phase cells of *Escherichia coli*: Relationship with cell death. *Appl. Environ. Microbiol.* 70, 1545–1554. doi: 10.1128/AEM.70.3.1545-1554.2004

Métris, A., George, S., Mackey, B., and Baranyi, J. (2008). Modeling the variability of single-cell lag times for *Listeria innocua* populations after sublethal and lethal heat treatments. *Appl. Environ. Microbiol.* 74, 6949–6955. doi: 10.1128/AEM.01237-08

Muñoz-Cuevas, M., Guevara, L., Aznar, M., Martínez, A., Periago, P., and Fernández, P. (2013). Characterisation of the resistance and the growth variability of *Listeria monocytogenes* after high hydrostatic pressure treatments. *Food Control* 29, 409–415. doi: 10.1016/j.foodcont.2012.05.047

Muntean, M.-V., Marian, O., Barbieru, V., Cătunescu, G. M., Ranta, O., Drocas, I., et al. (2016). High pressure processing in food industry – characteristics and applications. *Agric. Agric. Sci. Proc.* 10, 377–383. doi: 10.1016/j.aaspro.2016.09.077

Nikparvar, B., Andreevskay, M., Duru, I. C., Bucur, F. I., Grigore-Gurgu, L., Borda, D., et al. (2021). Analysis of temporal gene regulation of *Listeria monocytogenes* revealed distinct regulatory response modes after exposure to high pressure processing. *BMC Genomics* 22:266. doi: 10.1186/s12864-021-07461-0

Nikparvar, B., Subires, A., Capellas, M., Hernandez, M., and Bar, N. (2019). "A dynamic model of membrane recovery mechanisms in bacteria following high pressure processing," in *Proceedings of the 12th IFAC Symposium on Dynamics and Control of Process Systems, including Biosystems DYCOPS* (Florianópolis), 243–250.

Nikparvar, B., Subires, A., Capellas, M., Hernandez-Herrero, M., Crauwels, P., Riedel, C.U., et al. (2020). Images obtained by fluorescence microscopy technique for monitoring diffusion of PI molecules into pressure-treated *Listeria monocytogenes cells*, Dryad Digital Repository (dataset), Available online at: https://datadryad.org/stash/share/bP2iD9QM03-5tCl8njy_0BNrcQAHgX5dZvCwznZwmvw

Pagán, R., and Mackey, B. (2000). Relationship between membrane damage and cell death in pressure-treated *Escherichia coli* cells: differences between

exponential- and stationary-phase cells and variation among strains. *Appl. Environ. Microbiol.* 66, 2829–2834. doi: 10.1128/AEM.66.7.2829-2834.2000

Patterson, M. (2014). Food technologies: high pressure processing. *Food Sci.* 3, 196–201. doi: 10.1016/B978-0-12-378612-8.00262-6

Pluen, A., Netti, P., Jain, R., and Berk, D. (1999). Diffusion of macromolecules in agarose gels: comparison of linear and globular configurations. *Biophys. J.* 77, 542–552.

Ritz, M., Tholozan, J., Federighi, M., and Pilet, M. (2001). Morphological and physiological characterization of *Listeria monocytogenes* subjected to high hydrostatic pressure. *Appl. Environ. Microbiol.* 67, 2240–2247. doi: 10.1128/AEM.67.5.2240-2247.2001

Robinson, T., Ocio, M., Kaloti, A., and Mackey, B. (1998). The effect of the growth environment on the lag phase of *Listeria monocytogenes*. *Int. J. Food Microbiol.* 44, 83–92.

Rubio, B., Possas, A., Rincón, F., García-Gímeno, R. M., and Martínez, B. (2018). Model for *Listeria monocytogenes* inactivation by high hydrostatic pressure processing in spanish chorizo sausage. *Food Microbiol.* 69, 18–24. doi: 10.1016/j.fm.2017.07.012

Shi, L., Günther, S., Hübschmann, T., Wick, L., Harms, H., and Müller, S. (2007). Limits of propidium iodide as a cell viability indicator for environmental bacteria. *Cytom. Part A* 71A, 592–598. doi: 10.1002/cyto.a.20402

Singh, M., Mallick, A. K., Banerjee, M., and Kumar, R. (2016). Loss of outer membrane integrity in Gram-negative bacteria by silver nanoparticles loaded with *Camellia sinensis* leaf phytochemicals: plausible mechanism of bacterial cell disintegration. *Bull. Mater. Sci.* 39, 1871–1878. doi: 10.1007/s12034-016-1317-5

Smelt, J., Rijke, A., and Hayhurst, A. (1994). Possible mechanism of high pressure inactivation of microorganisms. *High Pressure Res.* 12, 199–203.

Subires, A., Yuste, J., and Capellas, M. (2013). Flow cytometry immunodetection and membrane integrity assessment of *Escherichia coli* o157:h7 in ready-to-eat pasta salad during refrigerated storage. *Int. J. Food Microbiol.* 169, 47–56. doi: 10.1016/j.ijfoodmicro.2013.10.013

Valdramidis, V., Patterson, M., and Linton, M. (2015). Modelling the recovery of *Listeria monocytogenes* in high pressure processed simulated cured meat. *Food Control* 47, 353–358. doi: 10.1016/j.foodcont.2014.07.022

Veening, J.-W., Smits, W., and Kuipers, O. (2008). Bistability, epigenetics, and bet-hedging in bacteria. *Annu. Rev. Microbiol.* 62, 193–210. doi: 10.1146/annurev.micro.62.081307.163002

Verkman, A. (2002). Solute and macromolecule diffusion in cellular aqueous compartments. *Trends Biochem Sci.* 27, 27–33. doi: 10.1016/S0968-0004(01)02003-5

Vigouroux, A., Cordier, B., Aristov, A., Alvarez, L., Özbaykal, G., Chaze, T., et al. (2020). Class-A penicillin binding proteins do not contribute to cell shape but repair cell-wall defects. *eLife* 9:e51998. doi: 10.7554/eLife.51998

Winter, R., and Jeworrek, C. (2009). Effect of pressure on membranes. *R. Soc Ch* 5, 3157–3173. doi: 10.1039/b901690b

Wortman, A. T., and Bissonnette, G. K. (1988). Metabolic processes involved in repair of *Escherichia coli* cells damaged by exposure to acid mine water. *Appl. Environ. Microbiol.* 54, 1901–1906. doi: 10.1128/AEM.54.8.1901-1906.1988

Yang, Y., Xiang, Y., and Xu, M. (2015). From red to green: the propidium iodide-permeable membrane of *Shewanella decolorationis* S12 is repairable. *Sci. Rep.* 5:18583. doi: 10.1038/srep18583

Yu, A., Loo, J., Yu, S., and S Kong, T.-F. C. (2014). Monitoring bacterial growth using tunable resistive pulse sensing with a pore-based technique. *Appl. Microbiol. Biotechnol.* 98, 855–862. doi: 10.1007/s00253-013-5377-9

Zarnitsyn, V., Rostad, C., and Prausnitz, M. (2008). Modeling transmembrane transport through cell membrane wounds created by acoustic cavitation. *Biophys. J.* 95, 4124–4138. doi: 10.1529/biophysj.108.131664

Zhen, H., Han, T., Fennell, D. E., and Mainelis, G. (2013). Release of free DNA by membrane-impaired bacterial aerosols due to aerosolization and air sampling. *Appl. Environ. Microbiol.* 79, 7780–7789. doi: 10.1128/AEM.02859-13

Conflict of Interest: The authors declare that the research was conducted in the absence of any commercial or financial relationships that could be construed as a potential conflict of interest.

This page intentionally left blank.

Chapter 3

Gene regulation analysis of *Listeria monocytogenes* after exposure to high pressure processing

Nikparvar *et al. BMC Genomics* (2021) 22:266
https://doi.org/10.1186/s12864-021-07461-0

BMC Genomics

Research article Open Access

Analysis of temporal gene regulation of *Listeria monocytogenes* revealed distinct regulatory response modes after exposure to high pressure processing

Bahareh Nikparvar[1], Margarita Andreevskaya[2], Ilhan C. Duru[2], Florentina I. Bucur[3], Leontina Grigore-Gurgu[3], Daniela Borda[3], Anca I. Nicolau[3], Christian U. Riedel[4], Petri Auvinen[2] and Nadav Bar[1*]

Abstract

Background: The pathogen *Listeria (L.) monocytogenes* is known to survive heat, cold, high pressure, and other extreme conditions. Although the response of this pathogen to pH, osmotic, temperature, and oxidative stress has been studied extensively, its reaction to the stress produced by high pressure processing HPP (which is a preservation method in the food industry), and the activated gene regulatory network (GRN) in response to this stress is still largely unknown.

Results: We used RNA sequencing transcriptome data of *L. monocytogenes* (ScottA) treated at 400 MPa and 8°C, for 8 min and combined it with current information in the literature to create a transcriptional regulation database, depicting the relationship between transcription factors (TFs) and their target genes (TGs) in *L. monocytogenes*. We then applied network component analysis (NCA), a matrix decomposition method, to reconstruct the activities of the TFs over time. According to our findings, *L. monocytogenes* responded to the stress applied during HPP by three statistically different gene regulation modes: survival mode during the first 10 min post-treatment, repair mode during 1 h post-treatment, and re-growth mode beyond 6 h after HPP. We identified the TFs and their TGs that were responsible for each of the modes. We developed a plausible model that could explain the regulatory mechanism that *L. monocytogenes* activated through the well-studied CIRCE operon via the regulator HrcA during the survival mode.

Conclusions: Our findings suggest that the timely activation of TFs associated with an immediate stress response, followed by the expression of genes for repair purposes, and then re-growth and metabolism, could be a strategy of *L. monocytogenes* to survive and recover extreme HPP conditions. We believe that our results give a better understanding of *L. monocytogenes* behavior after exposure to high pressure that may lead to the design of a specific knock-out process to target the genes or mechanisms. The results can help the food industry select appropriate HPP conditions to prevent *L. monocytogenes* recovery during food storage.

Keywords: Gene regulatory network, *Listeria monocytogenes*, High pressure processing, Network component analysis, Transcription factor, Target gene

*Correspondence: nadi.bar@ntnu.no
[1]Department of Chemical Engineering, Norwegian University of Science and Technology, Trondheim, Norway
Full list of author information is available at the end of the article

Introduction

Extensive studies revealed how bacteria respond to various environmental stresses such as heat/cold shock, hyperosmotic and oxidative stress, nutrient depletion, acid, and antibiotics [1–4]. These studies discovered some of the gene regulatory mechanisms that allow bacteria to survive intense stresses, including those necessary for repairing damages or restoring cellular homeostasis. However, bacterial response to high pressure stress has not been studied in-depth, despite its critical role in food preservation [5–7]. High pressure processing (HPP) is considered as an alternative to thermal treatment to preserve a wide variety of ready-to-eat food products such as dry fermented meat [8]. Pathogenic *L. monocytogenes* is one of the target organisms in HPP of food due to its ability to tolerate adverse conditions such as refrigeration temperatures [9, 10]. However, some authors showed that specific strains of *L. monocytogenes* could survive high pressure levels of up to 400 MPa [11–13], although the mechanisms that allow them to survive are unknown.

Although many studies indicated bacterial growth inhibition after HPP [14, 15], we lack temporal transcriptome data to explain the activated dynamics and mechanisms in response to this stress. Unlike other stress types, very few studies focused on changes in gene expression following high pressure stress. Exposure of *Escherichia (E.) coli* to relatively low hydrostatic pressures (30 and 50 MPa) revealed regulations by several DNA-binding proteins [16]. Bowman et al. [17] performed a microarray analysis to examine the effect of HPP (400 and 600 MPa) on gene expression in *L. monocytogenes*. However, as they only performed a single measurement of gene expression after exposure to high pressure, knowledge about the temporal gene regulatory response of bacteria is still missing.

As a bacterial response to many types of stress involves similar mechanisms [18], current information about general stress response in bacteria may give a better understanding of the response to HPP. The heat shock response of *E. coli* has been studied extensively [19–22], including temporal gene expression revealing the regulatory mechanism by sigma 32. Later, it was shown in *L. monocytogenes* and some other organisms that the transcription factors (TFs) CtsR, HrcA, and CcpA regulate several genes, including those encode for chaperones (responsible for refolding denatured proteins like GroESL, DnaKJ, GrpE or degrading unfolded proteins such as protease ClpC) and heat shock proteins such as DnaKJ and GroESL [23–27]. Some authors have studied bacteria's response, including *Bacillus subtilis* or *L. monocytogenes*, to acid and antibiotics [28–34]. These studies focused on critical gene regulatory networks (GRNs) such as the two-component signal transduction system (TCS) consisting of a sensor histidine kinase and a response regulator. LisRK, LiaRS, CesRK, and AgrCA are some of the TCSs in *L. monocytogenes* that were shown to be involved in the stress response.

Here, we focused on *L. monocytogenes*, ScottA and studied how GRN in this type of bacteria responded to HPP with time. We exposed the bacteria to the high pressure of 400 MPa at $8°C$ for 8 min. We performed RNA sequencing analysis at nine time points following HPP to extract differentially expressed genes, which we have described in detail in a separate work [35]. We then created a gene regulatory database and applied statistical analysis and optimization techniques to reveal hidden GRN during 48 h after HPP. We used the network component analysis (NCA) algorithm to derive the activity profile of regulators (TFs or response regulators) in *L. monocytogenes* over time after HPP, and then clustered the regulators into three different temporal groups.

We found that the transcriptome of *L. monocytogenes* operated in three distinct time phases in response to high pressure: an early-phase (0-10 min), a mid-phase (30-60 min), and a late-time phase (6-48 h) after HPP. Most importantly, we found that the regulatory function of the first phase might be related to survival by regulating genes encoding for chaperones, cell wall structure, DNA repair, and SOS response (a global response to DNA damage to arrest the cell cycle while repairing DNA). The second time phase involved GRN with a central role in synthesizing membrane components such as transmembrane proteins. The third phase appeared to regulate functions related to energy metabolism and re-growth. Furthermore, from our analysis, we derived a model of the regulation of chaperones production by HrcA as a TF at the first minutes after pressure treatment. This model, similar to the heat shock model [36, 37], showed that the negative regulation of the chaperonin system GroESL and DnaKJ by HrcA was suppressed after pressure treatment to enable the immediate (0-10 min) expression of chaperone genes, which are critical for the survivability of bacteria under stress condition [38, 39].

This temporal GRN division indicated a well-structured and timely response to stress, suggesting that bacteria could be evolved to switch the functionality mode with a strong priority to survive stress, repair, and re-initiate growth.

Results

Predicted connectivity network

A database that includes the network information between TFs and their TGs in *L. monocytogenes* is missing. We created a connectivity network between 37 TFs and 1113 TGs in *L. monocytogenes* (Table S1). To identify the specific GRN which is involved in bacterial response to high pressure stress, we further analyzed and reduced

the network: first we created a sub-network of this curated database with 26 TFs and 678 TGs, connected by 991 edges, that satisfies the three NCA criteria (stated in "Network component analysis" section), and defines the topology matrix **A** of the NCA. Second, our results of the matrix decomposition indicated that 5% (54/991) of the connections between the TFs and TGs in our initial network were not relevant in response to high pressure stress (TGs with connectivity strength (CS) values less than 0.1 in **A**). Removing connections with CS< 0.1 resulted in a network between 26 TFs and 533 TGs (Fig. 1). The Content of the matrix **A** is given by Table S2. According to the current information in the literature that we collected as the TF-TG database and matrix **A**, these genes are associated with membrane components (129/533), cell wall (22/533), synthesis of chaperones and heat shock proteins and SOS response (32/533), virulence activity (14/533), ribosomal proteins (39/533), regulation of DNA replication and cell division (18/533), production of other transcription factors (15/533), and energy metabolism (95/533).

Temporal response of regulators following HPP

Next, we studied the temporal activities of the 26 TFs of the reduced network (Fig. 1) during the first 48 h after HPP. By running 100 simulations (No. of iterations = 100), we found that the coefficient of variation CV (ratio of the standard deviation to the mean value) for 85% of the TFs was less than 10% at most of the time points, indicating a good model consistency (Figure S1).

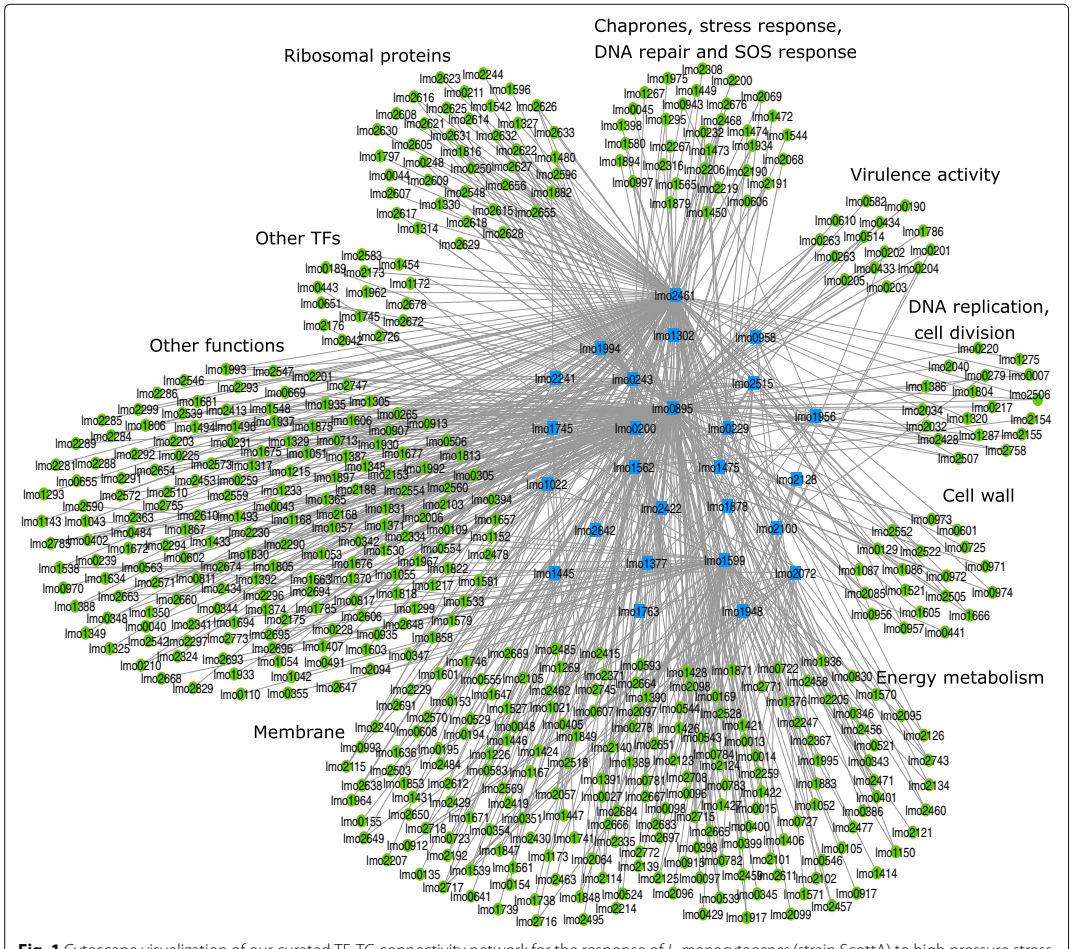

Fig. 1 Cytoscape visualization of our curated TF-TG connectivity network for the response of *L. monocytogenes* (strain ScottA) to high pressure stress. The blue squares and green circles represent TFs and TGs, respectively, clustered into nine functional groups. Each gene is marked with its locus-tag in EGD-e strain

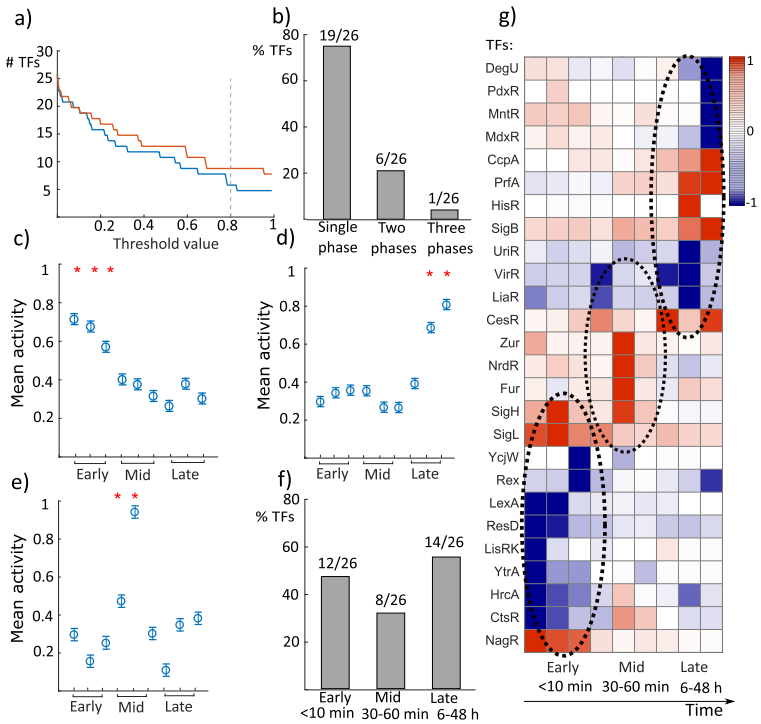

Fig. 2 TFs operate in three distinctive phases. **a** We set a threshold that defines whether a TF activity was regulated due to the exposure to high pressure at a time point to 0.8 (80% of maximum), the lowest stable value (see "Data analysis" section). Here only time point 0 (blue) and time point 48 h (red) are shown. **b** 73% of the TFs (19/26) were regulated in activity only during a single phase: either during the first 10 min (early), between 30-60 min (mid), or after 6 h (late) following HPP. 23% of the TFs (6/26) were activity-regulated during two phases, and only one TF activity was regulated for the whole duration of the experiment. **c**-**e** The mean values for activity during the first time points (0, 5, 10 min) were significantly different (ANOVA, $F(8, 90) = 7.15$, $p = 2.7 \times 10^{-7}$) from the remaining time points for the early-phase group. The mean values for TF activity during the last time points (24 and 48 h) were significantly different (ANOVA $F(8, 126) = 5.81$, $p = 2.61 \times 10^{-6}$) from the remaining time points for the late-phase group. For the TFs that were exclusively activity-regulated in the mid-phase, the mean value for TF activity was significantly different (ANOVA, $F(8, 2691) = 331.89$, $p = 0$) from the other time points. In parts c, d, and e, the y-axis represents the absolute value of the mean value for TF activity. **f** 46% of the TFs (12/26) were activity-regulated within the first 10 min after pressure stress, 31% (8/26) during the second phase, and 54% (14/26) in the last phase. **g** The TFs which belonged to the three separate phases are depicted in the temporal activity map (blue for repression and red for activation): early (0, 5, and 10 min), mid (30, 45, and 60 min), and late (6, 24, and 48 h) after HPP

We identified a list of differentially expressed genes in pressure-treated samples compared to control samples by RNA sequencing analysis [35]. As changes in gene expression levels result from changes in GRN, we concluded that TFs that regulate transcription levels of differentially expressed genes were themselves activity-regulated in response to HPP.

To investigate if a TF activity was influenced and regulated (irrespective of whether it was increased or decreased) in response to HPP compared to control, we set a threshold value found by simulations, Fig. 2a (see "Data analysis" section). We identified the TFs which were activity-regulated above that threshold (80%) for each time point compared to control. The results of the analysis were interesting: first, we found that the activities of 19/26 TFs were regulated either within the first 10 min, or 30-60 min, or 6-48 h after HPP, but not during more than one of these time groups. In contrast, the activities of 7/26 TFs were regulated in at least two time groups (Fig. 2b).

Second, we ran the analysis of variance (one-way ANOVA) and found that for the TFs that were activity-regulated during the first time points (0, 5, 10 min), the mean value (over 100 simulations) of activity was significantly different at $p < 0.05$ level (ANOVA, $F(8, 90) = 7.15$, $p = 2.7 \times 10^{-7}$) from the remaining time points (Fig. 2c). We ran the same analysis for the second (30, 45, 60 min) and third temporal groups (6, 24, 48 h). For the third group, we found a similar result (Fig. 2d), i.e., the mean value of activity for each TF that belonged to this group at $t = 24$ h and $t = 48$ h was significantly

different at $p < 0.05$ level (ANOVA, $F(8, 126) = 5.81$, $p = 2.61 \times 10^{-6}$) from the other time points. The second group contained several TFs that belonged to the first or third groups as well. By taking the TFs that were activity-regulated only during the second period, we found that the second group was also significantly different at $p < 0.05$ level (ANOVA, $F(8, 2691) = 331.89, p = 0$) from the first and third groups (Fig. 2e).

Taken together, these results suggest three clusters of TFs, grouped according to their activity profiles: TFs belonged to early-phase (0-10 min), mid-phase (30-60 min), and late-phase (6-48 h) after HPP. We found that the activities of 12/26 TFs were regulated during the early-phase, i.e., the first 10 min post-treatment (Fig. 2f). These TFs depicted the first response of bacteria to HPP and regulated the transcriptome response accordingly. 8/26 TFs were activity-regulated through the second phase or mid-phase (30-60 min), and the activities of 14/26 TFs were regulated during the late-phase, i.e., 6-48 h (note the overlap of seven TFs which were activity-regulated through more than one group). The three clusters are well-illustrated in the temporal activity map (Fig. 2g).

Next, we investigated the functionality of the TFs in each of the three phases.

The functionality of the TFs belonged to the early-phase

The map of temporal activity ratios of the TFs that were clustered in the early-phase is shown in Fig. 3a. Most of the TFs activities were negatively regulated immediately after high pressure (shown in blue). Among the TFs that belonged to the early-phase (NagR, SigL, SigH, CtsR, HrcA, YtrA, LisRK, ResD, LexA, LiaR, Rex, and YcjW), we excluded SigL, SigH, ResD, LiaR, and Rex as SigH and SigL regulate a large number of genes (based on our database and matrix **A** given by Tables S1 and S2, 177 and 73 genes, respectively) within different functional groups, ResD and Rex activity displayed a large coefficient of variation (CV) over 100 simulations (Figure S1); and LiaR was mostly involved during the late-phase (Fig. 2g). In the resulting sub-network (Fig. 3b), we revealed that 13/20 TGs are associated with the initial stress response in bacteria, including the production of heat/cold shock proteins and chaperones; biosynthesis of the cell wall, i.e., the envelope layer in Gram-positive bacteria (Firmicute); or involved in DNA repair and SOS response (Table S2). Fisher's exact test rejected the null hypothesis of non-association between having a gene related to the stress response or cell wall group and having the gene differentially expressed through the early-mode at a 5% significance level. The results may suggest that this cluster of TFs regulated TGs, which are critical for survival immediately after high pressure stress, as the regulation of chaperones and components related to the cell wall are the first line of defense in stress response [38, 39]. We collected the functional annotation of the full list of TFs and TGs that belonged to each phase and their functional groups in Table S2.

The functionality of the TFs belonged to the mid-phase

We studied the second phase of the bacterial response to HPP and found that the activities of the majority (6/8) of the TFs in this phase were regulated positively (Fig. 4a). We also examined the function of the genes that are regulated by these TFs. According to our curated TF-TG

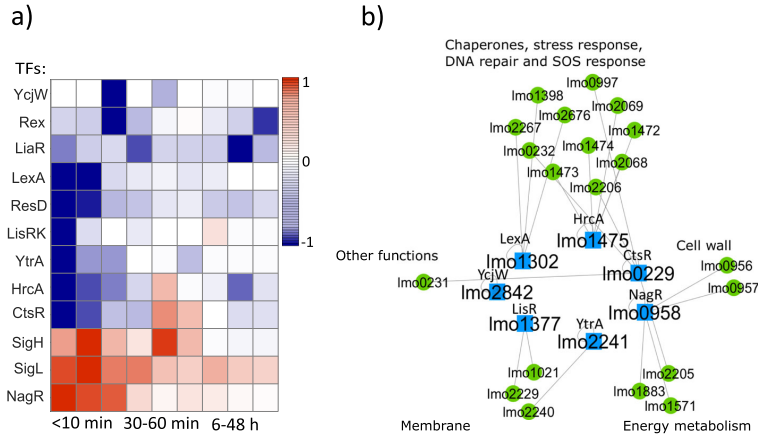

Fig. 3 According to our database and the matrix **A** (Table S2), TFs in the early-phase mostly regulated genes that encode for chaperone molecules, cell wall components, and SOS response. **a** List of TFs in the early-phase and their temporal activities. **b** The Cytoscape network shows that 65% (13/20) of the regulated genes by the TFs that belonged to the early-phase are associated with cell wall biosynthesis, chaperones production, or DNA repair and SOS response (Table S2)

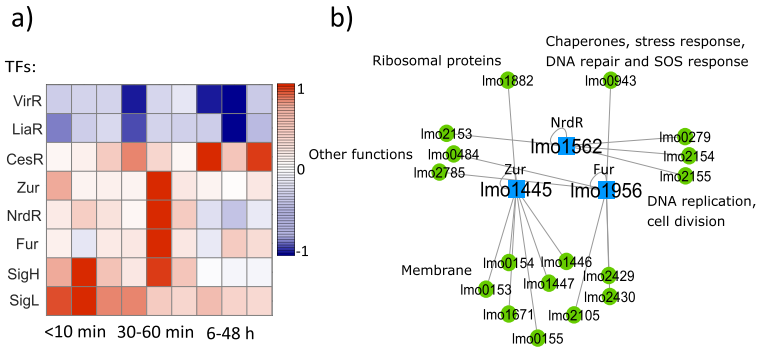

Fig. 4 According to our database and the matrix **A** (Table S2), TFs in the mid-phase mostly regulated genes that encode for membrane components. **a** Temporal activities of the TFs that belonged to the mid-phase (30-60 min after HPP). **b** 53% (9/17) of the regulated genes by the TFs NrdR, Fur, and Zur, which were exclusively clustered in the mid-phase, are associated with membrane components production such as transmembrane proteins and transporters (Table S2)

database and specifically the matrix **A** (Table S2), We found that 9/17 genes which are regulated by the TFs that exclusively belonged to this group (Fur, NrdR, and Zur) encode for the membrane components such as transmembrane proteins, Fig. 4b. Fisher's exact test showed that there is an association at a 5% significance level between being differentially expressed during the mid-phase and being related to the membrane. This can be interpreted as the presence of a recovery process in the membrane as the membrane is one of the most susceptible cell sites to pressure-induced damages [40, 41].

The functionality of the TFs belonged to the late-phase

More than half of the TFs (14/26) were involved in

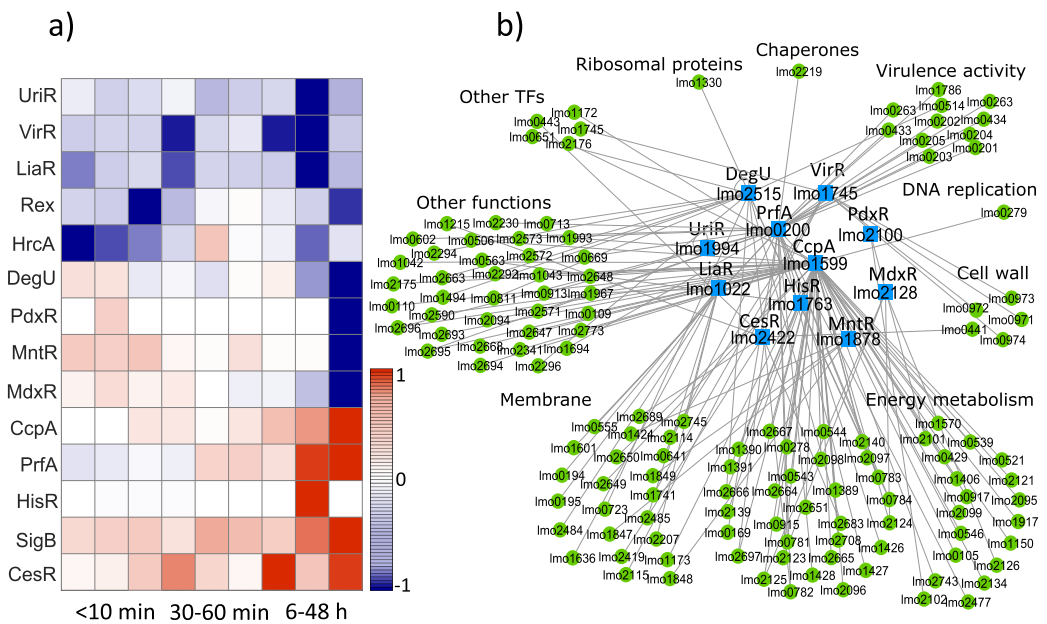

Fig. 5 According to our database and the matrix **A** (Table S2), TFs in the late-phase mostly regulated genes which are involved in energy metabolism. **a** Temporal activities of the TFs presented in the late-phase (6-48 h after HPP). **b** The Cytoscape network shows the regulatory network that acted exclusively during the late-phase. 38% (50/133) of the regulated genes in this group are involved in energy metabolism pathways (Table S2)

the late-phase, (Fig. 5a). Among this group (CesR, SigB, HisR, PrfA, CcpA, MdxR, MntR, PdxR, DegU, HrcA, Rex, LiaR, VirR, and UriR), we excluded SigB which is a well-known stress-response regulator in bacteria and regulate many genes (218 genes, Table S1); HrcA that was mostly involved in the early-phase; and Rex that displayed a large coefficient of variation (CV) over 100 simulations (Figure S1). In this phase, the remaining TFs regulate 133 genes from which 50 are involved in energy metabolism (Fig. 5b), for example by encoding for phosphotransferase (PTS) systems or different sub-components in the glycolysis pathway (Table S2). Fisher's exact test rejected the null hypothesis of non-association between having a gene related to the energy metabolism group and having the gene differentially expressed within the late-phase at a 5% significance level. This may suggest that by employing the GRN in this phase, bacteria started consuming more energy and preparing for growth and cell division again after the potential recovery process. As the time transition from the second phase (mid-phase) to the third phase (late-phase) was not abrupt (no significant statistical difference between hour 6 and mid-points, Fig. 2d), the TFs that belonged to the late-phase still regulate many genes related to the membrane components as well (Table S2).

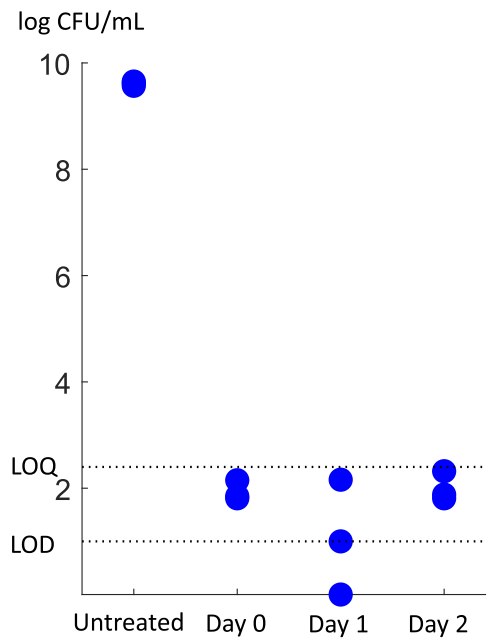

Fig. 6 Growth evaluation. We found that the number of colonies formed per each plate (non-selective medium) until the second day after HPP was less than LOQ (limit of quantification, i.e., the lower limit of acceptably accurate cell counts). Therefore, we concluded that no significant growth happened during the first two days after treatment. LOD (limit of detection) and LOQ in our plating method were 1.00 and 2.40 log CFU/ml, respectively

Discussion

Our results, that were based on time-series transcriptome data analysis using the optimization tool NCA [42] and our *L. monocytogenes* TF-TG network topology (Table S2), indicated that the regulatory network in *L. monocytogenes* strain ScottA responded to high pressure stress in three distinct phases:

1. Survival phase lasting 0-10 min after HPP, and based on our database (Table S2), regulating genes that are responsible for immediate survival and structural integrity (mostly chaperones and cell wall).
2. Repair phase, in which gene expressing enzymes and proteins related to the membrane repair were regulated during 30-60 min after HPP.
3. Pre-growth phase, in which genes that are responsible for energy metabolism and re-growth were regulated during 6-48 h after HPP.

This temporal response in three distinct phases, that may reveal the existence of a well-structured and timely mechanism embedded in bacteria to overcome stress conditions, have never been shown before for high pressure stress.

According to plating experiments for evaluating growth, we did not observe growth higher than the limit of quantification (LOQ) during the first 48 h post-treatment (Fig. 6). In accordance with [43], the generation time in *L. monocytogenes* in average lasted 13 h at pH 7 and temperature $10°C$. Therefore, it is less likely that the regulation of gene expression related to the cell wall and membrane biosynthesis and production of DNA repair proteins that we observed during the first and second phases were associated with growth and proliferation. In other words, since we did not observe any growth at the population level in the first two days after HPP, the gene expression regulations were more likely associated with the repair rather than growth, strengthening the hypothesis of the three phases.

Several previous studies support the existence of a temporally structured gene expression in bacteria in response to stress [44–46]. Veen et al. [44] showed that heat shock response of *L. monocytogenes* included upregulation of SOS response, heat shock, and cell wall associated genes during the first 3 min after heat exposure while genes encoding for cell division proteins were upregulated later. Another work [45] reported an early acid stress response followed by a later SOS response in *E. coli* after antibiotic treatment with TMP (trimethoprim). In [46], the authors showed two distinct responses during arsenic stress in *Herminiimonas arsenicoxydans*; an early (0-2 h)

response of arsenic resistance, oxidative stress, chaperone synthesis and sulfur metabolism, and a late (8 h) response of arsenic metabolism, phosphate transport and motility. These temporal regulations are consistent with our observations for the timely-ordered response of *L. monocytogenes* following HPP.

LexA is a repressor for the SOS regulon in *L. monocytogenes* which consists of genes encoding proteins associated with translesion DNA synthesis and repair [47]. Accumulation of single-stranded DNA under stress conditions results in the activation of RecA (DNA recombinase A) protein which acts as a co-protease that cleaves LexA from DNA, inducing the expression of SOS regulon [47, 48]. As shown in Fig. 3a, LexA regulator was among the TFs that were involved in the first phase of *L. monocytogenes* response to HPP by regulating the SOS response, thereby likely contributing to survival. Our NCA results showed a reduced activity for the repressor LexA over the first 10 min after pressure treatment suggesting the upregulation of LexA-regulated genes including DNA repair genes of SOS regulon. RNA sequencing results revealed upregulation of *lexA*, *recA*, and several other LexA-regulated genes such as DNA polymerase IV and V of *L. monocytogenes* after exposure to HPP at 400 MPa and 8 min [35], arguing strongly in favour of the results obtained from NCA.

According to the NCA results, the activity of CtsR protein which regulates heat shock genes negatively was suppressed in response to HPP. Nair et al. [23] demonstrated the negative regulation of stress tolerance genes such as *clpP* and *clpE* by the repressor CtsR of *L. monocytogenes*. The lower activity of CtsR that we found in the pressure-treated sample compared to the control might allow the expression of stress tolerance genes and contribute to survival of *L. monocytogenes* upon exposure to high pressure stress. Our RNA sequencing results indicated that *clpP* and *clpE* genes were upregulated during the first 10 min after HPP [35].

NagR which is a TF involved in N-acetylglucosamine utilization pathway in *L. monocytogenes* regulates the expression of *nagA* and *nagB* genes [49]. Popowska et al. [50] reported NagA (N-acetylglucosamine-6-phosphate deacetylase) as an essential enzyme for the metabolism and recycling of amino sugars and biosynthesis of cell wall. According to our results, a high activity of NagR regulator at the first 10 min after pressure treatment (Fig. 3a) could be associated with cell wall peptidoglycan and teichoic acid to repair damages in bacterial cell envelope. This result agrees with the upregulated expression of nagA and nagB genes in *L. monocytogenes* after HPP at 400 MPa and 8 min reported in [35].

Our predicted regulon for CcpA as a TF in *L. monocytogenes* included several genes encoding for PTS systems (mainly galacticol and cellbiose transporters). NCA results suggested that CcpA activity was higher in pressure-treated bacteria compared to untreated ones mainly during the late phase (Fig. 5a). The reason that the upregulation of CcpA-dependent PTS systems was delayed until the late phase, despite their role as energy metabolism source, might be due to the existence of a high number of PTS genes in *L. monocytogenes* [51] regulated by other TFs which may provide enough energy efficiently. Moreover, Stoll et al. [52] reported that *L. monocytogenes* mutants impaired in glucose, mannose and cellobiose transport could efficiently grow as the wild-type, which could be a reason for prioritized DNA, chaperonin system, and cell wall repairs and postponed upregulation of PTS system-associated genes observed in our pressure-treated *L. monocytogenes*.

Our observations suggested that the chaperonin group played a critical role in the first line of bacterial response to high pressure. Two operons (*dnaKJ* and *groESL*) encoding for molecular chaperones were identified in the previous decades as the CIRCE (controlling inverted repeat of chaperone expression) operons [36, 53]. The repressor gene *hrcA* (heat shock regulation at CIRCE) is the gene encoding for the repressor protein binding to the CIRCE element. The GroE chaperonin system is responsible for creating an equilibrium between active and inactive forms of the repressor HrcA, where the inactive form is unable to bind to its operator [36]. In the following, we proposed that the regulation of the repressor HrcA in *L. monocytogenes* might be essential during the early-phase after HPP.

The HrcA regulation network facilitated the survival phase

Negative regulation of the repressor HrcA was detected under some stress conditions such as heat shock stress and growth in nitrate [36, 54]. Hanawa et al. [55] showed that a *dnaK* mutant of *L. monocytogenes* was not able to grow neither at temperature higher than $39°C$ nor under acidic conditions, suggesting the role of the repressor HrcA in heat and acid stress resistance. Hu et al. [56] reported that deletion of the *hrcA* gene had an effect on heat resistance of *L. monocytogenes*. The activity of the repressor HrcA is modulated after heat shock by the GroE chaperonin system. In the absence of heat shock, HrcA is maintained in an active conformation able to bind to CIRCE through the GroE system. Under stress, since unfolded proteins titrate the GroE chaperonin system, it is no longer available to activate HrcA, leading to an increase in the amount of inactive repressor HrcA and transcription of the groE and dnaK operons [36, 54]. The reconstructed activity for the repressor HrcA extracted from NCA method in this work combined with the gene expression data suggested that the regulation of HrcA activity in *L. monocytogenes* was important during the first 10 min after HPP as well, i.e. during the survival phase.

Firstly, our results suggested a similar behavior following high pressure stress; An immediate increase of the expression of the chaperonin *groESL* and *dnaKJ* systems occurred during the first 10 min, expression levels that could not be mediated in the absence of pressure stress when the active repressor HrcA is present (Fig. 7a, sample points 1-3). Although during the first 10 min post-treatment, *hrcA* expression experienced a positive peak as shown in Fig. 7b, sample points 1-3, most likely no free GroE was present (being titrated by unfolded proteins damaged under pressure) such that the repressor HrcA remained inactive, results that the NCA output predicted as well (low activity for HrcA during the first 10 min, Fig. 7c, sample points 1-3). As the chaperonin proteins were expressed, free GroE proteins bound to and activated the repressor HrcA (predicted by our analysis, Fig. 7c, around 30-60 min, sample points 4-6). Active HrcA bound to the promoters of the CIRCE operon and suppressed its own expression (substantial decrease in its expression at time 30-60 min, Fig. 7b, sample points 4-6), and the expression of the chaperonin systems *groELS* and *dnaKJ* (Fig. 7a, 30-60 min, sample points 4-6). Our above findings suggested that the GRN that consists of the repressor HrcA and chaperonin system (CIRCE operon)

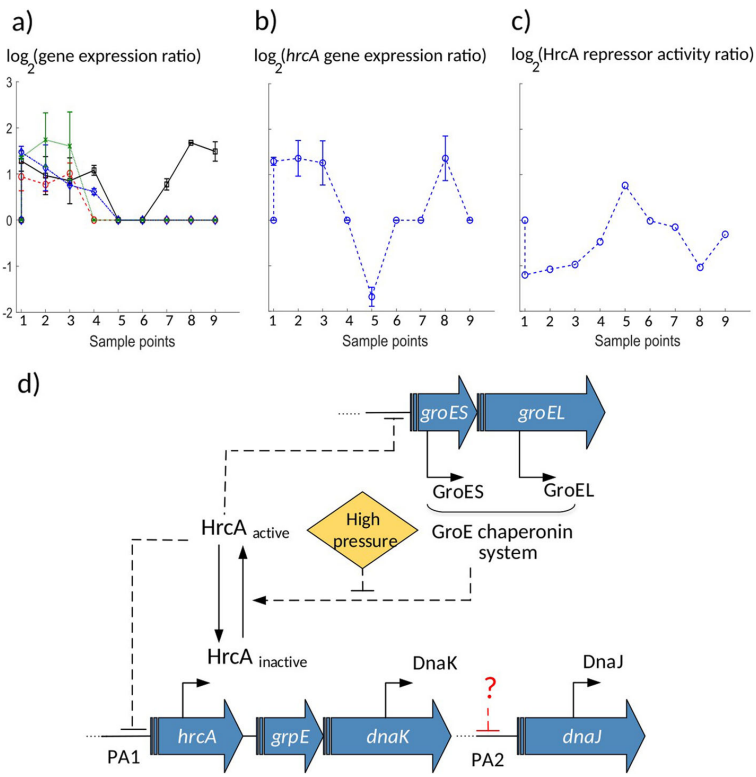

Fig. 7 The HrcA-chaperones GRN. **a** Expression levels ($\log(mRNA_{HPP}(t)/mRNA_{ctrl}(t))$) for the chaperonin genes *dnaJ* (red 'o' marks and dashed line), *dnaK* (black square marks and solid line), *groEL* (green 'x' marks and dotted line), and *groES* (blue diamond marks and dashedotted line) in *L. monocytogenes* were elevated during the first 10 min (sample points 1-3) after HPP, then suppressed to their original levels, except the *dnaK*, which was highly expressed during the later time. To make early time points distinguishable, the x-axis represents sample points for 9 time points (1-9) corresponding to 0, 5, 10, 30, 45, 60 min and 6, 24, 48 h, respectively. Error bars show the standard deviation of the three experimental replicates from the average value. **b** Expression level of the *hrcA* gene was high during the first 10 min (sample points 1-3) after pressure, followed by a suppression around 45 min (sample point 5), and elevated again during the late time (sample point 8). The x-axis is the same as part a. Error bars show the standard deviation of the three experimental replicates from the average value. In part a and b, at several time points, the p value for the fold change was higher than 0.05 (the adjusted threshold for differentially expressed genes), and therefore we set the expression ratio at those points to zero without error bars. **c** Activity of the regulator HrcA ($log(TFA_{HPP}(t)/TFA_{ctrl}(t))$ calculated by the NCA algorithm) was suppressed during the early-phase, then activated during the mid-phase, followed by another suppression at the late-phase. The x-axis is the same as part a. **d** A schematic illustration for the HrcA-chaperones GRN. Since according to part b the gene expression ratio for *hrcA* increased or remained unchanged (and not decayed) over almost all time points, the pressure effect might make HrcA not degraded but inactive that can be a reversible reaction

might mediate the ability of bacteria to survive HPP in addition to heat shock.

Recently it was shown that it is the degradation of HrcA that regulates the expression of chaperonin genes in *Mycobacterium tuberculosis* exposed to nitrate stress [57]. However, according to our analysis using NCA algorithm, three arguments suggest that it was more likely the HrcA inactivation, rather than its degradation, that modulated the expression of chaperones after HPP in *L. monocytogenes*: 1) The expression of *hrcA* (Fig. 7b) was likely suppressed by its negative self-regulation after 10 min (sample point 3), indicating the presence of the active repressor HrcA rather than its absence due to degradation. 2) The active HrcA molecules were immediately depleted to facilitate the rapid expression (Fig. 7a) of the *groESL* chaperonin system, a mechanism which would take longer by degradation pathways. 3) Our NCA model indicated the inactivation of the repressor HrcA rather than degradation, which is consistent with the measured expression levels of the *hrcA* gene (Fig. 7b,c). Taken together, we suggest that our model (Fig. 7d) likely represents the mechanism which regulated the chaperonin system following high pressure stress.

According to our observations shown in Fig. 7a, although *dnaK* and *dnaJ* belong to the same operon, the expression of *dnaJ* returned to its normal level 60 min post-treatment (sample point 6), whereas *dnaK* was highly over-expressed (compared to control) at 24 and 48 h after treatment (sample points 8, 9). This suggests that another factor than the active HrcA might regulate the transcription of *dnaJ* and switched *dnaJ* (but not *dnaK*) expression back to its normal level via a second promoter (Fig. 7d). It has been reported in the literature for *Bacillus subtilis* that the *dnaK* operon is under the control of two promoters, one (PA1) precedes the whole operon, activated under stress conditions, whereas the other (PA2) is located between *dnaK* and *dnaJ* [36]. Moreover our result is in line with cDNA sequencing results revealed the existence of a transcription start site (TSS) between *dnaK* and *dnaJ* genes in *L. monocytogenes* [58]. Some previous studies [56, 59]) identified overlapping interactions between HrcA, SigB and SigH regulons in *L. monocytogenes*. Hu et al. [56] reported an interaction between HrcA and SigB either through SigB-dependent transcription of *hrcA*, or co-regulation of other genes in HrcA regulon by SigB. Chaturongakul et al. [59] reported both HrcA and SigB as repressors for transcription of *dnaJ* and *groEL* of *L. monocytogenes*, which may again explain the difference we observed between the expression behaviour of *dnaJ* and *dnaK*. They also indicated that the expression of *groES*, in addition to HrcA, might be under control of SigB and SigH, a co-regulation that is required to be considered to improve the model in the future works.

Predictions in this work were based on an optimal model that guarantees a unique solution [42] for reconstructed activity of TFs. However, experimental evidence with deletion mutants is required in the future to verify the generated hypothesis and predictions from NCA analysis. Moreover, although our work focused only on regulation of transcription, regulation may occur at different levels, including translation, mRNA stability and protein degradation, and therefore mRNA levels may not always correlate with the proteins levels. Studies in other strains of *L. monocytogenes* such as RO15 is essential as well to understand better the role of GRN in more barotolerant strains.

Conclusions

The regulatory response of pathogenic *L. monocytogenes* to HPP is mostly unknown. Here we created a gene regulatory database (Table S1) for TF-TG connections in *L. monocytogenes* (strain ScottA), which was then used to input the NCA algorithm to reconstruct the activity of regulators (TFs) during 48 h after pressure treatment at 400 MPa, 8°, for 8 min. Our transcriptome analysis following HPP in *L. monocytogenes* indicated a timely structured response that corresponds to three distinct time phases: an early-phase (the first 10 min after HPP), which was shown to be associated with survival by regulation of genes encoding for chaperones, cell wall components, and SOS response; a mid-phase (30-60 min after HPP), which was related to the regulatory networks with the primary role in the repair of membrane components; and a late-phase (6-48 h following HPP), in which the activity of TFs which are involved in energy metabolism pathways and re-growth were regulated. Based on our observations the chaperonin group played a central role in the initial response of *L. monocytogenes* to high pressure. Therefore, we studied the regulation of this group in more detail. We proposed a model that could explain the modulation of HrcA activity after HPP, which facilitated the expression of chaperone genes in response to pressure stress. We believe that our results provide a better understanding of *L. monocytogenes* behavior after high pressure exposure that may help with the development of a specific knock-out process to target critical genes and increase the efficiency of HPP in the food industry.

Methods

High pressure processing

L. monocytogenes Scott A was statically grown in full BHI broth (Oxoid, Basingstoke Hampshire, England), at 37°*C*, until reaching the early stationary phase (≈ 1.3 OD600). The culture was then transferred to 2 mL Eppendorf tubes, which were fully filled and carefully sealed by avoiding the formation of air bubbles inside. Prior to HPP, both controls and samples to be treated were cooled-down by

storing at $4°C$ for one hour. The samples were treated at 400 MPa, $8°C$, for 8 min, in a multi-vessel high pressure equipment (Resato, Roden, the Netherlands) with the compression rate applied during pressure build-up being 100 MPa/min. The pressure-transmitting fluid was a mixture of water and propylene glycol (TR15, Resato). An additional minute, after the come-up time, was considered as the equilibration time necessary for the treatment. The decompression of vessels was carried out automatically, in less than 5 seconds. After decompression, both treated and control samples were stored at $8°C$, at atmospheric pressure (0.1 MPa), for certain times, considered as recovery time points: 5, 10, 30, 45, and 60 min and 6, 24, and 48 h. At each mentioned time point, both treated samples (5 replicates) and corresponding control samples (4 replicates) were mixed with 4 mL of RNA protect reagent (Qiagen, Hilden, Germany), for RNA stabilization, incubated at room temperature for 5 min, pelleted by centrifugation at 5000 rpm and stored at $-80°C$, until RNA extraction procedure.

Growth experiment

We measured the number of viable *L. monocytogenes* cells by using the spread plate count method before exposure to high pressure (untreated) and at days 0, 1, and 2 after HPP (400 MPa, $8°C$ for 8 min). Dilutions (in peptone saline solution: 1 g/L neutralized bacteriological peptone [Oxoid/ThermoFisher Scientific] and 8.5 g/L NaCl in water) of samples were plated on the nonselective medium tryptone soya agar supplemented with 0.6% (w/v) yeast extract (TSAYE; Oxoid/ThermoFisher Scientific) and incubated at $37°C$ for 48 h before counting.

Transcriptome analysis

RNA sequencing and analysis of the data for obtaining differentially expressed genes were described in a separate work [35]. Briefly, RNA was extracted with NucleoSpin RNA kit (Macherey-Nagel, Düren, Germany) as described previously [13]. RNA-seq libraries were prepared using QIAseq stranded Total RNA Lib kit (Qiagen) and were sequenced using NextSeq 500 (Illumina). It ended up 76 base pair (bp) single-end reads. Quality and rRNA filtering was performed using Trimmomatic v0.36 [60] and SortmeRNA v2.1b [61]. The reads were mapped to ScottA genome (GenBank: CM001159.1) using Bowtie2 [62]. HTseq v2.3.4.3 [63] was used to obtain raw gene counts. Raw counts were normalized and pairwise differential expression analysis between control and treated samples was performed using DESeq2 [64]. The threshold for differentially expressed genes was set adjusted, p-value $\leq$ 0.05 and $\log_2$ fold change ($\log_2$ FC) $\geq$ 0.6. Normalized read counts and $\log_2$ FC data were used for analysis. RNA-seq data is available in the European Nucleotide Archive (ENA) under accession code PRJEB34771.

Building a database of TF-TG for *L. monocytogenes*

We built a connectivity network (Table S1) for *L. monocytogenes* EGD-e connecting 37 TFs and 1113 TGs, mainly using the current information in the Regprecise database [49] and some published articles [28, 30, 32, 59, 65–70]. We predicted the regulons in *L. monocytogenes* EGD-e for three TFs (Rex, CtsR, and CcpA) by verifying binding sites (BS) using a comparative genomics approach. We took six complete genomes of different *Listeria* species/subspecies (including EGD-e) and *Bacilli* TFBS (transcription factor binding sites) profiles for the three TFs mentioned above. First, we predicted homologs in all the genomes using GET_HOMOLOGUES [71]. Then, upstream regions (up to 300 bps) of genes in all the genomes were searched for the presence of TFBS using the *Bacilli* TFBS profiles and the FIMO tool (MEME suite [72]) with the q-value (adjusted p-value) threshold of 0.05 and with the account of genome background HMM. For each TF, genes in EGD-e strain with BS that had homologs with BS in at least two other genomes were pre-selected (conserved BS) and manually reviewed to choose genes that are predicted to be either part of the corresponding *Bacilli* regulons or other species (based on the RegPrecise database and literature mentioned above) or have a relevant function (related to the TF in question). The upstream regions of the pre-selected genes were used to create a new *Listeria* specific TFBS profile, which was then used to search the genomes again, presumably giving more accurate results. Again, only the genes in EGD-e strain with BS that had homologs with BS in at least two other genomes were selected for the final list of regulons in EGD-e strain. Predicted regulons for the three mentioned TFs is given by Table S1.

Network component analysis

We employed Network Component Analysis (NCA) [73, 74] to predict the activities of TFs/response regulators in *L. monocytogenes* following HPP. The NCA solves a matrix decomposition problem presented as:

$$\mathbf{E}(t) = \mathbf{A} \cdot \mathbf{P}(t). \tag{1}$$

, where the matrix $\mathbf{E}$ is the differentially expressed gene values, i.e. $\log_2$ FC for each gene, $\log_2(mRNA_{HPP}(t)/mRNA_{ctrl}(t))$, at different recovery time points obtained from RNA sequencing experiments. $mRNA_{HPP}(t)$ and $mRNA_{ctrl}(t)$ are mRNA counts in pressure-treated and control sample, respectively. In this matrix, each row corresponds to one TG, and each column corresponds to one time point (nine time points in our case: 0, 5, 10, 30, 45, and 60 min and 6, 24, and 48 h after HPP). We used our curated connectivity network (Table S1) to build a connectivity matrix $\mathbf{A}$ which gives the strength of regulation in the expression of each TG

by each TF. In the matrix **A**, each row corresponds to one TG, and each column corresponds to one TF. The Content of the matrix **A** is given by Table S2. We used the differentially expressed gene matrix (**E**) and a random initial guess for the matrix **A** that preserves the null space of this connectivity matrix as inputs to the NCA algorithm. The algorithm then predicts a number as the CS between each regulatory layer (TF) and its TG (matrix **A**), as well as the matrix **P**, the reconstructed activity for TFs over time, $log(TFA_{HPP}(t)/TFA_{ctrl}(t))$ (where TFA is TF activity). In the matrix **P**, each row represents one TF, and each column represents one time point. The dimensions of **E**, **A**, and **P**, are $N \times M$, $N \times L$, and $L \times M$, respectively, where N is the number of TGs, M is the number of time points, and L is the number of TFs.

The decomposition problem in Eq. 1 is a bilinear optimization problem and can be solved numerically by minimizing the Frobenius norm of $\mathbf{E} - \mathbf{AP}$:

$$min||\mathbf{E} - \mathbf{AP}||_F \; s.t. \mathbf{A} \in \mathbf{Z_A}, \quad \text{where } \mathbf{Z_A} = \left\{\mathbf{A} \in \mathbf{R}^{N \times L} | a_{ij} = 0\right\}. \tag{2}$$

The decomposition of **E** to **A** and **P** is unique up to a scaling factor **X** if **A** and **P** satisfy a set of mathematical criteria [42]:

1. The connectivity matrix **A** must be full-rank in columns.
2. When we remove a TF with all the TGs connected to it, the remaining sub-network must have a connectivity matrix **A** which is still full-rank in columns.
3. The matrix **P** must be full-rank in rows. To satisfy the third criterion, the number of time points for each gene must be greater than or equal to the number of TFs regulating that gene. This criterion was not valid in our case, and therefore we used a modified NCA algorithm [74] that allows signal extraction based on relatively few data points.

Our connectivity network contains the information about 37 TFs and their TGs from which we extracted the matrix **A** with L=26 TFs and N=678 TGs such that the three criteria above are satisfied. To initialize the **A** matrix, we defined a set of constraints such that if TG_i is positively (negatively) regulated by TF_j, $a_{ij} = 1$ ($a_{ij} = -1$), and if TG_i is not regulated by TF_j, $a_{ij} = 0$ ($j = \{1, ..., L\}$ and $i = \{1, ..., N\}$). We used the software Cytoscape [75] to illustrate the connectivity network of TFs-TGs (Fig. 1). We grouped TGs into 9 groups according to the functional annotations we found for each gene of EGD-e strain using the Uniprot database [76]. The gene expression matrix **E** contains expression values for 678 genes over nine time points.

Data analysis

We used the software Matlab (Mathworks Inc) to run the NCA algorithm and the analysis of variance (ANOVA). The homoscedasticity and normality condition were checked. The activity matrix **P** contains normalized units of 26 TFs at nine time points, all relative to the control. We normalized the activity of each TF (rows of **P**) at each time point (columns of **P**) to its maximum level. We defined that the activity of a TF_j at any given time point t_k in the normalized matrix **P** ($j = \{1, ..., L\}$, $L = 26$ and $k = \{1, ..., M\}$, $M = 9$) was regulated (either activated or suppressed) when the absolute value in that time point in the matrix **P** exceeds a cut-off value. To determine this cut-off value, we increased threshold values incrementally (at steps of 0.01) and counted, at each time t_k, the number of TFs with activity values above this threshold. Then at each time point t_k, $k = \{1, ..., M\}$ we chose a threshold that reached a stable number of TFs, and computed the average of these thresholds over time. By doing so, we set a cut-off value of 0.8 to represent a stable threshold (see Fig. 2a).

Abbreviations

L. monocytogenes: *Listeria monocytogenes*; HPP: High pressure processing; TF: Transcription factor; TG: Target gene; GRN: Gene regulatory network; NCA: Network component analysis; TFA: TF activity; CS: Connectivity strength; CV: Coefficient of variation; BS: Binding site; TFBS: Transcription factor binding site; CIRCE: Controlling inverted repeat of chaperone expression; LOQ: Limit of quantification; LOD: Limit of detection

Supplementary Information

The online version contains supplementary material available at https://doi.org/10.1186/s12864-021-07461-0.

Additional file 1: Table S1 (.xls format): TF-TG network in *L. monocytogenes*.

Additional file 2: Figure S1 (.pdf format): TF activity (TFA) ratio. Error bars show the mean and standard deviation of TFA at each time point over 100 simulations. To make early time points distinguishable, the x-axis represents sample points for 9 time points (1-9) corresponding to 0, 5, 10, 30, 45, 60 min and 6, 24, 48 h, respectively.

Additional file 3: Table S2 (.xls format): Content of the matrix **A** with connectivity strength (CS) values for each TF-TG connection.

Acknowledgements

The authors wish to acknowledge Alicia Subires and Marta Capellas at the Autonomous University of Barcelona for help in running growth experiments.

Authors' contributions

NB and BN conceptualized the study. BN, MA, and CUR built the TF-TG dataset. BN and NB did the NCA and statistical analysis. ICD and BN did the Cytoscape visualization. FIB, LGG, DB, and AIN collected the samples and performed the pressure treatments. NB, BN, MA, ICD, and FIB drafted the manuscript. NB supervised the work. All authors have read, commented and approved the manuscript.

Funding

This study was supported within the ERA-IB2 consortium "SafeFood" (ID: ERA712IB-16- 247 014) by grants of the the Research Council of Norway (to NB,

grant number 263499), the Academy of Finland (to PA, grant numbers 311717, 307856); the Executive Agency for Higher Education, Research, Development and Innovation Funding in Romania (to AIN, International and European Cooperation–250 Subprogramme 3.2–Horizon 2020–Contract No. 15/2017), and the German Ministry for Education and Research (to CUR, grant number: 031B0268). The funders had no role in the design of the study and collection, analysis, and interpretation of data and in writing the manuscript.

Availability of data and materials
RNA sequencing data have been deposited in the European Nucleotide Archive (ENA) under accession code PRJEB34771.

Declarations

Ethics approval and consent to participate
Not applicable.

Consent for publication
Not applicable.

Competing interests
The authors declare that they have no competing interests.

Author details
[1]Department of Chemical Engineering, Norwegian University of Science and Technology, Trondheim, Norway. [2]Institute of Biotechnology, University of Helsinki, Helsinki, Finland. [3]Faculty of Food Science and Engineering, Dunarea de Jos University of Galati, Galati, Romania. [4]Institute of Microbiology and Biotechnology, Ulm University, Ulm, Germany.

Received: 2 December 2020 Accepted: 10 February 2021
Published online: 14 April 2021

References

1. Roncarati D, Scarlato V. Regulation of heat-shock genes in bacteria: from signal sensing to gene expression output. FEMS Microbiol Rev. 2017;41(4):549–74. https://doi.org/10.1093/femsre/fux015.
2. Battesti A, Majdalani N, Gottesman S. The RpoS-mediated general stress response in *Escherichia coli*. Ann Rev Microbiol. 2011;65(1):189–213. https://doi.org/10.1146/annurev-micro-090110-102946.
3. Cotter PD, Hill C. Surviving the acid test: Responses of Gram-positive bacteria to low pH. Microbiol Mol Biol Rev. 2003;67(3):429–53. https://doi.org/10.1128/mmbr.67.3.429-453.2003.
4. Goh E-B, Yim G, Tsui W, McClure J, Surette MG, Davies J. Transcriptional modulation of bacterial gene expression by subinhibitory concentrations of antibiotics. Proc Natl Acad Sci. 2002;99(26):17025–30. https://doi.org/10.1073/pnas.252607699.
5. Cheftel JC. Review : High-pressure, microbial inactivation and food preservation. Food Sci Technol Int. 1995;1(2-3):75–90. https://doi.org/10.1177/108201329500100203.
6. Monteiro MLG, Mársico ET, Mano SB, Alvares TS, Rosenthal A, Lemos M, Ferrari E, Lázaro CA, Conte-Junior CA. Combined effect of high hydrostatic pressure and ultraviolet radiation on quality parameters of refrigerated vacuum-packed tilapia (*Oreochromis niloticus*) fillets. Sci Rep. 2018;8(1):. https://doi.org/10.1038/s41598-018-27861-9.
7. Heinz V, Buckow R. Food preservation by high pressure. J Verbr Lebensm. 2009;5(1):73–81. https://doi.org/10.1007/s00003-009-0311-x.
8. Neetoo H, Chen H. Application of high hydrostatic pressure technology for processing and preservation of foods. In: Bhat R, Alias AK, Paliyath G, editors. Progress in Food Preservation, vol. 1. 1st edn. New Jersey: Wiley; 2012. p. 247–76.
9. Hill C, Cotter PD, Sleator RD, Gahan CGM. Bacterial stress response in *Listeria monocytogenes*: jumping the hurdles imposed by minimal processing. Int Dairy J. 2002;12(2-3):273–83. https://doi.org/10.1016/s0958-6946(01)00125-x.
10. Bucur FI, Grigore-Gurgu L, Crauwels P, Riedel CU, Nicolau AI. Resistance of *Listeria monocytogenes* to stress conditions encountered in food and food processing environments. Front Microbiol. 2018;9:. https://doi.org/10.3389/fmicb.2018.02700.
11. Bozoglu F, Alpas H, Kaletunç G. Injury recovery of foodborne pathogens in high hydrostatic pressure treated milk during storage. FEMS Immunol Med Microbiol. 2004;40(3):243–7. https://doi.org/10.1016/s0928-8244(04)00002-1.
12. Ferreira M, Almeida A, Delgadillo I, Saraiva J, Cunha Â. Susceptibility of *Listeria monocytogenes* to high pressure processing: A review. Food Rev Int. 2015;32(4):377–99. https://doi.org/10.1080/87559129.2015.1094816.
13. Duru IC, Andreevskaya M, Laine P, Rode TM, Ylinen A, Løvdal T, Bar N, Crauwels P, Riedel CU, Bucur FI, Nicolau AI, Auvinen P. Genomic characterization of the most barotolerant *Listeria monocytogenes* RO15 strain compared to reference strains used to evaluate food high pressure processing. BMC Genom. 2020;21(455):. https://doi.org/10.1080/87559129.2015.1094816.
14. Bover-Cid S, Belletti N, Garriga M, Aymerich T. Model for *Listeria monocytogenes* inactivation on dry-cured ham by high hydrostatic pressure processing. Food Microbiol. 2011;28(4):804–9. https://doi.org/10.1016/j.fm.2010.05.005.
15. Rubio B, Possas A, Rincón F, García-Gímeno RM, Martínez B. Model for *Listeria monocytogenes* inactivation by high hydrostatic pressure processing in spanish chorizo sausage. Food Microbiol. 2018;69:18–24. https://doi.org/10.1016/j.fm.2017.07.012.
16. Ishii A, Oshima T, Sato T, Nakasone K, Mori H, Kato C. Analysis of hydrostatic pressure effects on transcription in *Escherichia coli* by DNA microarray procedure. Extremophiles. 2004;9(1):65–73. https://doi.org/10.1007/s00792-004-0414-3.
17. Bowman JP, Bittencourt CR, Ross T. Differential gene expression of *Listeria monocytogenes* during high hydrostatic pressure processing. Microbiology. 2008;154(2):462–75. https://doi.org/10.1099/mic.0.2007/010314-0.
18. Gottesman S. Trouble is coming: Signaling pathways that regulate general stress responses in bacteria. J Biol Chem. 2019;294(31):11685–700. https://doi.org/10.1074/jbc.rev119.005593.
19. Straus DB, Walter WA, Gross CA. The heat shock response of *E. coli* is regulated by changes in the concentration of σ^{32}. Nature. 1987;329(6137):348–51. https://doi.org/10.1038/329348a0.
20. Zhou YN, Kusukawa N, Erickson JW, Gross CA, Yura T. Isolation and characterization of *Escherichia coli* mutants that lack the heat shock sigma factor sigma 32. Journal of Bacteriology. 1988;170(8):3640–9. https://doi.org/10.1128/jb.170.8.3640-3649.1988.
21. Nagai H, Yuzawa H, Yura T. Regulation of the heat shock response in *E coli*: involvement of positive and negative *cis*-acting elements in translational control of σ^{32} synthesis. Biochimie. 1991;73(12):1473–9. https://doi.org/10.1016/0300-9084(91)90180-9.
22. Guisbert E. A chaperone network controls the heat shock response in *E. coli*. Genes Dev. 2004;18(22):2812–21. https://doi.org/10.1101/gad.1219204.
23. Nair S, Derre I, Msadek T, Gaillot O, Berche P. CtsR controls class III heat shock gene expression in the human pathogen *Listeria monocytogenes*. Mol Microbiol. 2000;35(4):800–11. https://doi.org/10.1046/j.1365-2958.2000.01752.x.
24. Derre I, Rapoport G, Msadek T. CtsR, a novel regulator of stress and heat shock response, controls *clp* and molecular chaperone gene expression in Gram-positive bacteria. Mol Microbiol. 1999;31(1):117–31. https://doi.org/10.1046/j.1365-2958.1999.01152.x.
25. Schulz A, Schumann W. *hrcA*, the first gene of the *Bacillus subtilis dnak* operon encodes a negative regulator of class I heat shock genes. J Bacteriol. 1996;178(4):1088–93. https://doi.org/10.1128/jb.178.4.1088-1093.1996.
26. Minder AC, Fischer H-M, Hennecke H, Narberhaus F. Role of HrcA and CIRCE in the heat shock regulatory network of *Bradyrhizobium japonicum*. J Bacteriol. 2000;182(1):14–22. https://doi.org/10.1128/jb.182.1.14-22.2000.
27. Castaldo C, Siciliano RA, Muscariello L, Marasco R, Sacco M. CcpA affects expression of the *groESL* and *dnak* operons in *Lactobacillus plantarum*. Microb Cell Factories. 2006;5(1):. https://doi.org/10.1186/1475-2859-5-35.
28. Cotter PD, Guinane CM, Hill C. The LisRK signal transduction system determines the sensitivity of *Listeria monocytogenes* to Nisin and Cephalosporins. Antimicrob Agents Chemother. 2002;46(9):2784–90. https://doi.org/10.1128/aac.46.9.2784-2790.2002.
29. Mascher T, Zimmer SL, Smith T-A, Helmann JD. Antibiotic-inducible promoter regulated by the cell envelope stress-sensing two-component

system LiaRS of *Bacillus subtilis*. Antimicrob Agents Chemother. 2004;48(8):2888–96. https://doi.org/10.1128/aac.48.8.2888-2896.2004.
30. Nielsen PK, Andersen AZ, Mols M, Veen S, Abee T, Kallipolitis BH. Genome-wide transcriptional profiling of the cell envelope stress response and the role of LisRK and CesRK in *Listeria monocytogenes*. Microbiology. 2012;158(4):963–74. https://doi.org/10.1099/mic.0.055467-0.
31. Ohki R, Giyanto, Tateno K, Masuyama W, Moriya S, Kobayashi K, Ogasawara N. The BceRS two-component regulatory system induces expression of the bacitracin transporter, BceAB, in *Bacillus subtilis*. Mol Microbiol. 2003;49(4):1135–44. https://doi.org/10.1046/j.1365-2958.2003.03653.x.
32. Fritsch F, Mauder N, Williams T, Weiser J, Oberle M, Beier D. The cell envelope stress response mediated by the LiaFSR$_{Lm}$ three-component system of *Listeria monocytogenes* is controlled via the phosphatase activity of the bifunctional histidine kinase LiaS$_{Lm}$. Microbiology. 2011;157(2):373–86. https://doi.org/10.1099/mic.0.044776-0.
33. Kallipolitis BH, Ingmer H, Gahan CG, Hill C, Søgaard-Andersen L. CesRK, a two-component signal transduction system in *Listeria monocytogenes*, responds to the presence of cell wall-acting antibiotics and affects β-lactam resistance. Antimicrob Agents Chemother. 2003;47(11):3421–9. https://doi.org/10.1128/aac.47.11.3421-3429.2003.
34. Garmyn D, Augagneur Y, Gal L, Vivant A-L, Piveteau P. *Listeria monocytogenes* differential transcriptome analysis reveals temperature-dependent Agr regulation and suggests overlaps with other regulons. PLOS ONE. 2012;7(9):43154. https://doi.org/10.1371/journal.pone.0043154.
35. Duru IC, Bucur FI, Andreevskaya M, Nikparvar B, Ylinen A, Grigore-Gurgu L, Rode TM, Crauwels P, Laine P, Paulin L, Løvdal T, Riedel CU, Bar N, Borda D, Nicolau AI, Auvinen P. High-pressure processing-induced transcriptome response during recovery of *Listeria monocytogenes*. BMC Genom. 2021;22(117). https://doi.org/10.1186/s12864-021-07407-6.
36. Schumann W. The *Bacillus subtilis* heat shock stimulon. Cell Stress Chaperones. 2003;8(3):207. https://doi.org/10.1379/1466-1268(2003)008.
37. Mogk A. The GroE chaperonin machine is a major modulator of the CIRCE heat shock regulon of *Bacillus subtilis*. EMBO J. 1997;16(15):4579–90. https://doi.org/10.1093/emboj/16.15.4579.
38. Hartl FU, Bracher A, Hayer-Hartl M. Molecular chaperones in protein folding and proteostasis. Nature. 2011;475(7356):324–32. https://doi.org/10.1038/nature10317.
39. Kumar A, Balbach J. Targeting the molecular chaperone SlyD to inhibit bacterial growth with a small molecule. Sci Rep. 2017;7(1):. https://doi.org/10.1038/srep42141.
40. Pagán R, Mackey B. Relationship between membrane damage and cell death in pressure-treated *Escherichia coli* cells: differences between exponential- and stationary-phase cells and variation among strains. Appl Environ Microbiol. 2000;66(7):2829–34. https://doi.org/10.1128/aem.66.7.2829-2834.2000.
41. Klotz B, Mañas P, Mackey BM. The relationship between membrane damage, release of protein and loss of viability in *Escherichia coli* exposed to high hydrostatic pressure. Int J Food Microbiol. 2010;137(2-3):214–20. https://doi.org/10.1016/j.ijfoodmicro.2009.11.020.
42. Liao JC, Boscolo R, Yang Y-L, Tran LM, Sabatti C, Roychowdhury VP. Network component analysis: Reconstruction of regulatory signals in biological systems. Proc Natl Acad Sci. 2003;100(26):15522–27. https://doi.org/10.1073/pnas.2136632100.
43. Begot C, Lebert I, Lebert A. Variability of the response of 66 *Listeria monocytogenes* and *Listeria innocua* strains to different growth conditions. Food Microbiol. 1997;14(5):403–12. https://doi.org/10.1006/fmic.1997.0097.
44. Veen S, Hain T, Wouters JA, Hossain H, Vos WM, Abee T, Chakraborty T, Wells-Bennik MHJ. The heat-shock response of *Listeria monocytogenes* comprises genes involved in heat shock, cell division, cell wall synthesis, and the SOS response. Microbiology. 2007;153(10):3593–607. https://doi.org/10.1099/mic.0.2007/006361-0.
45. Mitosch K, Rieckh G, Bollenbach T. Noisy response to antibiotic stress predicts subsequent single-cell survival in an acidic environment. Cell Syst. 2017;4(4):393–4035. https://doi.org/10.1016/j.cels.2017.03.001.
46. Cleiss-Arnold J, Koechler S, Proux C, Fardeau M-L, Dillies MA, Coppee JY, Arsène-Ploetze F, Bertin PN. Temporal transcriptomic response during arsenic stress in *Herminiimonas arsenicoxydans*. BMC Genom. 2010;11(1):709. https://doi.org/10.1186/1471-2164-11-709.
47. Veen S, Schalkwijk S, Molenaar D, Vos WM, Abee T, Wells-Bennik MHJ. The SOS response of *Listeria monocytogenes* is involved in stress resistance and mutagenesis. Microbiology. 2010;156(2):374–84. https://doi.org/10.1099/mic.0.035196-0.
48. Simmons LA, Cohen SE, Foti JJ, Walker GC. The SOS regulatory network. EcoSal Plus. 2008;3(1):. https://doi.org/10.1128/ecosalplus.5.4.3.
49. Novichkov PS, Laikova ON, Novichkova ES, Gelfand MS, Arkin AP, Dubchak I, Rodionov DA. RegPrecise: a database of curated genomic inferences of transcriptional regulatory interactions in prokaryotes. Nucleic Acids Res. 2009;38(suppl_1):111–8. https://doi.org/10.1093/nar/gkp894.
50. Popowska M, Osińska M, Rzeczkowska M. N-acetylglucosamine-6-phosphate deacetylase (NagA) of *Listeria monocytogenes* EGD, an essential enzyme for the metabolism and recycling of amino sugars. Arch Microbiol. 2011;194(4):255–68. https://doi.org/10.1007/s00203-011-0752-3.
51. Glaser P, Frangeul L, Buchrieser C, Rusniok C, Amend A, Baquero F, et al. Comparative genomics of *Listeria* species. Science. 2001;294(5543):849–52. https://doi.org/10.1126/science.1063447.
52. Stoll R, Goebel W. The major PEP-phosphotransferase systems (PTSs) for glucose, mannose and cellobiose of *Listeria monocytogenes*, and their significance for extra- and intracellular growth. Microbiology. 2010;156(4):1069–83. https://doi.org/10.1099/mic.0.034934-0.
53. Chaturongakul S, Raengpradub S, Wiedmann M, Boor KJ. Modulation of stress and virulence in *Listeria monocytogenes*. Trends Microbiol. 2008;16(8):388–96. https://doi.org/10.1016/j.tim.2008.05.006.
54. Reischl S, Wiegert T, Schumann W. Isolation and analysis of mutant alleles of the *Bacillus subtilis* HrcA repressor with reduced dependency on GroE function. J Biol Chem. 2002;277(36):32659–67. https://doi.org/10.1074/jbc.m201372200.
55. Hanawa T, Fukuda M, Kawakami H, Hirano H, Kamiya S, Yamamoto T. The *Listeria monocytogenes* Dnak chaperone is required for stress tolerance and efficient phagocytosis with macrophages. Cell Stress Chaperones. 1999;4(2):118–28.
56. Hu Y, Oliver HF, Raengpradub S, Palmer ME, Orsi RH, Wiedmann M, Boor KJ. Transcriptomic and phenotypic analyses suggest a network between the transcriptional regulators HrcA and σ^B in *Listeria monocytogenes*. Appl Environ Microbiol. 2007;73(24):7981–91. https://doi.org/10.1128/aem.01281-07.
57. Becker SH, Jastrab JB, Dhabaria A, Chaton CT, Rush JS, Korotkov KV, Ueberheide B, Darwin KH. The *Mycobacterium tuberculosis* pup-proteasome system regulates nitrate metabolism through an essential protein quality control pathway. Proc Natl Acad Sci. 2019;116(8):3202–10. https://doi.org/10.1073/pnas.1819468116.
58. Wurtzel O, Sesto N, Mellin JR, Karunker I, Edelheit S, Bécavin C, Archambaud C, Cossart P, Sorek R. Comparative transcriptomics of pathogenic and non-pathogenic *Listeria* species. Mol Syst Biol. 2012;8(1):583. https://doi.org/10.1038/msb.2012.11.
59. Chaturongakul S, Raengpradub S, Palmer ME, Bergholz TM, Orsi RH, Hu Y, Ollinger J, Wiedmann M, Boor KJ. Transcriptomic and phenotypic analyses identify coregulated, overlapping regulons among PrfA, CtsR, HrcA, and the alternative sigma factors σ^B, σ^C, σ^H, and σ^L in *Listeria monocytogenes*. Appl Environ Microbiol. 2010;77(1):187–200. https://doi.org/10.1128/aem.00952-10.
60. Bolger AM, Lohse M, Usadel B. Trimmomatic: a flexible trimmer for illumina sequence data. Bioinformatics. 2014;30(15):2114–20. https://doi.org/10.1093/bioinformatics/btu170.
61. Kopylova E, Noé L, Touzet H. SortMeRNA: fast and accurate filtering of ribosomal RNAs in metatranscriptomic data. Bioinformatics. 2012;28(24):3211–7. https://doi.org/10.1093/bioinformatics/bts611.
62. Langmead B, Salzberg SL. Fast gapped-read alignment with bowtie 2. Nat Methods. 2012;9(4):357–9. https://doi.org/10.1038/nmeth.1923.
63. Anders S, Pyl PT, Huber W. HTSeq–a python framework to work with high-throughput sequencing data. Bioinformatics. 2014;31(2):166–9. https://doi.org/10.1093/bioinformatics/btu638.
64. Love MI, Huber W, Anders S. Moderated estimation of fold change and dispersion for RNA-seq data with DESeq2. Genome Biol. 2014;15(12):. https://doi.org/10.1186/s13059-014-0550-8.

65. Larsen MH, Kallipolitis BH, Christiansen JK, Olsen JE, Ingmer H. The response regulator ResD modulates virulence gene expression in response to carbohydrates in *Listeria monocytogenes*. Mol Microbiol. 2006;61(6):1622–35. https://doi.org/10.1111/j.1365-2958.2006.05328.x.
66. Riedel CU, Monk IR, Casey PG, Waidmann MS, Gahan CGM, Hill C. AgrD-dependent quorum sensing affects biofilm formation, invasion, virulence and global gene expression profiles in *Listeria monocytogenes*. Mol Microbiol. 2009;71(5):1177–89. https://doi.org/10.1111/j.1365-2958.2008.06589.x.
67. Mandin P, Fsihi H, Dussurget O, Vergassola M, Milohanic E, Toledo-Arana A, Lasa I, Johansson J, Cossart P. VirR, a response regulator critical for *Listeria monocytogenes* virulence. Mol Microbiol. 2005;57(5):1367–80. https://doi.org/10.1111/j.1365-2958.2005.04776.x.
68. Hain T, Hossain H, Chatterjee SS, Machata S, Volk U, Wagner S, Brors B, Haas S, Kuenne CT, Billion A, Otten S, Pane-Farre J, Engelmann S, Chakraborty T. Temporal transcriptomic analysis of the *Listeria monocytogenes* EGD-e σ^B regulon. BMC Microbiol. 2008;8(1):20. https://doi.org/10.1186/1471-2180-8-20.
69. Milohanic E, Glaser P, Coppée J-Y, Frangeul L, Vega Y, Vázquez-Boland JA, Kunst F, Cossart P, Buchrieser C. Transcriptome analysis of *Listeria monocytogenes* identifies three groups of genes differently regulated by PrfA. Mol Microbiol. 2003;47(6):1613–25. https://doi.org/10.1046/j.1365-2958.2003.03413.x.
70. Williams T, Joseph B, Beier D, Goebel W, Kuhn M. Response regulator DegU of *Listeria monocytogenes* regulates the expression of flagella-specific genes. FEMS Microbiol Lett. 2005;252(2):287–98. https://doi.org/10.1016/j.femsle.2005.09.011.
71. Contreras-Moreira B, Vinuesa P. GET_HOMOLOGUES, a versatile software package for scalable and robust microbial pangenome analysis. Appl Environ Microbiol. 2013;79(24):7696–701. https://doi.org/10.1128/aem.02411-13.
72. Bailey TL, Boden M, Buske FA, Frith M, Grant CE, Clementi L, Ren J, Li WW, Noble WS. MEME SUITE: tools for motif discovery and searching. Nucleic Acids Res. 2009;37(Web Server):202–8. https://doi.org/10.1093/nar/gkp335.
73. Tran LM, Brynildsen MP, Kao KC, Suen JK, Liao JC. gNCA: A framework for determining transcription factor activity based on transcriptome: identifiability and numerical implementation. Metab Eng. 2005;7(2):128–41. https://doi.org/10.1016/j.ymben.2004.12.001.
74. Galbraith SJ, Tran LM, Liao JC. Transcriptome network component analysis with limited microarray data. Bioinformatics. 2006;22(15):1886–94. https://doi.org/10.1093/bioinformatics/btl279.
75. Shannon P. Cytoscape: A software environment for integrated models of biomolecular interaction networks. Genome Res. 2003;13(11):2498–504. https://doi.org/10.1101/gr.1239303.
76. Consortium TU. UniProt: a worldwide hub of protein knowledge. Nucleic Acids Res. 2018;47(D1):506–15. https://doi.org/10.1093/nar/gky1049.

Publisher's Note

Chapter 4

An integrated model for the early response of bacteria to high pressure processing

This paper is awaiting publication and is not included in NTNU Open

Chapter 5

Discussion

The main purpose of this Ph.D. project was to find answers for the three research questions mentioned in chapter 1. In this section, we summarize our approach to address these questions.

5.1 Response of bacterial membrane to high pressure processing

Research question 1. *What is the impact of HPP on the bacterial membrane and how does the bacterium respond to any potential pressure-induced damage?*

As explained in chapter 2 in detail, we used three independent techniques (electron microscopy: SEM and TEM, flow cytometry, and fluorescence microscopy) to detect potential membrane damages in *L. monocytogenes* after exposure to HPP. Our observation using TEM technique led us to conclude that membrane might be damaged and became perforated under pressure.

This observation motivated us to design a new set of experiments using a flow cytometry technique combined with a dynamic model to quantify the scale of membrane damages after HPP at 400 MPa, 8 and 20 min. The flow cytometry results with two fluorescent molecules of different sizes suggested the existence of a recovery process in the membrane after pressure treatment. The model calibrated to the flow cytometry data predicted that membrane disintegrity resulted from pressure-created damages was repaired such that full integrity in membrane could be accomplished after four days. This is consistent with the reported recovery time in *L. monocytogenes* before restart of growth after HPP at 450 and 550 MPa [13].

As measurements with flow cytometer performed over a population of cells (and not in the level of each individual cell), there might be some limitations to describe network responses accurately in the case of a non-homogeneous population [23]. Therefore we increased the level of monitoring to each individual pressure-treated cell by using a high frequency fluorescence microscopy technique combined with PI staining. Similar to flow cytometry methodology, damaged cells were detected from penetration of PI molecules that emit red intensity after binding to DNA. The dynamics of the repair process over four consecutive days after HPP were

investigated by monitoring the change in the red fluorescence intensity resulted from PI uptake. In other words, we assumed that the diffusion rate of PI molecules into the cell (which was estimated from the slope of the intensity curve vs. time) was positively correlated with the scale of pressure-induced damage.

First, fluorescence microscopy images indicated large variations in the degree of membrane damage among single cells, an observation reported in [56] as well after PI staining of pressure-treated *L. monocytogenes*. This broad distribution of red fluorescence intensity for cells taking up PI was probably originated from different structural strengths of the cellular envelope due to various possible drivers of intrapopulation heterogeneity [9, 68].

Second, following a clustering analysis using the k-means algorithm, we found out that the rate of diffusion of PI, particularly in the cluster with the lowest slope (corresponding to the least-damaged cells), was reduced during four days after pressure exposure. This observation suggested the existence of a recovery process activated in this type of bacteria in response to high pressure to repair damaged membrane.

Third, the synergy of our mass transfer mechanistic model with pre-designed fluorescence microscopy experiments led us to estimate the total size of the pressure-created pores at any time point after treatment at 400 MPa, 8 min, 8°C. We assumed that the main damage occurred in a single membrane pore area. Although this assumption might affect the prediction of the size of individual pores, the total diffusion of molecules through the cell membrane was only dependent on the total surface of the pores [71]. Therefore, cell fate, which is strongly affected by the total diffusion via the loss of cytosol material, was not be affected by the wrong estimation of the number of pores. Additionally, we could not find any evidence supporting the creation of multiple small pores due to high pressure. In other words, we believe that once a pore area was formed under pressure, further damage most likely happened at the same area, which was weaker than the remaining parts of the membrane.

Fourth, the estimated pore size over four days after HPP showed a linear decay trend as a function of time, suggesting the ability of damaged cells to reseal membrane pores. This is consistent with a reported dynamics for small membrane wounds (with sizes less than 20 nm) closure in human cells after sonication in which the authors used a series of fluorescent molecules with different sizes to measure the size of the finer pores in a wounded area indirectly [71].

The results of our growth evaluation experiments showed that colony formation was stopped in the culture medium at the population level during the four days of the experiments such that cell counts exceeded the limit of quantification (LOQ) only after seven days. The increased time required to start division can be attributed to the metabolic processes needed for the repair of damaged cell components and is therefore indicative of the presence of sub-lethally injured cells [30, 45]. This observation guided us to conclude that the lower number of PI-positive cells we obtained over the four consecutive days after HPP was not originated from the proliferation of new cells but was likely due to an increasing number of recovered cells.

Finally, it should be noted that it was the combination of model outputs and experimental data that enabled us to predict the membrane pore size in dam-

aged cells after pressure exposure. Although the results about membrane recovery dynamics obtained in this study were related to *L. monocytogenes* exposed to specific HPP conditions (400 MPa, 8 or 20 min, 8°C) and may not be generalized to other conditions and microorganisms, they can be inspiring for similar works in the future.

5.2 Modulation of the gene regulatory network in response to high pressure

Research question 2. *What is the impact of HPP on gene regulatory network and regulators' activities in L. monocytogenes?*

In chapter 3 we focused on the response of *L. monocytogenes*, strain ScottA, to HPP at the level of the genes, i.e., the modulation of gene regulatory network and particularly the activity of TFs, under high pressure. We used a time-series transcriptome data of *L. monocytogenes* exposed to HPP at 400 MPa, 8 min, 8°C [20] combined with a TF-TG topology network (A.2) as inputs to an optimization algorithm to uncover hidden regulatory signals involved in response to HPP. The optimization algorithm, which is known as NCA [25, 41], is a matrix decomposition method that provides the reconstructed activities of the TFs over time as an output.

Our results indicated a timely structured response that corresponds to three distinct (statistically different) time phases:

1. Survival phase (early-phase) lasting 0-10 min after HPP: regulation of genes that are responsible for immediate survival (e.g., the SOS response) and structural integrity (mostly chaperones and cell wall).
2. Repair phase (mid-phase) during 30-60 min after HPP: regulation of genes expressing enzymes and proteins related to the membrane repair.
3. Pre-growth phase (late-phase) during 6-48 h after HPP: regulation of genes involved in energy metabolism and re-growth.

As our growth experiments showed no growth higher than LOQ for the first 48 h after HPP, the expression of genes that encode for proteins associated with DNA repair, cell wall, and membrane biosynthesis during the early- and mid- phases was most likely due to a repair process rather than newly proliferated cells.

Analysis of the NCA results provided further new insights into the regulators and genes involved in each temporal phase. For instance, the results indicated a reduced activity for LexA, which as mentioned in 1, is a key regulator (TF) in the SOS response pathway by repressing the transcription of the SOS response regulon [67], during the first 10 min post-treatment. This could imply the up-regulation of LexA-regulated genes, including DNA repair genes of SOS regulon, as revealed by RNA-seq data as well [20].

CtsR and HrcA are two TFs that control the expression of heat-shock (stress tolerance) and chaperone proteins in bacteria, respectively [49, 59]. The NCA results showed that the activities of these two regulators were suppressed in response to HPP. The negative regulation in the activity of CtsR might allow the expression

of stress tolerance genes and contribute to the survival of *L. monocytogenes* upon exposure to high pressure stress. As explained in 1.5, the expressions of *dnaKJ* and *groESL* that encode for molecular chaperones (responsible for correct foldings of proteins) are under the control of the repressor HrcA. It has been shown that Under heat stress, HrcA is kept in its inactive form such that groE and dnaK operons can be transcribed to produce chaperones [59]. The lower activity of HrcA that we found in the pressure-treated sample compared to the control sample can lead to an up-regulation in the transcription of chaperonin genes to facilitate the repair process in the protein system and thereby survivability after HPP.

5.3 Early response of bacteria to HPP

Research question 3. *How can we employ a system modelling approach to develop a comprehensive multi-scale model that describes the initial response of L. monocytogenes to HPP?*

According to our findings in Chapter 3, the immediate response of *L. monocytogenes* to HPP included the regulation of the SOS response and chaperonin system. It has been shown that some of the SOS response associated genes in *E. coli*, such as DNA polymerases, contribute to survival by providing essential functions to ensure replication of repaired DNA [70]. In [29] the authors revealed that chaperonin systems (particularly DnaK and DnaJ proteins) facilitate survivability of *E. Coli* during early exposure to antibiotics stress. Therefore due to the significant contribution of the SOS response and chaperonin system regulation in the survivability of bacteria during the early period after stress exposure, we focused on these two subnetworks. The combination of time-series RNA-seq experimental data (at nine time points 0, 5, 10, 30, 45, 60 min, 6, 24, 48 min following HPP) and mathematical model simulations provided us a new insight into the behavior and dynamics of these two subnetworks as parts of an initial recovery process in *L. monocytogenes* in response to HPP.

It should be noted that for the nonlinear model developed in this work, a lower number of experimental points than the number of parameters caused sloppiness, which is a universal characteristic of the nonlinear multiparameter models [31]. Although the estimation of individual parameters of sloppy models is usually accompanied by significant uncertainties, a useful prediction could be extracted from a fit which might be resulted from more than one set of parameters [31].

Our model predictions provided us some new insights into the dynamics of the SOS response in *L. monocytogenes* following high pressure stress. First, the simulation results obtained from an optimization algorithm calibrated with the experimental data showed an oscillatory behavior for the dynamics of the two key regulators of the SOS response pathway, i.e., LexA and RecA. This oscillatory behavior was originated from specific compartments of the model configuration, which was developed from biological knowledge on the SOS and chaperonin system response to stress [7, 32, 46, 54, 59, 60]. It has been shown that delayed negative feedback can cause oscillations [62]. In our wiring diagram (Figure 1 in 4), delayed activation of RecA protein via signals from multiple proteins (RsbV, HU, and

SigB), following the formation of ssDNA after HPP stress contributed to a negative feedback loop closed by DNA_{ss} and $RecA_A$ (Figure 1 in 4). A two-step gene expression modelling consists of transcription and translation processes separately is the source for an extra delay in our developed model. Moreover, the interaction between LexA and RecA, which depends on other proteins such as HU, SigB, and UmuC, adds to the complexity of the model, which can be a cause for oscillations rather than a simpler network including only the regulation by LexA [6, 23]. A mutual antagonism structure between LexA and RecA, where an increase in one protein implies the decrease in the other, and the positive feedback loop formed between RsbV and SigB proteins can contribute to oscillations as well.

Second, we compared two different strains of *L. monocytogenes*, ScottA and RO15, in the characteristics of the SOS response dynamics following HPP. By optimizing the model parameters using time-series experimental data for each of the two strains separately, we found that the oscillation frequency of RecA response in the RO15 strain was higher than the ScottA strain. Furthermore, our simulation results showed a shift in the critical point of the bifurcation diagram (where for a particular parameter, increasing the parameter over a specific value changed the dynamics from damped oscillations to sustained oscillations) towards higher parameter values in the RO15 strain. This finding may explain the higher resistibility of the RO15 strain to HPP in comparison to the ScottA strain, which was reported in [20]. From a dynamic perspective, a rapid convergence (by short damped oscillations) to a stable, post-SOS response steady state is more desirable for survival than a longer oscillatory convergence, which can take a considerable more time to reach the same homeostasis. Because reaching this post-SOS response increases the likelihood to survive the stress, it is plausible that a wider parameter range that yields homeostasis promotes the ability of the bacteria to withstand high pressure stress, i.e., increases the bacterial resistibility.

Our sensitivity analysis indicated that although in the primary network configuration, the two subnetworks SOS response and chapronin system have impact on each other through RsbV and SigB proteins, perturbing the parameters associated with the SOS response system has a minor effect on the dynamics of the chaperonin system. Therefore, we concluded that the chaperonin system impacts the SOS response network but not vice versa. The protection of UmuC protein (in the SOS response system) from degradation by GroEL (a chaperone protein) in *E. coli* after exposure to UV radiation reported in [19] may strengthen our hypothesis of the effect of the chaperones on the the model outputs for the SOS response pathway.

Furthermore, the results of inhibition analysis suggested that that the parameters associated with the production or activity of the HU protein have a significant effect on the characteristics of the SOS response. This is in agreement with an observation in [46] where the authors reported a significant reduction in the induction of the SOS response and particularly the activation of the RecA protein in *hupA-hupB* (genes encode for HU) mutant versions of *E. coli* cells after exposure to UV radiation. This finding may suggest *hupA-hupB* as TGs for knockdown/out processes to investigate its impact on the efficiency of HPP.

Our further analysis suggested a relationship between the degree of damage induced by high pressure and the number of peaks appearing in the oscillatory response of SOS variables. We compared the results for two pressure values, 200

and 400 MPa (both at 8 min), and detected an extra initial peak in response to 400 MPa in comparison to the response to 200 MPa while the second peaks were simultaneous in response to both pressure levels. This is consistent with the results in [23] where the authors observed a highly structured oscillatory behavior for the SOS variables after UV treatment in *E. coli* cells with the number of peaks increased with the damage level.

5.4 The thesis as a whole, and the EU project SafeFooD

5.4.1 The thesis as a whole

Figure 5.1 summarizes the outcome of this Ph.D. thesis as four manuscripts published in (or submitted to) international journals.

We started our study of the response of *L. monocytogenes* to high pressure by observing the morphology of pressure-treated cells using SEM and TEM techniques. As the next step, we designed experiments employing the flow cytometry technique to investigate the status of the membrane in a population of treated bacteria. The analysis of this data, together with the results of growth evaluation experiments, led us to conclude the existence of a repair mechanism in the membrane after being damaged under high pressure (Paper 1, Dycops 2019). We then took a deeper level of complexity and investigated the membrane damage and the repair mechanisms in individual *L. monocytogenes* cells by designing a set of experiments using the fluorescence microscopy technique (paper 2, Frontiers in Microbiology) to measure the diffusion rate of fluorescent molecules into damaged bacteria. Based on this data, we developed a model that enabled us to quantify the scale of membrane damage and predict the time required for repair until full membrane integrity was re-obtained.

To understand the repair process at the level of the genes, we went deeper into gene regulatory networks involved in response to pressure-induced damages. We took a set of time-series RNA-seq data (A.3) together with a database we built for TF-TG connections in *L. monocytogenes* (A.2) as inputs of the NCA algorithm and obtained the reconstructed activity of key regulators. The analysis of the results surprisingly revealed three distinctive temporal phases in the regulatory response of *L. monocytogenes* to HPP (Paper 3, BMC Genomics). Among other important findings, the results suggested the significance of the early-phase in the survivability of damaged bacteria by activation of the SOS response and regulation of the chaperonin system. This led us to focus on these two pathways by developing a model to describe the interaction between genes, mRNA molecules, and proteins. Interestingly, our results suggested a damped oscillatory response for the main regulators of the SOS response pathway, which might be a result of complex interactions through a well-structured gene regulatory network including negative feedback and mutual antagonism structures (Paper 4, submitted).

All these subprojects provide a better overview of the response of *L. monocytogenes* to HPP, from an overall response (cellular structure and growth) to more specific structures such as the membrane, SOS-response pathway, and chaperonin system regulations. Although there is much more to be done to receive the complete picture of this response to HPP, the thesis took a large step in this direction

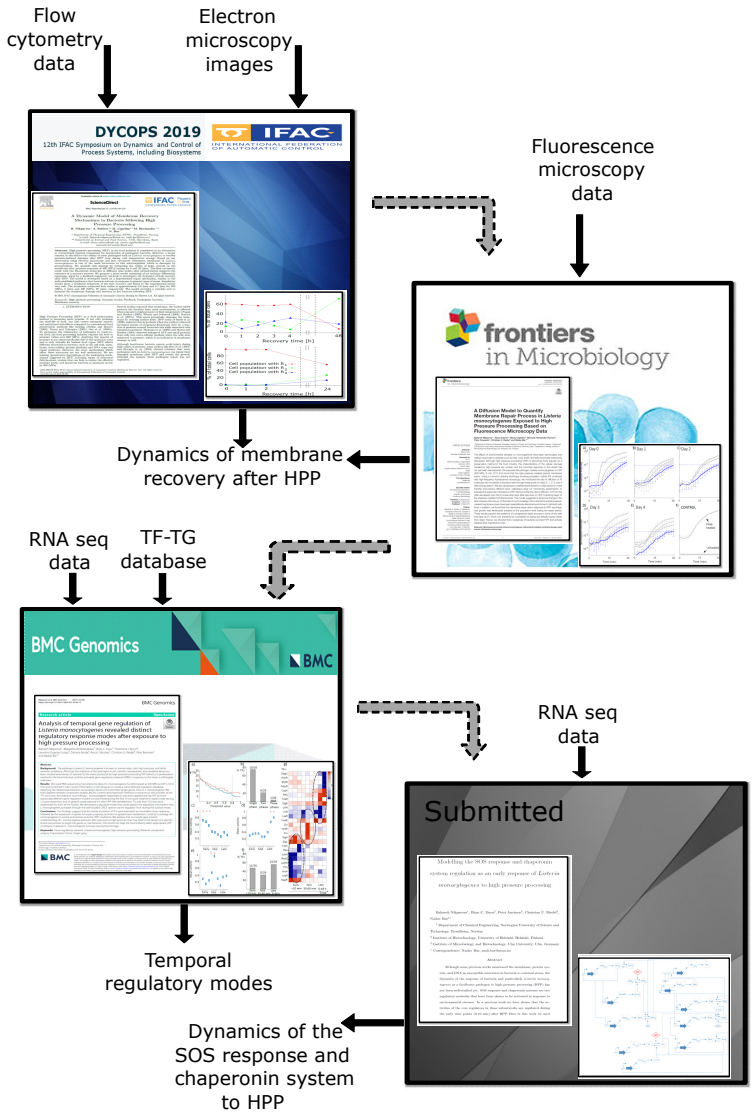

Figure 5.1: Published (submitted) papers as the outcome of this Ph.D. project.

and contributed to a better understanding of the behavior of *L. monocytogenes* specifically and bacteria generally to high pressure stress.

5.4.2 The project SafeFood

This thesis was a part of the transnational SafeFood industrial biotechnology project with the title: "Development of a novel industrial process for safe, sustainable and higher quality foods, using biotechnology and cybernetic approach".

SafeFood united eight groups from 6 countries across Europe, with the purpose to turn food safer by inactivating *L. monocytogenes*. The consortium consisted of experts in bioinformatics, molecular biology, simulation and modelling, and the food preservation industry.

The main objective of the project was to turn food products (ready-to-eat products based on meat, fish, and vegetables) safer and more durable by reducing or inhibit the ability of *L. monocytogenes* to recover after HPP. This can extend the shelf-life of food, increasing its resistance to food-related bacteria (by rendering the food "non-hospitable" for this type of bacteria) and decrease the amount of food waste from processing and throughout the food chain. Cutting edge biotechnological methods were applied in this project to achieve the following objectives:

- **O1.** to discover how recovery mechanisms of *L. monocytogenes* operate over time and with varying pressures. This will result in a novel knowledge database, mapping the food-related bacterial genetic regulatory networks involved in the recovery from pressure stress.
- **O2.** to predict the most promising potential genes and circuits that can suppress *L. monocytogenes* recovery from HPP, based on a unique dynamic model (cybernetic approach). The model can be served as a predictive tool and enables to focus on very few specific gene pathways that are responsible for efficient *L. monocytogenes* recovery.
- **O3.** to verify the prediction of the candidate genes by neutralizing the recovery mechanism using gene deletion and HPP treatment.
- **O4.** to produce zero-listeria food and increase shelf-life of existing food products, by a new concept strategy of HPP, i.e., targeting the mechanisms that prevent *L. monocytogenes* inactivation and allow its survival of HPP treatments.

Figure 5.2 summarizes the concept of SafeFood project as work packages assigned to each scientific group of the consortium. The objective of each work package is explained in the following:

- WP1: Project coordination and management.
- WP2: 1. Prepare and provide two *L. monocytogenes* strains for further research to other partners, including HPP stressed strains. 2. Conduct response (culture-based survival/recovery) studies of HPP stressed *L. monocytogenes* (both strains). 3. Assess HPP-induced sublethal injury, cell envelope integrity and ability to recover of selected *L. monocytogenes* strains by flow cytometry.
- WP3: 1. Develop a novel database, integrating all published knowledge about bacterial recovery (genes and pathways) due to HPP, mapping the genes and their interactions that are known to be involved in the recovery systems of bacteria in general (not only *L. monocytogenes*). This will result in a gene regulation/cell signaling map. 2. Measure gene expression of *L. monocytogenes* exposed to HPP of several thousands of genes (RNA-seq), and focus on selected highly expressed genes (qPCR). 3. Analyse the large RNA-seq data by advanced bioinformatics tools. 4. High precision gene expression qPCR measurements of selected genes that are differentially expressed.

- **WP4:** 1. Integrate the previous knowledge into an interconnected network of regulatory circuits, resulting in a qualitative integrated network model of the recovery processes. 2. Develop a novel dynamic model of the recovery processes and implement it in computer programming for later simulations (Matlab). 3. Estimate the model parameters so the response of the recovery model simulations will reflect our observations of recovery time. 4. Develop a novel, sophisticated predictive tool that can predict the key genes responsible for regulation. 5. Predict regulatory key genes and circuits and their effect when turned on/off on recovery response by advance simulation analysis.
- WP5: 1. Classical gene deletion approaches (for non-essential genes), performed using a widely used and well-established system for mutagenesis of *L. monocytogenes* based on a suicide vector. 2. Advanced knockdown strategies (for essential genes). For this strategy, called conditional gene knockdown, a dCas9/CRISPRi system for *L. monocytogenes* will be devised. 3. Both approaches will be applied to the well-established laboratory strain *L. monocytogenes* EGDe. 4. Experimental confirmation of the impact of the deleted genes (or circuits) on the susceptibility of *L. monocytogenes* towards HPP.
- WP6: Main goal is to evaluate a new HPP design based on the data obtained/modelled. 1. Based on target gene candidates, there will be a screening for suitable additives (salts, organic acids, etc.) that will impair recovery of *L. monocytogenes*. Several concentrations and combinations will be tested to find the most optimal additive(s). 2. Run pilot experimental evaluation of the concept on selected food products (e.g., cured meat and/or smoked salmon) inoculated with *L. monocytogenes*. 3. Run industrial experimental evaluation of the concept in real food matrices. 4. Evaluate the quality (taste, texture, color) of food products treated with the new HPP design.

In addition to the accomplishment of the five objectives of WP4 entirely (which was specifically assigned to NTNU according to Figure 5.2), we actively contributed to WP2 by evaluation of HPP-induced sublethal damages, cell envelope integrity, and ability to recover of selected *L. monocytogenes* strains by electron microscopy, flow cytometry, and fluorescence microscopy techniques. The TF-TG database (WP3) we built was also one of the results of the collaboration between NTNU and the University of Helsinki.

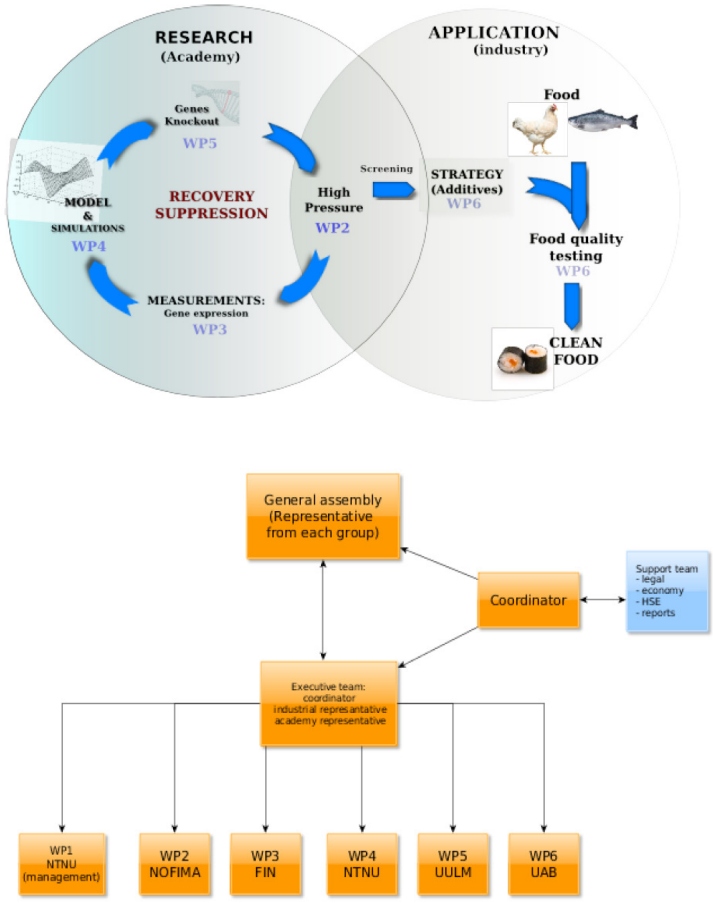

Figure 5.2: The SafeFood concept. Left circle: academic work, right circle: industrial work. nomenclature: WP: Work package; NTNU: Norwegian University of Science and Technology; NOFIMA: The Norwegian Institute of Food, Fisheries and Aquaculture Research; FIN: Finland (University of Helsinki); UULM: Ulm University; UAB: Autonomous University of Barcelona. University of Galati and University of Porto were two other partners of the project which are not shown in the figure.

Chapter 6

Conclusion and future work

6.1 Conclusion

In this chapter, we present a summary of the main conclusions of this Ph.D. study followed by possible research directions suggested as future works for interested readers. The topic of the thesis relies on the modelling and analysis of the response of *L. monocytogenes*, a kind of foodborne pathogenic Gram-positive bacteria, to high pressure treatment. We presented three research questions (see 1.7) and explained our approaches to address these questions (Chapters 2, 3, and 4), thereby providing new insight into the bacterial reaction to environmental stimuli including high pressure. The outcome of this thesis includes four original research papers published in (or submitted to) international journals or conference proceedings. The topics focus on understanding, modelling, and analysis of the response of *L. monocytogenes* to HPP. The answers to the research questions illuminate the effect of HPP on the bacterial membrane and the response of bacteria to any potential pressure-induced damages in the membrane; modulation of the gene regulatory network in response to high pressure; and the early response of bacteria to HPP, which contributes to the survivability of damaged cells.

First, in Chapter 2 we focused on the membrane as one of the most susceptible structures in the cell to HPP and investigated the existence of a recovery process in the membrane to repair any potential damage created due to the high pressure. We developed a dynamic model to quantify the degree of damage in pressure-treated bacteria. The synergy between our diffusion model and microscopy experiments revealed that some *L. monocytogenes* cells exposed to HPP repaired their damaged membrane approximately linearly on a time scale of days. This is the first time that membrane pores created by HPP have been quantitatively described and shown to diminish.

Second, in Chapter 3 we presented the results of our study about the regulatory response of *L. monocytogenes* to HPP at the level of the genes. We created a gene regulatory database for TF-TG connections in *L. monocytogenes* (strain ScottA), which was then used to input the NCA algorithm to reconstruct the activity of regulators (TFs) during 48 h after pressure treatment at 400MPa, 8°C, for 8 min. Our analysis indicated a structured temporal response in *L. monocytogenes*

after HPP which led to three distinct time phases: 0-10 min (early-phase), 30-60 min (mid-phase), and 6-48 h (late-phase) post-treatment. The results suggested an association between the activity of TFs involved during the early-phase with survival by regulation of genes encoding for chaperones, cell wall components, and the SOS response. Similarly, according to the results, the mid and late -phases were related to the regulatory networks with the primary role in repairing of membrane components, energy metabolism pathways, and regrowth, respectively.

Third, our results suggesting the role of the regulations during the early-phase in the survivability of pressure-treated bacteria inspired us to focus on the initial response to HPP in *L. monocytogenes* (particularly the SOS response and chaperonin system regulations), which was the topic of Chapter 4. This chapter introduced a dynamic model developed as a set of ODEs and calibrated with time-series RNA-seq data. Our experimental results and model outputs indicated a damped oscillatory response for the main regulators of the SOS response pathway (LexA and RecA), suggesting the existence of complex interactions through a well-structured gene regulatory network. The oscillatory behavior was expected due to the presence of delayed negative feedback and mutual antagonism structures in the wiring diagram of the model. Our findings suggested that a plausible explanation for the increase in the resistibility of the bacterial strains is a rapid convergence to homeostasis by shorter damped oscillations in the SOS response dynamics. Additionally, according to the results of inhibition analysis, HU protein played a critical role in the activation of RecA protein and thereby the induction of the SOS response following HPP. Finally, our results proposed that increasing the pressure value and holding time affected the response by increasing the number of peaks and the first peak amplitude, respectively. Taken together, the model gives an idea about how *L. monocytogenes* survives high pressure stress, provides an explanation for the increased resistance of some strains to HPP, and can be used as a basis to model survivability under other stress types.

We believe that our results provide a better understanding of *L. monocytogenes* behavior after high pressure exposure that may help with the development of a specific knockout process to target critical genes and increase the efficiency of HPP in the food industry.

6.2 Future work

The findings and ideas in this Ph.D. work might be extended for other HPP conditions and other microorganisms.

The diffusion model that quantified the membrane repair process in *L. monocytogenes* after HPP can be extended and improved such that the fidelity of the results is increased by adding more experimental points, repeating the experiments for some other fluorescent molecules and other microorganisms. It will be interesting as well to compare the results of the model for two strains with different sensitivity to high pressure, e.g. ScottA and RO15 of *L. monocytogenes*.

Predictions obtained from the NCA results in this work were based on an optimal model that guarantees a unique solution for the reconstructed activity of TFs.

However, experimental evidence with deletion mutants is required in the future to verify the generated hypothesis and predictions from the NCA analysis. Moreover, although our work focused only on the regulation of transcription, regulation may occur at different levels, including translation, mRNA stability, and protein degradation, and therefore mRNA levels may not always correlate with the proteins levels. As we focused on the ScottA strain of *L. monocytogenes*, studies in other strains such as RO15 are essential as well to understand better the role of gene regulatory networks in more barotolerant strains.

The model developed for the SOS response and chaperonin system regulation in this work can increase the understanding of the repair process in pressure-treated *L. monocytogenes* cells. However, more work is needed to obtain results with higher fidelity and accuracy. First, the configuration network proposed here presented the interactions between genes and proteins and consisted of one representative protein of each group with the same function. An extended network including more proteins that are in reality involved in these two pathways will increase the accuracy of the results. Second, more experimental data with shorter measurement intervals is required to obtain higher fidelity from a more complex model. For example, the characteristics of the oscillatory behavior suggested in this work for the SOS response after HPP can be extracted more precisely from an increased number of measurement points.

This page intentionally left blank.

Appendices

Appendix A

Supplementary information

A.1 Images obtained by fluorescence microscopy technique

Images obtained by fluorescence microscopy technique for monitoring diffusion of PI molecules into pressure-treated *L. monocytogenes* cells are available at The Dryad Digital Repository via the following link:
https://doi.org/10.5061/dryad.np5hqbzq6

A.2 TF-TG database of *L. monocytogenes*

The database is available at https://doi.org/10.1186/s12864-021-07461-0 as Additional file 1.

A.3 RNA-seq data

RNA-seq data have been deposited in the European Nucleotide Archive (ENA) under accession code PRJEB34771.

References

[1] doi: 10.1016/s0921-0423(02)80105-8.

[2] European centre for disease prevention and control. listeriosis. In: Ecdc. Annual epidemiological report for 2017. Stockholm: Ecdc, 2020. URL https://www.ecdc.europa.eu/sites/default/files/documents/listeriosis-annual-epidemiological-report-2017.pdf. (Retrieved July 2021).

[3] High pressure processing, 2021. URL https://hpp-systems.com/hpp-technology/. (Retrieved June 2021).

[4] High pressure processing in food industry, 2021. URL https://www.foodbuddies.in/high-pressure-processing-in-food-industry/. (Retrieved June 2021).

[5] T. Abee, W. van Schaik, and R. J. Siezen. Impact of genomics on microbial food safety. *Trends in Biotechnology*, 22(12):653–660, Dec. 2004. doi: 10.1016/j.tibtech.2004.10.007. URL https://doi.org/10.1016/j.tibtech.2004.10.007.

[6] A. Aertsen, K. Vanoirbeek, P. D. Spiegeleer, J. Sermon, K. Hauben, A. Farewell, T. Nystrom, and C. W. Michiels. Heat shock protein-mediated resistance to high hydrostatic pressure in *Escherichia coli*. *Applied and Environmental Microbiology*, 70(5):2660–2666, May 2004. doi: 10.1128/aem.70.5.2660-2666.2004. URL https://doi.org/10.1128/aem.70.5.2660-2666.2004.

[7] S. V. Aksenov. Dynamics of the inducing signal for the SOS regulatory system in *Escherichia coli* after ultraviolet irradiation. *Mathematical Biosciences*, 157 (1-2):269–286, Mar. 1999. doi: 10.1016/s0025-5564(98)10086-x. URL https://doi.org/10.1016/s0025-5564(98)10086-x.

[8] K. Aronsson, U. Rönner, and E. Borch. Inactivation of *Escherichia coli*, *Listeria innocua* and *Saccharomyces cerevisiae* in relation to membrane permeabilization and subsequent leakage of intracellular compounds due to pulsed electric field processing. *International Journal of Food Microbiology*, 99(1):19–32, Mar. 2005. doi: 10.1016/j.ijfoodmicro.2004.07.012. URL https://doi.org/10.1016/j.ijfoodmicro.2004.07.012.

[9] S. V. Avery. Microbial cell individuality and the underlying sources of heterogeneity. *Nature Reviews Microbiology*, 4(8):577–587, Aug. 2006. doi: 10.1038/nrmicro1460. URL https://doi.org/10.1038/nrmicro1460.

[10] Z. Baharoglu and D. Mazel. SOS, the formidable strategy of bacteria against aggressions. *FEMS Microbiology Reviews*, 38(6):1126–1145, Nov. 2014. doi: 10.1111/1574-6976.12077. URL https://doi.org/10.1111/1574-6976.12077.

[11] A. Battesti, N. Majdalani, and S. Gottesman. The RpoS-mediated general stress response in *Escherichia coli*. *Annual Review of Microbiology*, 65(1):189–213, Oct. 2011. doi: 10.1146/annurev-micro-090110-102946. URL https://doi.org/10.1146/annurev-micro-090110-102946.

[12] A. M. Bowman, O. M. Nesin, O. N. Pakhomova, and A. G. Pakhomov. Analysis of plasma membrane integrity by fluorescent detection of Tl(+) uptake. *The Journal of Membrane Biology*, 236(1):15–26, July 2010. doi: 10.1007/s00232-010-9269-y. URL https://doi.org/10.1007/s00232-010-9269-y.

[13] F. Bozoglu, H. Alpas, and G. Kaletunc. Injury recovery of foodborne pathogens in high hydrostatic pressure treated milk during storage. *FEMS Immunology & Medical Microbiology*, 40(3):243–247, 2004. doi: 10.1016/s0928-8244(04)00002-1. URL https://doi.org/10.1016/s0928-8244(04)00002-1.

[14] S. Chaturongakul, S. Raengpradub, M. Wiedmann, and K. J. Boor. Modulation of stress and virulence in *Listeria monocytogenes*. *Trends in Microbiology*, 16(8):388–396, Aug. 2008. doi: 10.1016/j.tim.2008.05.006. URL https://doi.org/10.1016/j.tim.2008.05.006.

[15] J. C. Cheftel. Review : High-pressure, microbial inactivation and food preservation. *Food Science and Technology International*, 1(2-3):75–90, Aug. 1995. doi: 10.1177/108201329500100203. URL https://doi.org/10.1177/108201329500100203.

[16] K. M. Considine, A. L. Kelly, G. F. Fitzgerald, C. Hill, and R. D. Sleator. High-pressure processing - effects on microbial food safety and food quality. *FEMS Microbiology Letters*, 281(1):1–9, Apr. 2008. doi: 10.1111/j.1574-6968.2008.01084.x. URL https://doi.org/10.1111/j.1574-6968.2008.01084.x.

[17] D. Cortezzo, K. Koziol-Dube, B. Setlow, and P. Setlow. Treatment with oxidizing agents damages the inner membrane of spores of *Bacillus subtilis* and sensitizes spores to subsequent stress. *Journal of Applied Microbiology*, 97(4):838–852, Oct. 2004. doi: 10.1111/j.1365-2672.2004.02370.x. URL https://doi.org/10.1111/j.1365-2672.2004.02370.x.

[18] P. D. Cotter and C. Hill. Surviving the acid test: Responses of Gram-positive bacteria to low pH. *Microbiology and Molecular Biology Reviews*, 67(3):429–453, Sept. 2003. doi: 10.1128/mmbr.67.3.429-453.2003. URL https://doi.org/10.1128/mmbr.67.3.429-453.2003.

[19] C. E. Donnelly and G. C. Walker. Coexpression of UmuD' with UmuC suppresses the UV mutagenesis deficiency of *groe* mutants. *Journal of Bacteriology*, 174(10):3133–3139, May 1992. doi: 10.1128/jb.174.10.3133-3139.1992. URL https://doi.org/10.1128/jb.174.10.3133-3139.1992.

[20] I. C. Duru, F. I. Bucur, M. Andreevskaya, B. Nikparvar, A. Ylinen, L. Grigore-Gurgu, T. M. Rode, P. Crauwels, P. Laine, L. Paulin, T. Løvdal, C. U. Riedel, N. Bar, D. Borda, A. I. Nicolau, and P. Auvinen. High-pressure processing-induced transcriptome response during recovery of *Listeria monocytogenes*. *BMC Genomics*, 22(1), Feb. 2021. doi: 10.1186/s12864-021-07407-6. URL https://doi.org/10.1186/s12864-021-07407-6.

[21] B. Ezraty, A. Gennaris, F. Barras, and J.-F. Collet. Oxidative stress, protein damage and repair in bacteria. *Nature Reviews Microbiology*, 15(7):385–396, Apr. 2017. doi: 10.1038/nrmicro.2017.26. URL https://doi.org/10.1038/nrmicro.2017.26.

[22] P. L. Foster. Stress responses and genetic variation in bacteria. *Mutation Research/Fundamental and Molecular Mechanisms of Mutagenesis*, 569(1-2): 3–11, Jan. 2005. doi: 10.1016/j.mrfmmm.2004.07.017. URL https://doi.org/10.1016/j.mrfmmm.2004.07.017.

[23] N. Friedman, S. Vardi, M. Ronen, U. Alon, and J. Stavans. Precise temporal modulation in the response of the SOS DNA repair network in individual bacteria. *PLoS Biology*, 3(7):e238, June 2005. doi: 10.1371/journal.pbio.0030238. URL https://doi.org/10.1371/journal.pbio.0030238.

[24] F. Fritsch, N. Mauder, T. Williams, J. Weiser, M. Oberle, and D. Beier. The cell envelope stress response mediated by the LiaFSR$_{Lm}$ three-component system of *Listeria monocytogenes* is controlled via the phosphatase activity of the bifunctional histidine kinase LiaS$_{Lm}$. *Microbiology*, 157(2):373–386, Feb. 2011. doi: 10.1099/mic.0.044776-0. URL https://doi.org/10.1099/mic.0.044776-0.

[25] S. J. Galbraith, L. M. Tran, and J. C. Liao. Transcriptome network component analysis with limited microarray data. *Bioinformatics*, 22(15):1886–1894, June 2006. doi: 10.1093/bioinformatics/btl279. URL https://doi.org/10.1093/bioinformatics/btl279.

[26] M. G. Gänzle and R. F. Vogel. On-line fluorescence determination of pressure mediated outer membrane damage in *Escherichia coli*. *Systematic and Applied Microbiology*, 24(4):477–485, Jan. 2001. doi: 10.1078/0723-2020-00069. URL https://doi.org/10.1078/0723-2020-00069.

[27] D. Garcia, P. Manas, N. Gomez, J. Raso, and R. Pagan. Biosynthetic requirements for the repair of sublethal membrane damage in *Escherichia coli* cells after pulsed electric fields. *Journal of Applied Microbiology*, 100(3): 428–435, Mar. 2006. doi: 10.1111/j.1365-2672.2005.02795.x. URL https://doi.org/10.1111/j.1365-2672.2005.02795.x.

[28] E.-B. Goh, G. Yim, W. Tsui, J. McClure, M. G. Surette, and J. Davies. Transcriptional modulation of bacterial gene expression by subinhibitory concentrations of antibiotics. *Proceedings of the National Academy of Sciences*, 99(26):17025–17030, Dec. 2002. doi: 10.1073/pnas.252607699. URL https://doi.org/10.1073/pnas.252607699.

[29] L. Goltermann, L. Good, and T. Bentin. Chaperonins fight aminoglycoside-induced protein misfolding and promote short-term tolerance in *Escherichia coli*. *Journal of Biological Chemistry*, 288(15):10483–10489, Apr. 2013. doi: 10.1074/jbc.m112.420380. URL https://doi.org/10.1074/jbc.m112.420380.

[30] L. Guillier, P. Pardon, and J.-C. Augustin. Influence of stress on individual lag time distributions of *Listeria monocytogenes*. *Applied and Environmental Microbiology*, 71(6):2940–2948, June 2005. doi: 10.1128/aem.71.6.2940-2948.2005. URL https://doi.org/10.1128/aem.71.6.2940-2948.2005.

[31] R. N. Gutenkunst, J. J. Waterfall, F. P. Casey, K. S. Brown, C. R. Myers, and J. P. Sethna. Universally sloppy parameter sensitivities in systems biology models. *PLoS Computational Biology*, 3(10):e189, Oct. 2007. doi: 10.1371/journal.pcbi.0030189. URL https://doi.org/10.1371/journal.pcbi.0030189.

[32] T. Hain, H. Hossain, S. S. Chatterjee, S. Machata, U. Volk, S. Wagner, B. Brors, S. Haas, C. T. Kuenne, A. Billion, S. Otten, J. Pane-Farre, S. Engelmann, and T. Chakraborty. Temporal transcriptomic analysis of the *Listeria monocytogenes* EGD-e σ^B regulon. *BMC Microbiology*, 8(1):20, 2008. doi: 10.1186/1471-2180-8-20. URL https://doi.org/10.1186/1471-2180-8-20.

[33] J. Hardin. *Becker's World of the cell*. Pearson, Boston, 2016. ISBN 9780134145792.

[34] V. Heinz and R. Buckow. Food preservation by high pressure. *Journal für Verbraucherschutz und Lebensmittelsicherheit*, 5(1):73–81, Aug. 2009. doi: 10.1007/s00003-009-0311-x. URL https://doi.org/10.1007/s00003-009-0311-x.

[35] C. Hill, P. D. Cotter, R. D. Sleator, and C. G. Gahan. Bacterial stress response in *Listeria monocytogenes*: jumping the hurdles imposed by minimal processing. *International Dairy Journal*, 12(2-3):273–283, Jan. 2002. doi: 10.1016/s0958-6946(01)00125-x. URL https://doi.org/10.1016/s0958-6946(01)00125-x.

[36] A. Jofre and T. Aymerich. Inactivation and recovery of *Listeria monocytogenes*, *Salmonella enterica* and *Staphylococcus aureus* after high hydrostatic pressure treatments up to 900 MPa. *International Microbiology*, (13):105–112, 2010. ISSN 1618-1905. doi: 10.2436/20.1501.01.115. URL https://doi.org/10.2436/20.1501.01.115.

[37] G. Kaletunc, J. Lee, H. Alpas, and F. Bozoglu. Evaluation of structural changes induced by high hydrostatic pressure in *Leuconostoc mesenteroides*.

Applied and Environmental Microbiology, 70(2):1116–1122, Feb. 2004. doi: 10.1128/aem.70.2.1116-1122.2004. URL https://doi.org/10.1128/aem.70.2.1116-1122.2004.

[38] B. Klotz, P. Mañas, and B. M. Mackey. The relationship between membrane damage, release of protein and loss of viability in *Escherichia coli* exposed to high hydrostatic pressure. *International Journal of Food Microbiology*, 137(2-3):214–220, Feb. 2010. doi: 10.1016/j.ijfoodmicro.2009.11.020. URL https://doi.org/10.1016/j.ijfoodmicro.2009.11.020.

[39] D. Knorr, V. Heinz, and R. Buckow. High pressure application for food biopolymers. *Biochimica et Biophysica Acta (BBA) - Proteins and Proteomics*, 1764(3):619–631, Mar. 2006. doi: 10.1016/j.bbapap.2006.01.017. URL https://doi.org/10.1016/j.bbapap.2006.01.017.

[40] B. Kramer and J. Thielmann. Monitoring the live to dead transition of bacteria during thermal stress by a multi-method approach. *Journal of Microbiological Methods*, 123:24–30, Apr. 2016. doi: 10.1016/j.mimet.2016.02.009. URL https://doi.org/10.1016/j.mimet.2016.02.009.

[41] J. C. Liao, R. Boscolo, Y.-L. Yang, L. M. Tran, C. Sabatti, and V. P. Roychowdhury. Network component analysis: Reconstruction of regulatory signals in biological systems. *Proceedings of the National Academy of Sciences*, 100(26):15522–15527, Dec. 2003. doi: 10.1073/pnas.2136632100. URL https://doi.org/10.1073/pnas.2136632100.

[42] P. Mañas and B. M. Mackey. Morphological and physiological changes induced by high hydrostatic pressure in exponential- and stationary-phase cells of *Escherichia coli*: Relationship with cell death. *Applied and Environmental Microbiology*, 70(3):1545–1554, Mar. 2004. doi: 10.1128/aem.70.3.1545-1554.2004. URL https://doi.org/10.1128/aem.70.3.1545-1554.2004.

[43] J. Marles-Wright and R. J. Lewis. Stress responses of bacteria. *Current Opinion in Structural Biology*, 17(6):755–760, Dec. 2007. doi: 10.1016/j.sbi.2007.08.004. URL https://doi.org/10.1016/j.sbi.2007.08.004.

[44] K. H. Maslowska, K. Makiela-Dzbenska, and I. J. Fijalkowska. The SOS system: A complex and tightly regulated response to DNA damage. *Environmental and Molecular Mutagenesis*, 60(4):368–384, Jan. 2019. doi: 10.1002/em.22267. URL https://doi.org/10.1002/em.22267.

[45] A. Metris, S. M. George, B. M. Mackey, and J. Baranyi. Modeling the variability of single-cell lag times for *Listeria innocua* populations after sublethal and lethal heat treatments. *Applied and Environmental Microbiology*, 74(22):6949–6955, Nov. 2008. doi: 10.1128/aem.01237-08. URL https://doi.org/10.1128/aem.01237-08.

[46] I. Miyabe, Q.-M. Zhang, Y. Kano, and S. Yo. Histone-like protein HU is required for recA gene-dependent DNA repair and SOS induction pathways in UV-irradiated *Escherichia coli*. *International Journal of Radiation Biology*,

76(1):43–49, Jan. 2000. doi: 10.1080/095530000138998. URL https://doi.org/10.1080/095530000138998.

[47] M. L. G. Monteiro, E. T. Mársico, S. B. Mano, T. S. Alvares, A. Rosenthal, M. Lemos, E. Ferrari, C. A. Lázaro, and C. A. Conte-Junior. Combined effect of high hydrostatic pressure and ultraviolet radiation on quality parameters of refrigerated vacuum-packed tilapia (*Oreochromis niloticus*) fillets. *Scientific Reports*, 8(1), June 2018. doi: 10.1038/s41598-018-27861-9. URL https://doi.org/10.1038/s41598-018-27861-9.

[48] M.-V. Muntean, O. Marian, V. Barbieru, G. M. Cătunescu, O. Ranta, I. Drocas, and S. Terhes. High pressure processing in food industry - characteristics and applications. *Agriculture and Agricultural Science Procedia*, 10:377–383, 2016. doi: 10.1016/j.aaspro.2016.09.077. URL https://doi.org/10.1016/j.aaspro.2016.09.077.

[49] S. Nair, I. Derre, T. Msadek, O. Gaillot, and P. Berche. CtsR controls class III heat shock gene expression in the human pathogen *Listeria monocytogenes*. *Molecular Microbiology*, 35(4):800–811, Feb. 2000. doi: 10.1046/j.1365-2958.2000.01752.x. URL https://doi.org/10.1046/j.1365-2958.2000.01752.x.

[50] H. Neetoo and H. Chen. Application of high hydrostatic pressure technology for processing and preservation of foods. In R. Bhat, A. K. Alias, and G. Paliyath, editors, *Progress in Food Preservation*, volume 1, pages 247–276. John Wiley & Sons Ltd, ISBN:9780470655856, 1st edition, 2012.

[51] R. J. Ouellette and J. D. Rawn. 14 - amino acids, peptides, and proteins. In R. J. Ouellette and J. D. Rawn, editors, *Principles of Organic Chemistry*, pages 371–396. Elsevier, Boston, 2015. ISBN 978-0-12-802444-7. doi: https://doi.org/10.1016/B978-0-12-802444-7.00014-8. URL https://www.sciencedirect.com/science/article/pii/B9780128024447000148.

[52] Z. Podlesek and D. Ž. Bertok. The DNA damage inducible SOS response is a key player in the generation of bacterial persister cells and population wide tolerance. *Frontiers in Microbiology*, 11, Aug. 2020. doi: 10.3389/fmicb.2020.01785. URL https://doi.org/10.3389/fmicb.2020.01785.

[53] T.-T. Qin, H.-Q. Kang, P. Ma, P.-P. Li, L.-Y. Huang, and B. Gu. Sos response and its regulation on the fluoroquinolone resistance. *Annals of Translational Medicine*, 3(22), 2015. ISSN 2305-5847. URL https://atm.amegroups.com/article/view/8610.

[54] S. Raengpradub, M. Wiedmann, and K. J. Boor. Comparative analysis of the σ^B-dependent stress responses in *Listeria monocytogenes* and *Listeria innocua* strains exposed to selected stress conditions. *Applied and Environmental Microbiology*, 74(1):158–171, Jan. 2008. doi: 10.1128/aem.00951-07. URL https://doi.org/10.1128/aem.00951-07.

[55] S. Reischl, T. Wiegert, and W. Schumann. Isolation and analysis of mutant alleles of the *Bacillus subtilis* HrcA repressor with reduced dependency on GroE function. *Journal of Biological Chemistry*, 277(36):32659–32667, Sept. 2002. doi: 10.1074/jbc.m201372200. URL https://doi.org/10.1074/jbc.m201372200.

[56] M. Ritz, J. L. Tholozan, M. Federighi, and M. F. Pilet. Morphological and physiological characterization of *Listeria monocytogenes* subjected to high hydrostatic pressure. *Applied and Environmental Microbiology*, 67(5): 2240–2247, May 2001. doi: 10.1128/aem.67.5.2240-2247.2001. URL https://doi.org/10.1128/aem.67.5.2240-2247.2001.

[57] D. Roncarati and V. Scarlato. Regulation of heat-shock genes in bacteria: from signal sensing to gene expression output. *FEMS Microbiology Reviews*, 41(4):549–574, Apr. 2017. doi: 10.1093/femsre/fux015. URL https://doi.org/10.1093/femsre/fux015.

[58] A. Russell. Lethal effects of heat on bacterial physiology and structure. *Science Progress*, 86(1-2):115–137, Feb. 2003. doi: 10.3184/003685003783238699. URL https://doi.org/10.3184/003685003783238699.

[59] W. Schumann. The *Bacillus subtilis* heat shock stimulon. *Cell Stress & Chaperones*, 8(3):207, 2003. doi: 10.1379/1466-1268(2003)008<0207:tbshss>2.0.co;2. URL https://doi.org/10.1379/1466-1268(2003)008<0207:tbshss>2.0.co;2.

[60] L. A. Simmons, J. J. Foti, S. E. Cohen, and G. C. Walker. The SOS regulatory network. *EcoSal Plus*, 3(1), Feb. 2008. doi: 10.1128/ecosalplus.5.4.3. URL https://doi.org/10.1128/ecosalplus.5.4.3.

[61] J. P. Smelt, A. F. Rijke, and A. Hayhurst. Possible mechanism of high pressure inactivation of microorganisms. *High Pressure Research*, 12(4-6):199–203, Nov. 1994. doi: 10.1080/08957959408201658. URL https://doi.org/10.1080/08957959408201658.

[62] Z. Szallasi. *System modeling in cellular biology : from concepts to nuts and bolts*. MIT Press, Cambridge, Mass, 2010. ISBN 9780262514224.

[63] P. Teixeira, H. Castro, C. Mohacsi-Farkas, and R. Kirby. Identification of sites of injury in *Lactobacillus bulgaricus* during heat stress. *Journal of Applied Microbiology*, 83:219–226, 1997.

[64] S. Tiwari, S. B. Jamal, S. S. Hassan, P. V. S. D. Carvalho, S. Almeida, D. Barh, P. Ghosh, A. Silva, T. L. P. Castro, and V. Azevedo. Two-component signal transduction systems of pathogenic bacteria as targets for antimicrobial therapy: An overview. *Frontiers in Microbiology*, 8, Oct. 2017. doi: 10.3389/fmicb.2017.01878. URL https://doi.org/10.3389/fmicb.2017.01878.

[65] J. A. Torres and G. Velazquez. Commercial opportunities and research challenges in the high pressure processing of foods. *Journal of Food Engineering*, 67(1-2):95–112, Mar. 2005. doi: 10.1016/j.jfoodeng.2004.05.066. URL https://doi.org/10.1016/j.jfoodeng.2004.05.066.

[66] L. M. Tran, M. P. Brynildsen, K. C. Kao, J. K. Suen, and J. C. Liao. gNCA: A framework for determining transcription factor activity based on transcriptome: identifiability and numerical implementation. *Metabolic Engineering*, 7(2):128–141, Mar. 2005. doi: 10.1016/j.ymben.2004.12.001. URL https://doi.org/10.1016/j.ymben.2004.12.001.

[67] S. van der Veen, S. van Schalkwijk, D. Molenaar, W. M. de Vos, T. Abee, and M. H. J. Wells-Bennik. The SOS response of *Listeria monocytogenes* is involved in stress resistance and mutagenesis. *Microbiology*, 156(2):374–384, Feb. 2010. doi: 10.1099/mic.0.035196-0. URL https://doi.org/10.1099/mic.0.035196-0.

[68] J.-W. Veening, W. K. Smits, and O. P. Kuipers. Bistability, epigenetics, and bet-hedging in bacteria. *Annual Review of Microbiology*, 62(1):193–210, Oct. 2008. doi: 10.1146/annurev.micro.62.081307.163002. URL https://doi.org/10.1146/annurev.micro.62.081307.163002.

[69] T. J. Welch, A. Farewell, F. C. Neidhart, and D. H. Bartlett. Stress response of *Escherichia coli* to elevated hydrostatic pressure. *Journal of Bacteriology*, 175(22):7170–7177, Sept. 1993. doi: 0021-9193/93/227170-0802.00/0. URL https://journals.asm.org/doi/pdf/10.1128/jb.175.22.7170-7177.1993.

[70] B. Yeiser, E. D. Pepper, M. F. Goodman, and S. E. Finkel. SOS-induced DNA polymerases enhance long-term survival and evolutionary fitness. *Proceedings of the National Academy of Sciences*, 99(13):8737–8741, June 2002. doi: 10.1073/pnas.092269199. URL https://doi.org/10.1073/pnas.092269199.

[71] V. Zarnitsyn, C. A. Rostad, and M. R. Prausnitz. Modeling transmembrane transport through cell membrane wounds created by acoustic cavitation. *Biophysical Journal*, 95(9):4124–4138, Nov. 2008. doi: 10.1529/biophysj.108.131664. URL https://doi.org/10.1529/biophysj.108.131664.

[72] C. P. Zschiedrich, V. Keidel, and H. Szurmant. Molecular mechanisms of two-component signal transduction. *Journal of Molecular Biology*, 428(19):3752–3775, Sept. 2016. doi: 10.1016/j.jmb.2016.08.003. URL https://doi.org/10.1016/j.jmb.2016.08.003.

ISBN 978-82-326-5717-9 (printed ver.)
ISBN 978-82-326-5411-6 (electronic ver.)
ISSN 1503-8181 (printed ver.)
ISSN 2703-8084 (online ver.)

NTNU

Norwegian University of
Science and Technology